2014

The electron transport within the wide energy gap compound semiconductors gallium nitride and zinc oxide

Walid Abdul Hadi
University of Windsor

The Electron Transport within the Wide Energy Gap Compound Semiconductors Gallium Nitride and Zinc Oxide

by

Walid Abdul Hadi

A Dissertation
Submitted to the Faculty of Graduate Studies
Through the Department of Electrical and Computer Engineering
In Partial Fulfillment of the Requirements for
The Degree of Doctor of Philosophy at the
University of Windsor

Windsor, Ontario, Canada

2013

The Electron Transport within the Wide Energy Gap Compound Semiconductors Gallium Nitride and Zinc Oxide

by

Walid Abdul Hadi

APPROVED BY:

Dr. R. Sobot
Western University

Dr. N. Zamani
Department of Mechanical, Automotive and Materials Engineering

Dr. M. Ahmadi
Department of Electrical and Computer Engineering

Dr. M. Mirhasani
Department of Electrical and Computer Engineering

Dr. R. Muscedere
Department of Electrical and Computer Engineering

Dr. S. K. O'Leary
Department of Electrical and Computer Engineering

Dr. M. Guarini, Chair of Defense
Department of Philosophy

Declaration of Co-Authorship / Previous Publication

I. Co-Authorship Declaration

I hereby declare that this thesis incorporates material that is the result of joint research undertaken with Dr. Michael S. Shur, of Rensselaer Polytechnic Institute, Mr. Reddiprasad Cheekoori, of The University of British Columbia, and my supervisor, Dr. S. K. O'Leary, of The University of British Columbia. In all cases, the key ideas, the primary contributions, and data analysis and interpretation, were performed by the author of this thesis, the contributions of the co-authors being primarily focused on providing simulation data, in addition to suggesting possible directions. Results related to this research are reported in Chapters 2 through 5, inclusive.

I am aware of the University of Windsor's Senate Policy on Authorship and I certify that I have properly acknowledged the contributions of the other researchers to my thesis, and I have obtained written permission from my co-authors to include the aforementioned materials in my thesis.

I certify that, with the above qualification, this thesis, and the research to which it refers to, is the product of my own work.

II. Declaration of Previous Publication

This thesis includes 3 original papers that have been previously published/submitted for publication to peer reviewed journals. It also includes one paper that is in the process of submission to a peer reviewed journal. These original papers are as follows:

Thesis Chapter	Publication Title/full citation	Publication status
Chapter 2	Transient electron transport in III-V compound semiconductors gallium arsenide and gallium nitride, W. A. Hadi, R. Cheekoori, M. S. Shur, and S. K. O'Leary, *Journal of Materials Science: Materials in Electronics*, vol. 24, no. 2, pp. 807-813, 2013.	Published
Chapter 3	On the applicability of a semi-analytical approach to determining the transient electron response of gallium arsenide, gallium nitride, and zinc oxide, W. A. Hadi, M. S. Shur, and S. K. O'Leary, *Journal of Materials Science: Materials in Electronics*, vol. 24, no. 5, pp. 1624-1634, 2013.	Published
Chapter 4	Determining the optimal applied electric field strength for a given electron displacement for the case of bulk wurtzite zinc oxide: A transient Monte Carlo analysis, W. A. Hadi, M. S. Shur, and S. K. O'Leary, submitted to *Journal of Applied Physics*.	Some revisions required
Chapter 5	On the applicability of a semi-analytical approach in determining the optimal applied electric field strength for a given electron displacement for the case of bulk wurtzite zinc oxide, W. A. Hadi, M. S. Shur, and S. K. O'Leary.	*To be submitted to the Journal of Materials Science: Materials in Electronics.*

I certify that I have obtained written permission from the copyright owner(s) to include the above published materials in my thesis. I certify that the above material describes work completed during my registration as a graduate student at the University of Windsor.

I declare that, to the best of my knowledge, my thesis does not infringe upon anyone's copyright nor violate any proprietary rights and that any ideas, techniques, quotations, or any other material from the work of other people included in my thesis, published or otherwise, are fully acknowledged in accordance with the standard referencing practices. Furthermore, to the extent that I have included copyrighted material that surpasses the bounds of fair dealing within the meaning of the Canada Copyright Act, I certify that I have obtained a written permission from the copyright owners to include such materials in my thesis.

I declare that this is a true copy of my thesis, including any final revisions, as approved by my thesis committee and the Graduate Studies office, and that this thesis has not been submitted for a higher degree to any other university or institution.

ABSTRACT

In this thesis, the electron transport that occurs within two wide energy gap semiconductors, gallium nitride and zinc oxide, is considered. Electron transport within gallium arsenide is also examined, albeit primarily for benchmarking purposes. The overarching goal of this thesis is to provide the materials community with tools for analysis and optimization to be used when evaluating the consequences of transient electron transport within these compound semiconductors. Providing fresh insights into the character of the electron transport within zinc oxide, with particular focus on the device implications, is another aim of this analysis.

Initially, Monte Carlo electron transport simulation results are used for a comparative analysis of the transient electron transport that occurs within bulk zinc-blende gallium arsenide and bulk wurtzite gallium nitride. It is found that for both materials the electron drift velocity and the average electron energy field-dependent "settling times" are strongly correlated and that the electric field resulting in the shortest electron transit-time is a function of channel length. Then, the applicability of the semi-analytical approach of Shur [M. S. Shur, "Influence of non-uniform field distribution on frequency limits of GaAs field-effect transistors," *Electronics Letters*, vol. 12, no. 23, pp. 615-616, 1976] in evaluating the transient electron transport response within gallium arsenide, gallium nitride, and zinc oxide is critically examined. In particular, a

comparison with Monte Carlo results is performed in order to establish the utility of this approach as a tool in studying the transient electron transport response. Next, a Monte Carlo analysis of the electron transport within bulk wurtzite zinc oxide is performed. The applied electric field strength that ensures the minimum electron time-to-transit across a given channel length is determined. These results are then used in order to provide an upper bound on the potential performance of zinc oxide based devices.

Finally, the utility of the semi-analytical approach of Shur, for the purposes of device design optimization, is considered for the specific case of bulk wurtzite ZnO. It is found that the results produced through the semi-analytical approach of Shur are, in many cases, imperceptibly different from those of the Monte Carlo simulations. This adds to the allure of the semi-analytical approach as a versatile tool for transient electron transport analyzes and device design.

DEDICATION

To Mom and Dad.

AKNOWLEDGEMENTS

The author would like to express his deep appreciation to Dr. Stephen O'Leary for his unlimited support, guidance, and endless hours of fruitful and extremely rewarding discussions throughout the years that led to the culmination of this work. His mentorship and knowledge has helped me finesse both my research and academic skills and will undoubtedly be a substantial contribution to my success in both my academic and research careers. I also extend my sincerest gratitude to my committee members Drs. R. Muscedere, A. Ahmadi, N. Zamani, and M. Mirhasani, for their valuable guidance and important suggestions. Their feedback has provided me with the motivation to find the right ideas to work on for my research. I would also like to thank Dr. R. Sobot for giving me the honor to be on my committee and examine my work.

I would also like to thank Dr. Sid Ahmed, Head of the Electrical and Computer Engineering Department, for his encouragement and guidance during my graduate studies pursuit. Special thanks goes to Ms. Andria Ballo, the graduate secretary, for her genuine assistance and care throughout my years of graduate studies at the University of Windsor.

I thank my brother Hussein for his care and support and our long phone conversations that have given me the strength when I needed it the most. I thank my parents Ali and

Rafica for everything they have done for me, there are no words that can describe the gratitude and love I feel towards you guys, nothing would have been possible without you. Children take their parents for granted and this is one of those moments of truth where I deeply realize everything you have done for me and all the things you have taught me. It is because of all the sacrifices that you have made throughout those many years that my accomplishments are made possible.

Last but not least I want to thank my wife Samar and daughters Leila and Angelina for their unparalleled support, patience, encouragement, and for their faith in my talent and ability to pursue my goals. I thank Samar for always being there for me in those moments where every graduate student feels lost in the midst of their research, she always managed to bring the sunshine to my grey skies. I thank Leila and Angelina for bringing a smile to my face and giving me the breeze of fresh air each time I took things too seriously.

Table of Contents

List of Tables

List of Figures

List of Abbreviations and Symbols

D_a	acoustic deformation potential
AlAs	aluminium arsenide
k_b	Boltzmann's constant
CdS	cadmium sulfide
C	carbon
$\hbar k$	crystal momentum
c-GaAs	crystalline gallium arsenide
c-Si	crystalline silicon
3C SiC	cubic zinc-blende silicon carbide polytype
f_T	cut-off frequency
ρ	density
L	device length
N_D	doping concentration
ξ	electric field strength
v	electron drift velocity
m^*	electron effective mass
τ	electron transit time
ε	electron energy

E_g	energy gap
$\tau_\varepsilon(\varepsilon)$	energy relaxation time
m_e	free electron mass
t_s	free flight time
GaSb	gallium antimonide
GaAs	gallium arsenide
GaN	gallium nitride
GaP	gallium phosphide
Ge	germanium
4H SiC	hexagonal wurtzite silicon carbide polytype
6H SiC	hexagonal wurtzite silicon carbide polytype
K_∞	high frequency dielectric constant
InSb	indium antimonide
InAs	indium arsenide
InN	indium nitride
InP	indium phosphide
D_{ij}	intervalley deformation potential
ε_{ij}	intervalley phonon energy
β	inverse screening length
τ_{min}	minimum time-to-transit
$\tau_m(\varepsilon)$	momentum relaxation time
α	non-parabolicity coefficient
Z_j	number of equivalent valleys

e_o	permittivity of vacuum
ε_{op}	polar optical phonon energy
λ_m	scattering rate
Si	silicon
v_s	sound velocity
K_o	static dielectric constant
$\xi_{ss}(\varepsilon)$	steady-state electric field strength
$v_{ss}(\varepsilon)$	steady-state electron drift velocity
v_{peak}	steady-state peak electron drift velocity
ε_o	thermal equilibrium energy
λ	total scattering rate
Γ	valley location
ZnO	zinc oxide

CHAPTER 1

Introduction

The development of the transistor in 1947 prompted a revolution in technology that continues to shape the course of human development today [1, 2]. The transistor lies at the heart of modern electronics. It allows for the amplification of analog signals and for the processing of digital signals with efficiencies that could not otherwise be achieved. In modern industrial societies, such as Canada's, transistors are ubiquitous. They are found in telephones, radios, televisions, automobiles, and many other commodities. They are being used for an ever broadening range of applications, including applications in sensing, processing, and data archiving. Given their hold on modern technology, transistors seem destined to continue to play a crucial role in technological development for at least this century, and perhaps beyond.

In 1965, Gordon Moore, the future chairman and a future founder of Intel Corporation, prophesized that the number of transistors on a silicon chip would double every 18 months for the next decade [3]. Moore's law, as this prophecy is now often referred to as today, has held for almost 5 decades now and the expectation is that it will continue to hold for at least another decade [4]; see Figure 1.1. In order to achieve this rate of technological progress, transistors have needed to become smaller, faster, cheaper,

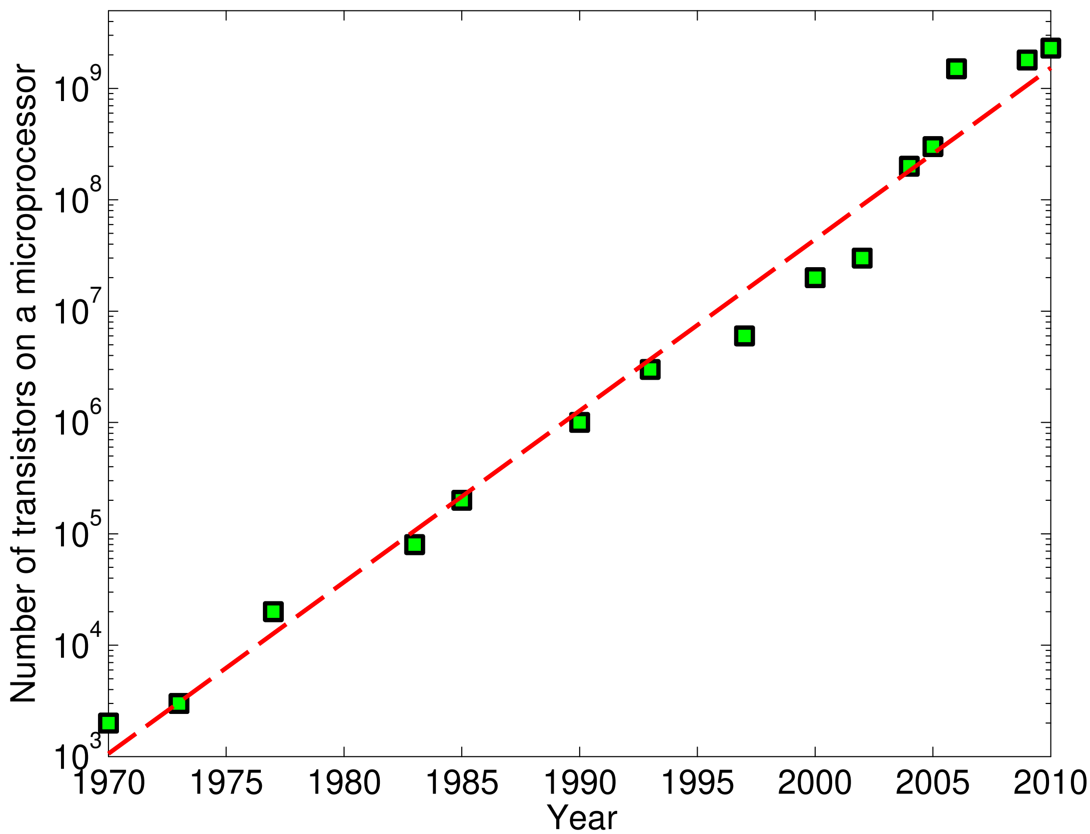

Figure 1.1: The number of transistors on an Intel microprocessor, from 1970 to 2010. A least-squares linear fit to this data is depicted with the dashed line. The data in this figure from Schwierz [4]. The online version is depicted in color.

and more reliable. This has required a detailed understanding of the material properties of the materials found within transistors [5]. Transistors are fabricated from insulators, conductors, and semiconductors. While the material properties of insulators and conductors were reasonably well known prior to development of the transistor, the material properties of semiconductors remained largely unknown at that time. Indeed, in 1947, semiconductors were considered more of a laboratory curiosity [6].

Since that time, however, there has been a tremendous amount of effort invested into the determination of the material characteristics of semiconductors. Experimental and theoretical studies have been performed on the structural, electronic, and optical characteristics of these materials. The scientific literature now burgeons with reports from such studies. As a consequence, a detailed and quantitative understanding of the material properties of a number of semiconductor materials has been achieved [7]. This understanding has allowed for the realization of many novel device designs, and thus, has played an indispensible role in the evolution of the field. Further innovations in device design will undoubtedly require an even greater understanding of the properties of these materials.

Thus far, most such semiconductor material studies have focused upon the material properties of either bulk silicon (Si) or bulk gallium arsenide (GaAs). Si is the workhorse upon which conventional microelectronics has been built. Unfortunately, as Si is an indirect energy-gap semiconductor, its utility for optoelectronic device applications is limited. GaAs, however, is a direct-gap III-V compound semiconductor with great optical properties. As a consequence, it is often used for optoelectronic device applications. Beyond Si and GaAs, there are many other semiconductor materials, some offering a unique constellation of material characteristics, making them ideal for certain niche device applications. In Figure 1.2, the energy gaps, corresponding to some of the more common elemental and compound semiconductors, are tabulated, the nature of these energy gaps, i.e., whether they are direct or indirect, being clearly indicated. Unfortunately, at the present moment at least, the understanding of the material properties of many of the non-traditional semiconductors, i.e, neither Si nor GaAs, remains rudimentary, at best. The understanding of the material properties of these non-traditional semiconductors, and the novel device designs engendered through this understanding, will undoubtedly remain a focus of semiconductor researchers for many years to come.

Wide energy gap semiconductors, i.e., semiconductors with energy gaps wider than those associated with the more conventional semiconductors [8], crystalline silicon (c-Si) and crystalline gallium arsenide (c-GaAs), offer considerable promise for novel electronic and optoelectronic device applications. Owing to the fact that wider energy gap semiconductors tend to possess higher polar optical phonon energies, the saturation electron drift velocities exhibited by these materials tend to be higher. In addition, the dielectric constants, both static and high-frequency, associated with the wider energy gap semiconductors tend to be smaller than those associated with the more conventional semiconductors. Both of these factors favor improved electron device performance [9]. An additional benefit of the wide energy gap semiconductors is their great tolerance to high applied electric field strengths, making them ideal for high-power device applications [10], the breakdown field of a semiconductor increasing with the magnitude of its energy gap [11,12]. Finally, the high thermal conductivities associated with these materials further adds to their allure.

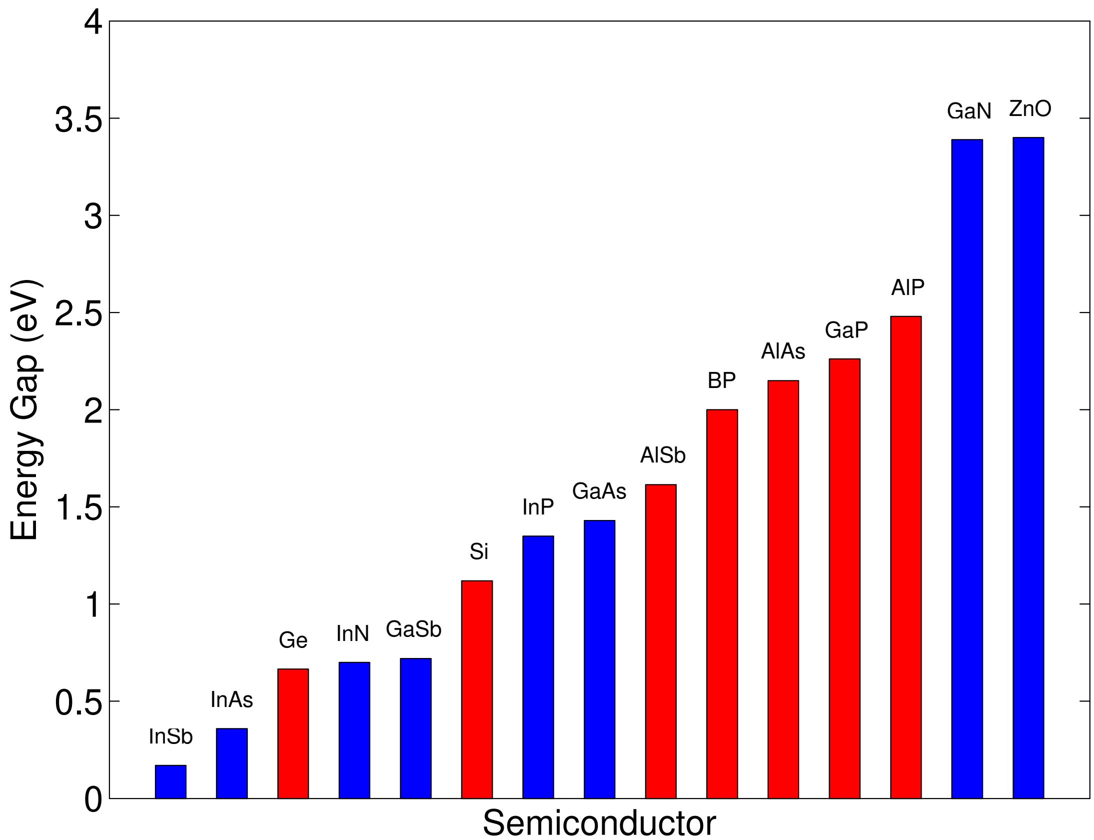

Figure 1.2: The energy gaps associated with a variety of elemental and compound semiconductors. The nature of the energy gaps are also indicated, the blue bars corresponding to direct energy gap semiconductors and the red bars corresponding to indirect energy gap semiconductors. The data in this figure from Adachi [12]. The online version is depicted in color.

Two wide energy gap compound semiconductors currently attracting attention are gallium nitride (GaN) and zinc oxide (ZnO) [13-18]. The wurtzite phase of GaN has a wide and direct energy gap; at room temperature, this energy gap is around 3.39 eV. Wurtzite GaN also exhibits a high breakdown field, elevated thermal conductivity, and superb electron transport characteristics [17-18]. These attributes make GaN ideally suited for both electronic and optoelectronic device applications. ZnO, while currently finding applications as a material for low-field thin-film transistor electron devices [19] and as a potential material for transparent conducting electrodes [20], also possesses a direct energy gap with a magnitude that is very similar to that exhibited by GaN. Thus, it might be expected that, with some further improvements in its material quality, ZnO may also be employed for some of the device roles currently implemented or envisaged for GaN.

It is widely recognized that improvements in the design of semiconductor based devices may be achieved through a greater understanding of the underlying electron transport mechanisms. The electrons within a semiconductor drift under the action of an applied electric field. The transport of electrons within such a semiconductor maybe quantified in terms of a distribution function, in which the distribution of electrons may be characterized in terms of their momentum and position at a particular instant in time. The evolution of this distribution function with respect to time is the fundamental issue at stake when one studies electron transport. For bulk semiconductors in thermal equilibrium, this evolution may be characterized through the solution of the Boltzmann transport equation [21]. Monte Carlo simulations of the electron transport are usually employed in order to solve for this equation [22, 23].

While the distribution function provides for a complete specification of the nature of the electron transport within a semiconductor, it is difficult to visualize and interpret. Moments of this distribution function are often used instead [23]. The electron drift velocity, i.e., the average electron velocity over the ensemble of electrons, provides an intuitive quantitative measure of the electron transport response within a semiconductor. It may be determined by averaging over the distribution function, i.e., it is a first-order moment of the distribution function. The average electron energy is another electron transport property that can be used in order to characterize the electron transport within a semiconductor. It may be determined through a second-order moment of the corresponding distribution function. These two measures of the electron transport, i.e., the electron drift velocity and the average electron energy, will be used throughout the analysis presented in this thesis.

There are two-types of electron transport that are considered in this analysis; (1) steady-state electron transport, and (2) transient electron transport. In steady-state electron transport, one considers what happens to the electron transport after all transients have expired. This form of electron transport is usually characterized in terms of the dependence of the electron drift velocity on the applied electric field strength, i.e., through the specification of the velocity-field characteristic. The velocity-field characteristic associated with GaAs, for the crystal temperature set to 300 K and the doping concentration set to 10^{17} cm^{-3}, is depicted in Figure 1.3. Transient electron transport, however, provides insight into how steady-state conditions are acquired. In Figure 1.4, the dependence of the electron drift velocity on the time elapsed since the application of a constant electric field is depicted for the case of GaAs, for the crystal

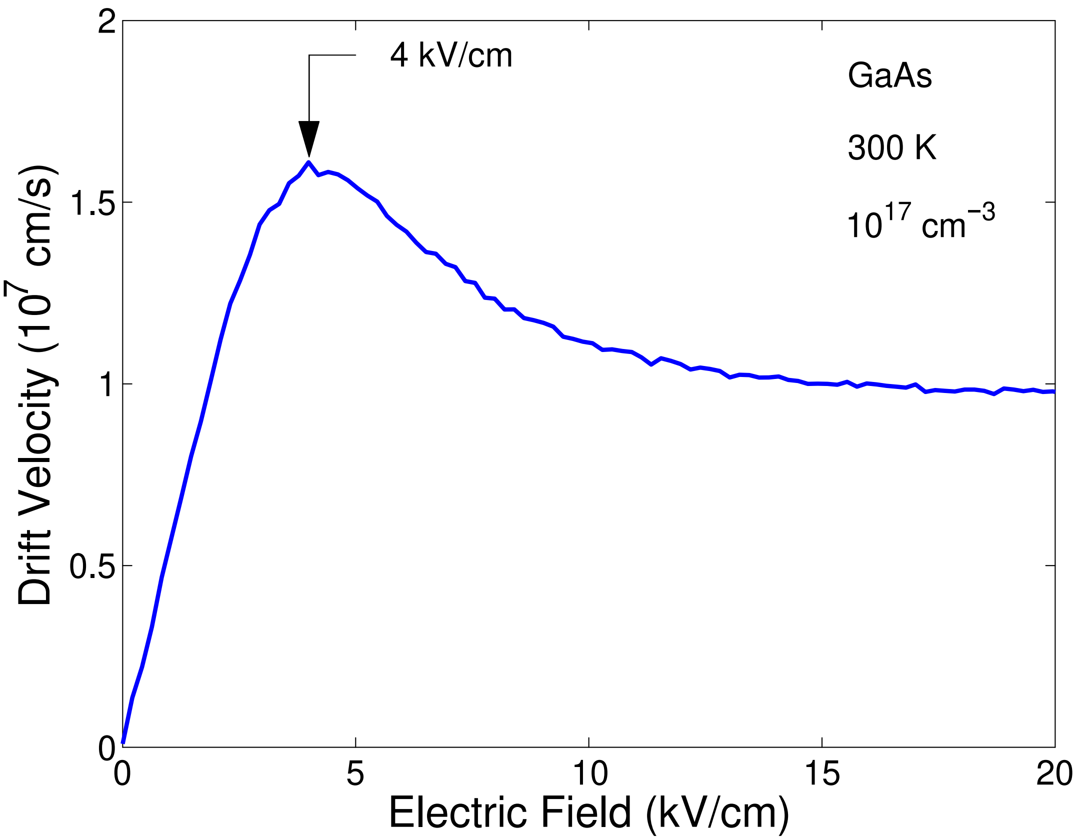

Figure 1.3: A plot of the steady-state velocity-field characteristic, i.e., the dependence of the steady-state electron drift velocity on the applied electric field strength, associated with GaAs, for the crystal temperature set to 300 K and the doping concentration set to 10^{17} cm^{-3}. These results are obtained from the simulations performed by O'Leary *et al.* [24]. The online version is depicted in color.

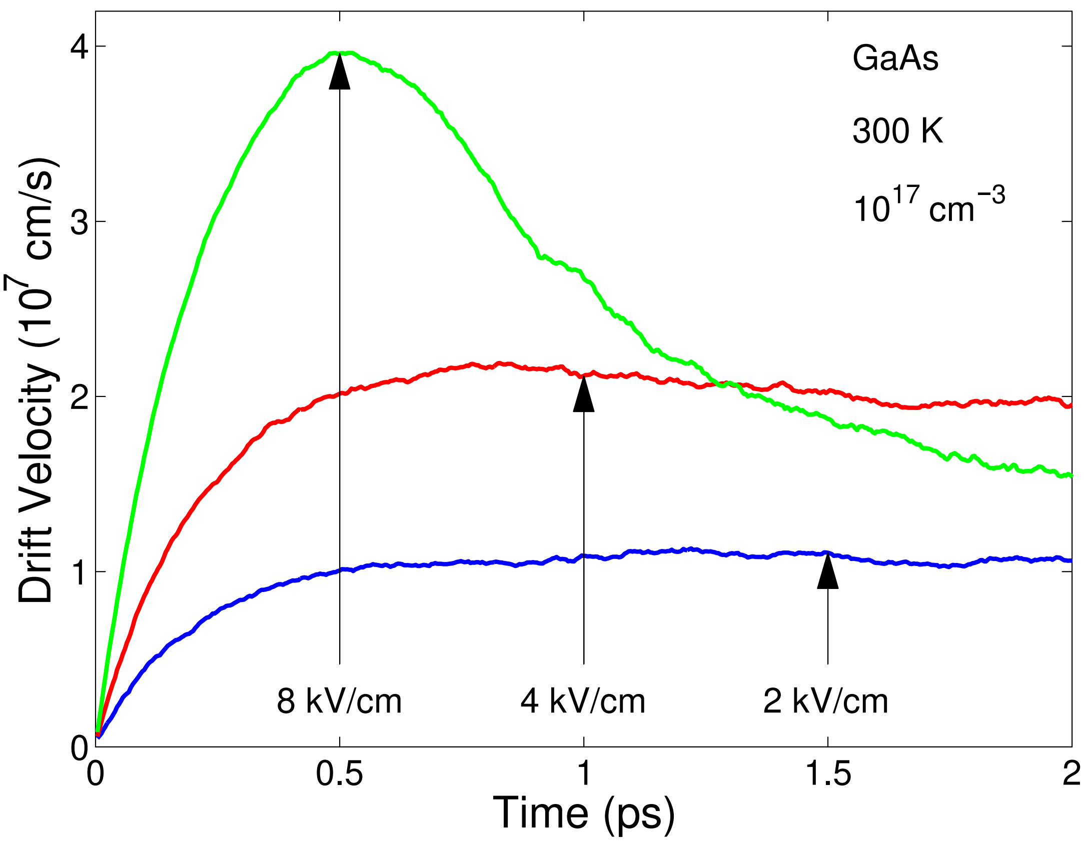

Figure 1.4: The dependence of the electron drift velocity on the time elapsed since the onset of the constant applied electric field. Three applied electric field strength selections are considered, i.e., 2, 4, and 8 kV/cm. For all cases, the crystal temperature is set to 300 K and the doping concentration is set to 10^{17} cm^{-3}. These results are from the simulations performed by O'Leary *et al.* [24]. The online version is depicted in color.

temperature set to 300 K and the doping concentration set to 10^{17} cm^{-3}. Three electric field strengths are considered for the case of this analysis, i.e., 2, 4, and 8 kV/cm. It is noted that as the time elapsed since the onset of the applied electric field becomes greater, the transients start to expire, and steady-state conditions are eventually achieved.

It is noted that the transient electron drift velocities may substantially exceed the corresponding steady-state electron drift velocities, i.e., velocity overshoots occur. These overshoots occur over brief periods of time immediately following the application of the electric field. For large device lengths, most of the transport will be steady-state in nature, i.e., the transients will quickly expire and the electrons will transit primarily with steady-state velocities. For shorter device lengths, however, transient electron transport effects may play a decisive role in determining the nature of the transport. Device feature scales are reducing as time progresses, and thus, while transient electron transport effects may not have been important in the past, they are starting to play a fundamental role in shaping the resultant device performance: the progress in device feature lengths, for Si-based electron devices, as a function of the year, is depicted in Figure 1.5, the feature scale of GaAs based devices exhibiting a similar contraction as the years have progressed. As device features become ever smaller, it is clear that transient electron transport effects will become an increasingly important consideration to take into account when evaluating device performance. Transient electron transport within compound semiconductors is the primary focus of the analysis presented in this thesis.

In this thesis, the electron transport that occurs within two particular wide energy gap semiconductors of current interest, GaN and ZnO, is considered. Electron transport within GaAs is also examined, albeit primarily for benchmarking purposes. The over-

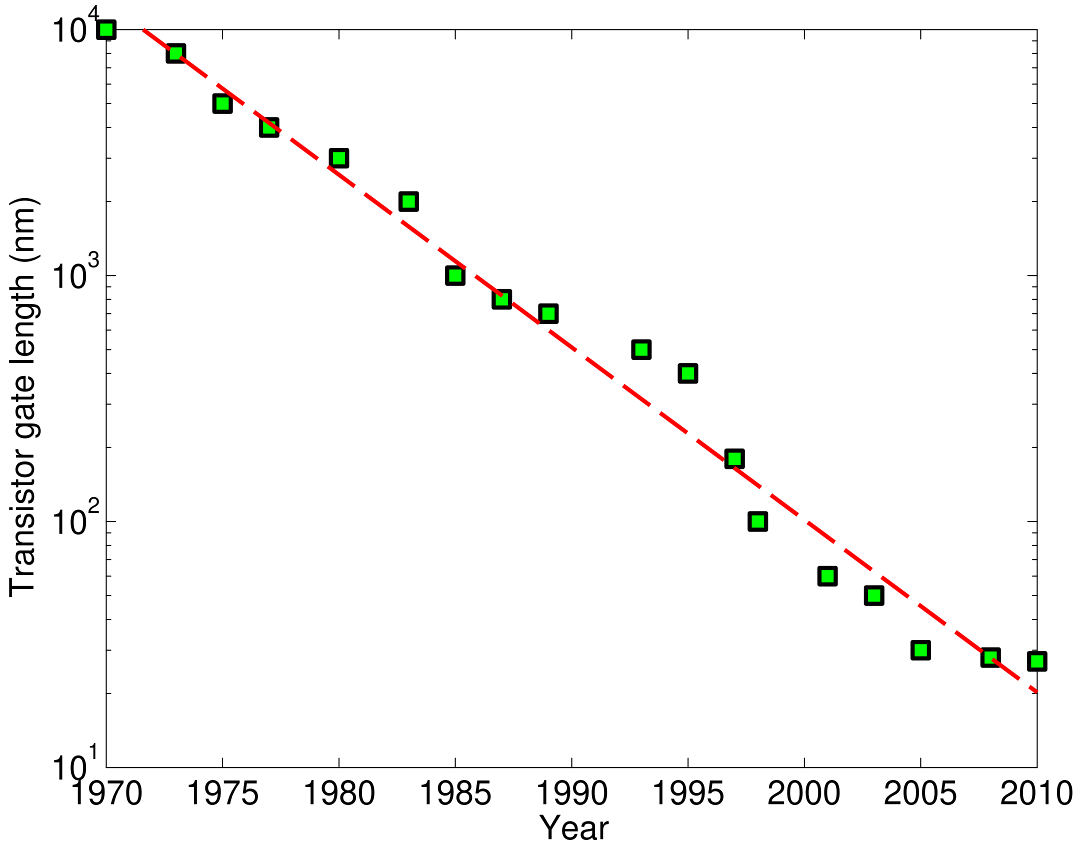

Figure 1.5: The gate length of Si-based electron devices as a function of year, from 1970 to 2010. A least-squares linear fit to this data is depicted with the dashed line. The data in this figure is from Schwierz [4]. The online version is depicted in color.

arching goal of this thesis is to provide the materials community with tools for analysis and optimization to be used when evaluating the consequences of transient electron transport within these compound semiconductors. Providing fresh insights into the character of the electron transport within ZnO, with particular focus on the device implications, is another central aim of this analysis. Device performance is assessed through the evaluation of the electron time-to-transit, τ, the cut-off frequency of a device being inversely proportional to this time, i.e.,

$$f_T = \frac{1}{2\pi\tau}. \tag{1.1}$$

In the initial phase of this analysis, a comparative critical analysis of the nature of the transient electron transport that occurs within bulk zinc-blende GaAs and bulk wurtzite GaN is performed. Monte Carlo electron transport simulation results are employed for the purposes of this analysis. The dependence of the electron drift velocity and the average electron energy on the time elapsed since the onset of a constant applied electric field is the primary means through which this analysis is performed. The relationship between the electron drift velocity and the average electron energy "settling-times" is a critical aim of this analysis. Developing a novel means of visualizing the advantages offered by transient electron transport, as compared with steady-state electron transport, and the potential of using this visualization technique for the purposes of optimizing the performance of short-channel devices, will arise as a consequence of this phase of the analysis. GaN is selected as a material as it is a wide energy gap semiconductor whose material properties are now relatively well understood. GaAs is used as a benchmark. The primary intellectual contribution from this study is the development of novel means of visualizing the impact of transient electron transport and in exploring its implications for short-channel device optimization.

In the next phase of the analysis, a critical examination of the utility of the semi-analytical approach of Shur [25] in evaluating the transient electron transport response within zinc-blende GaAs, wurtzite GaN, and wurtzite ZnO is provided. In particular, results obtained from the semi-analytical approach of Shur [25] are contrasted with those obtained using Monte Carlo simulations of the electron transport. Three aspects of the transient electron transport are considered: (1) the dependence of the electron drift velocity on the time elapsed since the onset of the applied electric field, (2) the dependence of the average electron energy on the time elapsed since the onset of the applied electric field, and (3) the dependence of the average electron displacement on the time elapsed since the onset of the applied electric field. The semi-analytical approach of Shur [25] offers a computational efficient means of resolving the transient electron transport response, and thus, if its results faithfully reproduce those of the corresponding Monte Carlo electron transport simulation, a substantial benefit may be accrued in terms of the scale of the computations required, especially in cases for which potentially thousands of simulation runs may be required. In addition, the semi-analytical approach may be employed for cases of non-uniform and time-varying fields, these situations being beyond the capability of the bulk Monte Carlo simulation approach that has been employed for the purposes of this analysis. In addition to GaAs and GaN, ZnO is considered in this analysis, as it is a material for which the understanding of its material properties is still relatively rudimentary. The primary intellectual contribution of this component of the analysis is the critical evaluation of the suitability of this semi-analytical approach in the characterization of the transient electron transport response.

In the next phase of this analysis, the electron transport that occurs within bulk wurtzite ZnO is critically examined. In particular, how electrons, initially in thermal equilibrium, drift under the action of an applied electric field, is considered. From Monte Carlo simulations of the electron transport within this material, for a variety of applied electric field strength selections, the dependence of the time-to-transit on the applied electric field strength is evaluated. For a given fixed electron displacement, the applied electric field strength that ensures the minimum time-to-transit, is determined. This analysis is performed over a wide range of fixed electron displacements. The results are then used in order to form an upper bound on the device performance of a ZnO-based device. The primary intellectual contribution of this component of the analysis is the application of a device optimization procedure to the specific case of wurtzite ZnO and the acquisition of an upper bound on the performance of ZnO based devices, that can be used by subsequent generations of device designers.

In the final phase of this analysis, the utility of the semi-analytical approach of Shur [25], for the purposes of device design optimization, is considered for the specific case of bulk wurtzite ZnO. In particular, the device optimization performed in the previous phase of this thesis is now performed within the framework of the semi-analytical approach of Shur [25]. How the results obtained through the Monte Carlo simulations compare with those produced through the semi-analytical approach is then critically examined, for each step of the analysis. The primary intellectual contribution of this component of the analysis is the assessment as to whether or not the semi-analytical approach of Shur [25] may be employed for device optimization purposes for the case of bulk wurtzite ZnO.

While results from Monte Carlo simulations of the electron transport are employed throughout this thesis, the author did not perform these simulations. The Monte Carlo simulation approach for characterizing the electron transport within semiconductors has been in use since 1966 when it was employed by Kurosawa [26] in the study of hot electron transport. It is a well-known approach and its results, particularly for the more common elemental and compound semiconductors, are well established. In this thesis, the objective is to add value to these Monte Carlo simulation results. In particular, novel means of visualization, optimization, and characterization are proposed, which can be applied to a much broader range of materials than those considered within this thesis, i.e., Monte Carlo results provide the input data for this analysis. In addition, Monte Carlo results corresponding to bulk wurtzite ZnO, a material whose electron transport characteristics were poorly understood prior to this investigation, are processed and interpreted. These contributions will aid in the development of this rapidly emerging field. Details, as to how these Monte Carlo simulations of electron transport were performed, are provided in Appendix A.

The results presented in this thesis are merely a sampling of the collection of results that were obtained throughout the investigations performed by the author and his collaborators [27-37]. The results presented touch on all aspects of the analysis, ranging from visualization to optimization. Further details, regarding the breadth of the analysis that was performed during this study, may be obtained through a reading of the relevant scientific literature.

This thesis is organized in the following manner. In Chapter 2, a new means of rendering transparent the benefits offered through transient electron transport is presented and applied to the specific case of GaAs and GaN. Then, in Chapter 3, the applicability of the semi-analytical approach of Shur [25] is examined for the cases of GaAs, GaN, and ZnO. Means of minimizing the time-to-transit across ZnO-based devices, for various electron device lengths, are then provided in Chapter 4, Monte Carlo results being employed. The applicability of the semi-analytical approach to the optimization analysis performed in Chapter 4 is then considered in Chapter 5. Finally, the conclusions of this thesis are drawn in Chapter 6, recommendations for further study also being provided in this chapter.

References

[1] J. Bardeen and W. H. Brattain, "The transistor, a semi-conductor triode," *Physics Review*, vol. 74, no. 2, pp. 2301-231, 1948.

[2] I. M. Ross, "The foundation of the silicon age," *Physics Today*, vol. 12, no. 12, pp. 34-41, 1997.

[3] G. E. Moore, "Cramming more components onto integrated circuits," *Proceedings of the IEEE*, vol. 86, no. 1, pp. 82-85, 1998.

[4] F. Schwierz, "Graphene transistors," *Nature Nanotechnology*, vol. 5, pp. 487-496, 2010.

[5] P. Y. Yu and M. Cardona. *Fundamentals of Semiconductors: Physics and Materials Properties*. Berlin, Germany: Springer, 1999.

[6] P. K. Bondyopadhyay, "In the beginning [junction transistor]," *Proceedings of the IEEE* , vol. 86, no.1, pp. 63-77, 1998.

[7] S. Sze, K. K. Ng, *Physics of Semiconductor Devices*. Hoboken, New Jersey : John Wiley and Sons, 2006.

[8] K. Takahashi, A. Yoshikawa, and A. Sandhu, *Wide Bandgap Semiconductors: Fundamental Properties and Modern Photonic and Electronic Devices*, New York, New York: Springer, 2007.

[9] D. K. Ferry, "High-field transport in wide-band-gap semiconductors," *Physical Review B*, vol. 12, no. 6, pp. 2361-2369, 1975.

[10] K. Shenai, M. Dudley, and R. F. Davis, "Current status and emerging trends in wide bandgap (WBG) semiconductor power switching devices," *Electro Chemical Society Journal of Solid State Science and Technology*, vol. 2, no. 8, pp. 3055-3063, 2013.

[11] J. L. Hudgins, G. S. Simin, E. Santi, and M. Asif Khan, "An Assessment of Wide Bandgap Semiconductors for Power Devices," *IEEE Transactions on Power Electronics,* vol. 18, no. 3, pp. 907-914, 2003.

[12] S. Adachi, *Properties of Group-IV, III-V and II-VI Semiconductors*. Chichester, England: John Wiley and Sons, 2005.

[13] Ü. Özgür, Ya. I. Alivov, C. Liu, A. Teke, M. A. Reshchikov, S. Doğan, V. Avrutin, S.-J. Cho, and H. Morkoç, "A comprehensive review of ZnO materials and devices," *Journal of Applied Physics*, vol. 98, no. 4, pp. 041301-1-103, 2005.

[14] A. Ashrafi and C. Jagadish, "Review of zincblende ZnO: stability of metastable ZnO phases," *Journal of Applied Physics*, vol. 102, no. 7, pp. 071101-1-12, 2007.

[15] R. P. Davies, C. R. Abernathy, S. J. Pearton, D. P. Norton, M. P. Ivill, and F. Ren, "Review of recent advances in transition and lanthanide metal-doped GaN and ZnO," *Chemical Engineering Communications*, vol. 196, no. 9, pp. 1030-1053, 2009.

[16] Ü. Özgür, D. Hofstetter, and H. Morkoç, "ZnO devices and applications: a review of current status and future prospects," *Proceedings of the IEEE*, vol. 98, no. 7, pp. 1255-1268, 2010.

[17] F. Scholz, "Semipolar GaN grown on foreign substrates: a review," *Semiconductor Science and Technology*, vol. 27, no. 2, pp. 024002-1-15, 2012.

[18] R. S. Pengelly, S. M. Wood, J. W. Milligan, S. T. Sheppard, and W. L. Pribble, "A Review of GaN on SiC High Electron-Mobility Power Transistors and MMICs," *IEEE Transactions on Microwave Theory and Techniques*, vol. 60, no. 6, pp. 1764-1783, 2012.

[19] P. F. Carcia, R. S. McLean, M. H. Reilly, and G. Nunes**,** "Transparent ZnO thin film transistor fabricated by rf magnetron sputtering," *Applied Physics Letters*, vol. 82, no. 7, pp. 1117-1119, 2003.

[20] J. H. Lee, K. H. Ko, and B. O. Park, "Electrical and optical properties of ZnO transparent conducting films by the sol–gel method," *Journal of Crystal Growth*, vol. 247, no. 1, pp. 119-125, 2003.

[21] P. A. Markowich, C. A. Ringhofer, and C. Schmeiser, *Semiconductor Equations.* New York, New York: Springer-Verlag, 1990.

[22] C. Jacoboni and L. Reggiani, "The Monte Carlo method for solution of charge transport in semiconductor with application to covalent materials," *Reviews of Modern Physics*, vol. 55, no. 3, pp. 645-705, 1983.

[23] B. Nag, *Electron Transport in Compound Semiconductors*. Berlin, Germany: Springer-Verlag, 1980.

[24] S. K. O'Leary, B. E. Foutz, M. S. Shur, and L. F. Eastman, "Steady-state and transient electron transport within the III–V Nitride semiconductors, GaN, AlN, and InN: A review," *Journal of Electronic Materials*, vol. 17, no. 2, pp. 87-126, 2006.

[25] M. S. Shur, "Influence of non-uniform field distribution on frequency limits of GaAs field-effect transistors," *Electronics Letters*, vol. 12, no. 23, pp. 615-616, 1976.

[26] T. Kurosawa, “Monte-Carlo simulation of hot electron problems,” *Journal of the Physical Society of Japan,* vol. 21, pp. 527-529, 1966.

[27] W. A. Hadi, E. Baghani, M. S. Shur, and S. K. O'Leary, “Electron transport within the two-dimensional electron gas formed at a ZnO/ZnMgO heterojunction: Recent progress,” in *Materials Research Society Symposium Proceedings*, 2013, vol. 1577.

[28] W. A. Hadi, M. S. Shur, and S. K. O'Leary, “Steady state and transient electron transport within bulk wurtzite zinc oxide and the resultant electron device performance,” in *Materials Research Society Symposium Proceedings*, 2013, vol. 1577.

[29] W. A. Hadi, M. S. Shur, and S. K. O'Leary, “The electron transport within bulk wurtzite zinc oxide in response to strong applied electric field pulses,” in *Materials Research Society Symposium Proceedings*, 2013, vol. 1577.

[30] W. A. Hadi, M. S. Shur, and S. K. O’Leary, “Steady-state and transient electron transport within wurtzite and zinc-blende indium nitride,” *Journal of Applied Physics*, vol. 113, no. 11, pp. 113709-1-6, 2013.

[31] W. A. Hadi, M. S. Shur, and S. K. O'Leary, “The sensitivity of the steady-state and transient electron transport within bulk wurtzite zinc oxide to variations in the crystal temperature, the doping concentration, and the non-parabolicity coefficient,” *Journal of Materials Science: Materials in Electronics*, vol. 24, no. 1, pp. 2-12, 2013.

[32] W. A. Hadi, R. Cheekoori, M. S. Shur, and S. K. O'Leary, “Transient electron transport in the III-V compound semiconductors gallium arsenide and gallium nitride,” *Journal of Materials Science: Materials in Electronics*, vol. 24, no. 2, pp. 807-813, 2013.

[33] W. A. Hadi, M. S. Shur, and S. K. O’Leary, “On the applicability of a semi-analytical approach to determining the transient electron response of gallium arsenide, gallium nitride and zinc oxide,” *Journal of Materials Science: Materials in Electronics*, vol. 24, no. 5, pp. 1624-1634, 2013.

[34] W. A. Hadi, M. S. Shur, and S. K. O’Leary, “A transient electron transport analysis of bulk wurtzite zinc oxide,” *Journal of Applied Physics*, vol. 112, no. 3, pp. 033720-1-5, 2012.

[35] W. A. Hadi, S. Chowdhury, M. S. Shur, and S. K. O'Leary, “A detailed characterization of the transient electron transport within zinc oxide, gallium nitride, and gallium arsenide,” *Journal of Applied Physics*, vol. 112, no. 12, pp. 123722-1-6, 2012.

[36] W. A. Hadi, S. K. O'Leary, M. S. Shur, and L.F. Eastman, "The sensitivity of the steady-state electron transport within bulk wurtzite zinc oxide to variations in the non-parabolicity coefficient," *Solid State Communications*, vol. 151, no. 12, pp. 874-878, 2011.

[37] W. A. Hadi, S. K. O'Leary, M. S. Shur, and L. F. Eastman, "Steady state and transient electron transport in Zinc Oxide: recent progress," in *Materials Research Society Spring Meeting*, San Francisco, CA, 2011, vol. 1327.

CHAPTER 2

Transient electron transport in the III-V compound semiconductors gallium arsenide and gallium nitride

A version of this manuscript was published in the Journal of Materials Science: Materials in Electronics.

"Reprinted with permission from Cheekoori, R., Shur, M. S., and O'Leary, S. K., Transient electron transport in III-V compound semiconductors gallium arsenide and gallium nitride, vol. 24, no. 2, pp. 807-813, Copyright [2013]"

Reprinted with permission from Springer-Verlag publishing.

2.1 Introduction

GaN is a useful material for a number of important electronic and optoelectronic device applications. In terms of electronics, its wide energy gap [1, 2], large breakdown field [3-5], high thermal conductivity [6], and favorable electron transport characteristics [7, 8], make GaN ideally suited for high-power and high-frequency electron device applications [9-12]. On the optoelectronics front, the direct nature of the energy gap associated with GaN, and the location of this energy gap, make it possible to use this material, and alloys of this material with other III–V nitride semiconductors, for a variety of novel optoelectronic device applications in the near-ultraviolet to visible frequency range [13-16]. While initial efforts to study this material were hindered by growth difficulties [17-20], improvements in the material quality have made possible the realization of a number of GaN-based electronic and optoelectronic devices.

In order to understand and improve the design of GaN based devices, an understanding of the nature of the electron transport that occurs within this material is useful. Accordingly, the electron transport that occurs within GaN has been extensively examined over the years [7, 8, 21-34]. While most such studies have focused upon the steady-state electron transport that occurs within this material, primarily the dependence of the electron drift velocity on the applied electric field strength, transient electron transport is also important, particularly for shorter-channel devices. While the steady-state electron drift velocity saturates for higher electric fields, as a consequence of the emission of polar optical phonons and intervalley transitions, the transient electron drift velocity that occurs may be much larger than the corresponding steady-state electron drift velocity. This occurs as there is a finite time required to emit polar optical phonons or engage in intervalley transitions. If the transit-time across a device is less than that required for either of these processes to occur, then dramatic enhancements in the exhibited electron drift velocity, beyond that expected for the case of steady-state, may occur. As was demonstrated by Foutz *et al.* [29, 31], transient electron transport can dramatically enhance the performance of GaN based devices.

In this paper, we will perform a detailed examination of the transient electron transport response of GaN. While most analyzes of the transient electron response within GaN, such as that of Foutz *et al.* [29, 31], have focused solely on the dependence of the electron drift velocity on the distance displaced since the onset of the applied electric field, in this paper we examine the dependence of the electron drift velocity on the time elapsed since the onset of the applied electric field. This will allow us to explicitly examine the electron drift velocity "settling time", i.e., how long it takes in order to achieve the corresponding steady-state electron drift velocity [35, 36]. Another unique feature of this analysis is that we will probe the dependence of the average electron energy on the time elapsed since the onset of the applied electric field, i.e., how long it takes in order to achieve the corresponding steady-state average electron energy [35, 36]. Exploring the relationship between the "settling time" associated with the electron drift velocity and that corresponding to the average electron energy, a heretofore unexplored aspect of the transient electron transport response of GaN, will also be a focus of our examination. Finally, by examining the dependence of the transient electron drift velocity on the applied electric field strength selection for a fixed selection of the time elapsed since the onset of the applied electric field, a new quantitative means of rendering transparent the electron drift velocity enhancement provided through transient electron transport is devised. In the interests of providing a comparison with another popular III-V compound semiconductor, a parallel analysis is provided for the case of GaAs. The device implications of these results are then commented upon.

This paper is organized in the following manner. In Section 2.2, we discuss the Monte Carlo simulations of the electron transport that we use for the purposes of this analysis. Then, in Section 2.3, we present a detailed analysis of the steady-state and transient electron transport that occurs within GaAs and GaN, with a focus on the determination of the velocity-field characteristics. How the electron drift velocity and the average electron energy respond to the sudden application of a constant applied electric field, and the development of a new quantitative means of rendering transparent the electron drift velocity enhancement provided through transient electron transport, is the focus of this analysis. The device implications of these results are then discussed in Section 2.4. Finally, the conclusions of our analysis are presented in Section 2.5.

2.2 Analysis

For the purposes of this analysis of the transient electron transport within GaAs and GaN, we assume the zinc blende phase of GaAs and the wurtzite phase of GaN. We employ an ensemble semi-classical three-valley Monte Carlo simulation approach. The scattering mechanisms considered are: (1) ionized impurity, (2) polar optical phonon, (3) piezoelectric, and (4) acoustic deformation potential. Intervalley scattering is also considered. The non-parabolicity of each valley is treated through the application of the Kane model [37][1]. We assume that all donors are ionized and that the free electron concentration is equal to the dopant concentration. For our steady-state electron transport simulations, the motion of 3,000 electrons is examined, while for our transient electron transport simulations, the motion of 10,000 electrons is considered. For our simulations, the crystal temperature is set to 300 K and the doping concentration is set to 10^{17} cm^{-3} for all cases. Electron degeneracy effects are accounted for by means of the rejection technique of Lugli and Ferry [38]. Electron screening is also accounted for following the Brooks-Herring method [39]. Further details of our Monte Carlo simulation approach are presented in the literature [7, 8, 31, 40-46].

---

[1] In the Kane model, the energy band of the lowest energy Γ valley is assumed to be non-parabolic, spherical, and of the form

$$E(1+\alpha E) = \frac{\hbar^2 k^2}{2m^*},$$

where $\hbar k$ denotes the crystal momentum, E represents the energy, m^* is the effective mass of the electrons within this valley, and the non-parabolicity coefficient, α, is given by

$$\alpha = \frac{1}{E_g}\left(1-\frac{m^*}{m_e}\right)^2,$$

where m_e and E_g denote the free electron mass and the energy gap, respectively [37].

2.3 Results

We start our analysis with a review of some steady-state electron transport results. In Figure 2.1, the dependence of the electron drift velocity on the applied electric field strength corresponding to the case of bulk zinc blende GaAs is depicted. For low applied electric field strengths, the electron drift velocity monotonically increases with the applied electric field strength, ultimately achieving a peak of about 1.6×10^7 cm/s at an applied electric field strength of around 4 kV/cm; we henceforth will refer to the applied electric field strength at which the peak in the velocity-field characteristic occurs as the peak field. After this peak, the electron drift velocity monotonically decreases in response to further increases in the applied electric field strength, saturating at a value of about 1.0×10^7 cm/s. In Figure 2.2, the corresponding velocity-field characteristic associated with bulk wurtzite GaN is depicted. For this case, the peak electron drift velocity is found to be about 2.9×10^7 cm/s, the corresponding peak field being around 140 kV/cm. Following this peak, the electron drift velocity monotonically decreases in response to further increases in the applied electric field strength, as with the case of GaAs, saturating at a value of about 1.4×10^7 cm/s for high applied electric fields.

Alongside these velocity-field characteristics, we also plot the corresponding average electron energy as a function of the applied electric field strength, these results being obtained from the same Monte Carlo simulations as those used to obtain the corresponding velocity-field characteristics. Starting from the thermal equilibrium result of $(3/2)\, k_b T$, corresponding to the specific case of the applied electric field being set to nil, it is seen that this average electron energy monotonically increases as the applied electric field strength is increased, achieving a value of around 0.35 eV when the applied

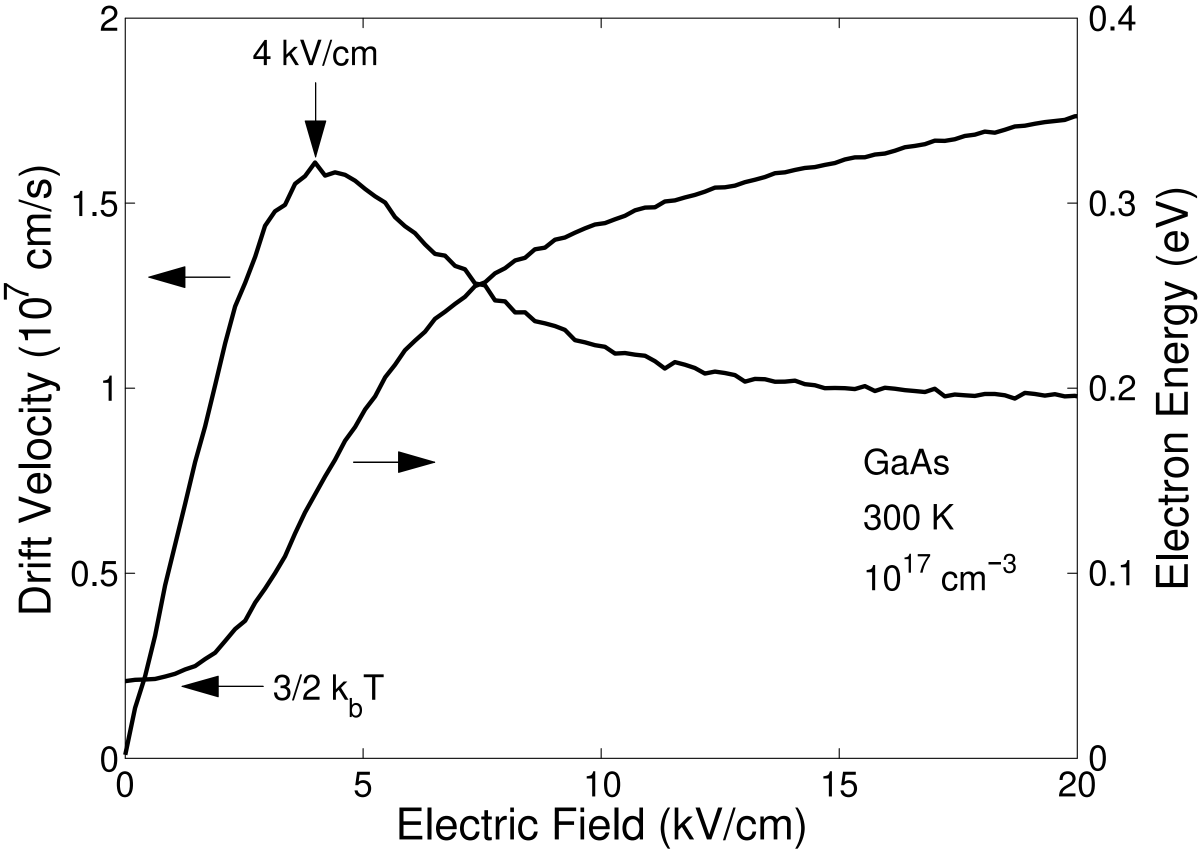

Figure 2.1: The dependence of the electron drift velocity on the applied electric field strength for the case of bulk zinc blende GaAs. The dependence of the average electron energy on the applied electric field strength is also depicted. These results were determined from a Monte Carlo simulation of the electron transport within this material. For the purposes of this particular simulation, the crystal temperature is set to 300 K and the doping concentration is set to 10^{17} cm^{-3}. The peak field is indicated with the arrow.

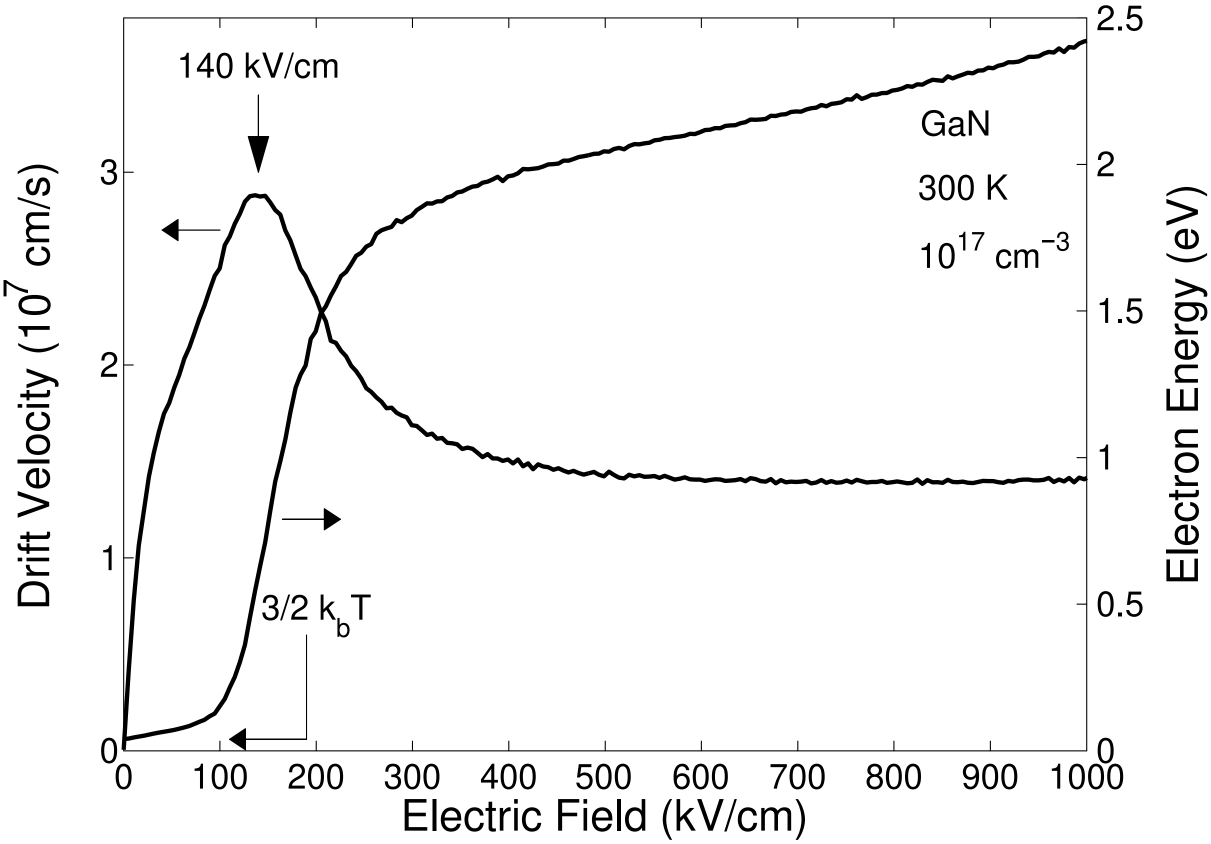

Figure 2.2: The dependence of the electron drift velocity on the applied electric field strength for the case of bulk wurtzite GaN. The dependence of the average electron energy on the applied electric field strength is also depicted. These results were determined from a Monte Carlo simulation of the electron transport within this material. For the purposes of this particular simulation, the crystal temperature is set to 300 K and the doping concentration is set to 10^{17} cm^{-3}. The peak field is indicated with the arrow.

electric field strength is set to 20 kV/cm for the case of bulk zinc blende GaAs and a value of about 2.4 eV when the applied electric field strength is set to 1,000 kV/cm for the case of bulk wurtzite GaN; these values do not represent saturated values, however, as these average electron energies appear to be continuing to increase in response to further increases in the applied electric field strength. It is noted that for both materials that the onset of the increases in the average electron energy roughly corresponds with that at which the peak in the velocity-field characteristic is achieved. Intervalley transitions, from the lower energy conduction band valley, where the electrons have a lighter effective mass, to higher energy conduction band valleys, where the electrons have heavier effective masses, are responsible for both the peak in the velocity-field characteristics and partially responsible for the increases in the average electron energy corresponding to these materials.

We now examine the transient electron transport that occurs within bulk zinc blende GaAs and bulk wurtzite GaN. In particular, following the approach of Foutz *et al.* [29, 31], we study how electrons, initially in thermal equilibrium, respond to the sudden application of a constant applied electric field. In Figure 2.3, we plot the electron drift velocity for bulk zinc blende GaAs as a function of the time elapsed since the electric field was initially applied, for a number of applied electric field strength selections. We note that for the applied electric field strength selections 2 and 4 kV/cm that the electron drift velocity reaches steady-state very quickly, with little or no velocity overshoot. In contrast, for applied electric field strength selections in excess of 4 kV/cm, significant velocity overshoot occurs. This result suggests that for bulk zinc blende GaAs that around 4 kV/cm is a critical applied electric field strength for the onset of velocity

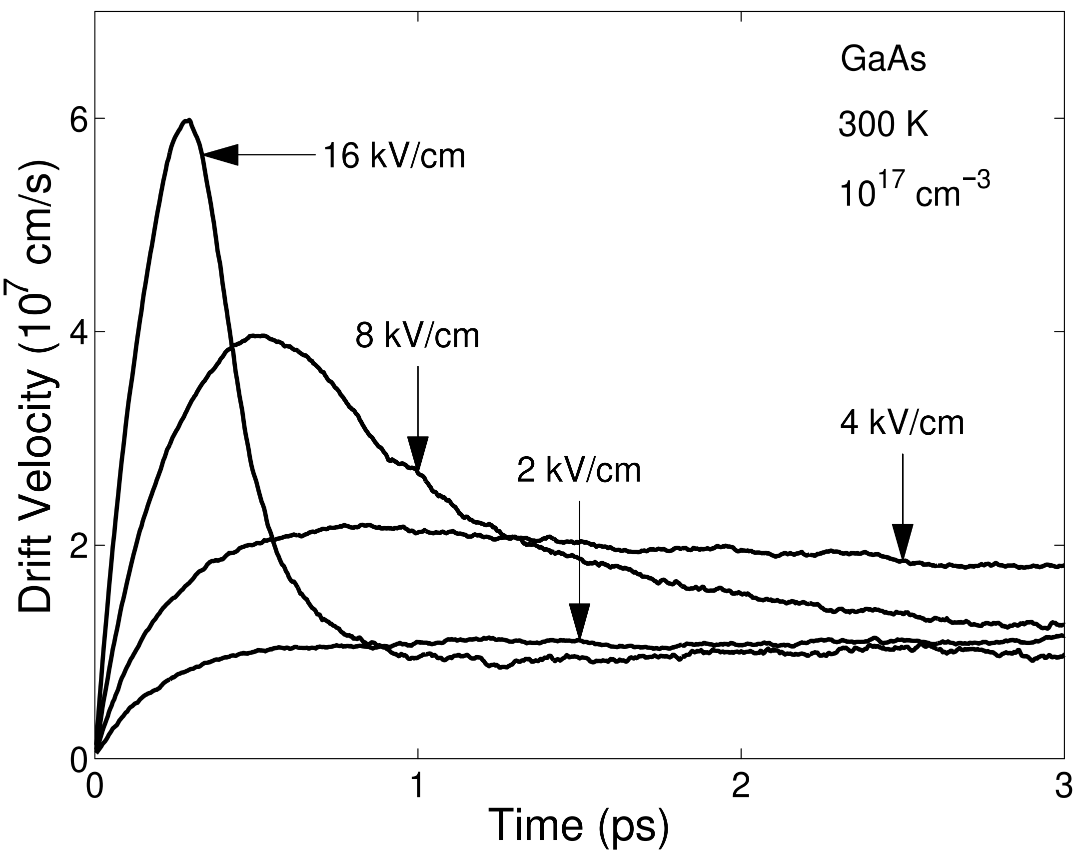

Figure 2.3: The dependence of the electron drift velocity on the time elapsed since the onset of the applied electric field for the case of bulk zinc blende GaAs. The various selections of the applied electric field strength are indicated. These results were determined from Monte Carlo simulations of the electron transport within this material. For the purposes of these simulations, the crystal temperature is set to 300 K and the doping concentration is set to 10^{17} cm^{-3}.

overshoot effects. As was mentioned earlier, around 4 kV/cm also corresponds to the peak field in the velocity-field characteristic associated with bulk zinc blende GaAs; recall Figure 2.1.

Similar results are found for the case of bulk wurtzite GaN. In Figure 2.4, we plot the electron drift velocity as a function of the time elapsed since the electric field was initially applied, for a number of applied electric field strength selections. We note that for the applied electric field strength selections 70 kV/cm and 140 kV/cm that the electron drift velocity reaches steady-state very quickly, with little or no velocity overshoot. In contrast, for applied electric field strength selections in excess of 140 kV/cm, significant velocity overshoot occurs. This result suggests that for bulk wurtzite GaN that around 140 kV/cm is a critical applied electric field strength for the onset of velocity overshoot effects. As with the case of GaAs, it is noted that around 140 kV/cm also corresponds to the peak field in the velocity-field characteristic associated with bulk wurtzite GaN; recall Figure 2.2. Similar results were found for the other III–V semiconductors considered by Foutz *et al.* [29, 31].

We now examine how the average electron energy evolves with time following the application of a constant applied electric field. In Figure 2.5, we plot the average electron energy within GaAs as a function of the time elapsed since the electric field was initially applied, for the same applied electric field strength selections made in Figure 2.3; the same Monte Carlo simulations of the electron transport within GaAs are employed for the purposes of this analysis. It is noted that in all cases the average electron energy monotonically increases with the time elapsed since the application of the constant electric field; for zero-time, all the results coincide at the thermal equilibrium result, i.e.,

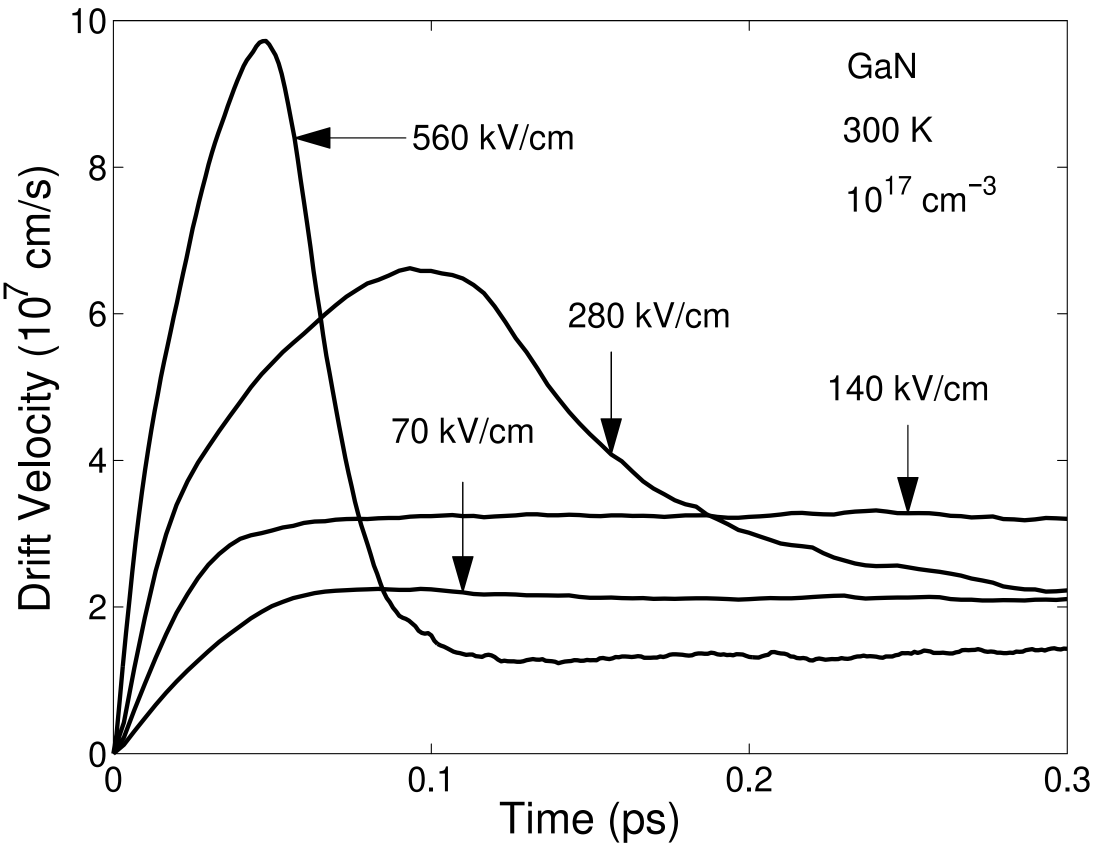

Figure 2.4: The dependence of the electron drift velocity on the time elapsed since the onset of the applied electric field for the case of bulk wurtzite GaN. The various selections of the applied electric field strength are indicated. These results were determined from Monte Carlo simulations of the electron transport within this material. For the purposes of these simulations, the crystal temperature is set to 300 K and the doping concentration is set to 10^{17} cm^{-3}.

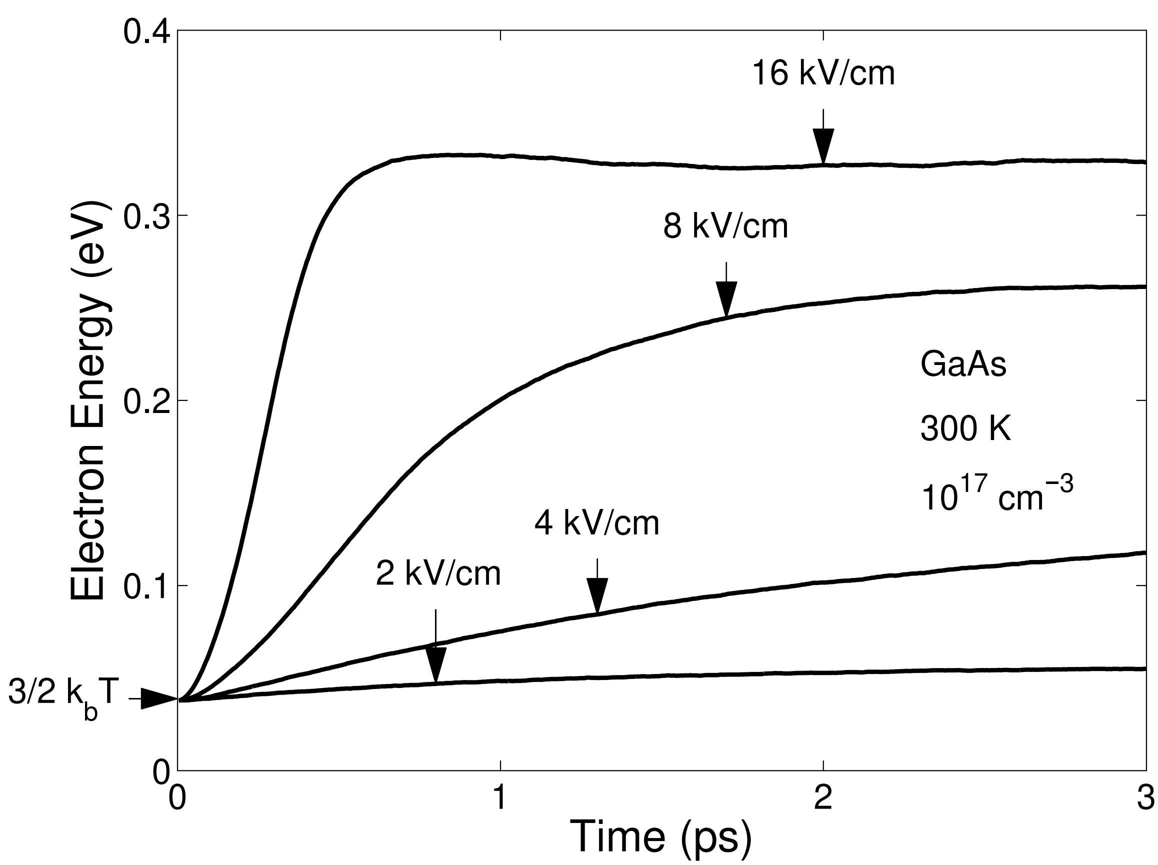

Figure 2.5: The dependence of the average electron energy on the time elapsed since the onset of the applied electric field for the case of bulk zinc blende GaAs. The various selections of the applied electric field strength are indicated. These results were determined from Monte Carlo simulations of the electron transport within this material; the same simulations as those employed to determine Figure 2.3. For the purposes of these simulations, the crystal temperature is set to 300 K and the doping concentration is set to 10^{17} cm^{-3}.

(3/2) $k_b T$. It is also noted that for applied electric field strength selections in excess of the peak field, the time required in order for the steady-state value to be achieved seems to decrease as the magnitude of the applied electric field strength is increased. It is interesting to note that the average electron energy ‘‘settling time’’ seems to be strongly correlated with the ‘‘settling time’’ required for the transient electron drift velocity to approach steady-state. It is noted that the ‘‘settling times’’ associated with bulk zinc blende GaAs, observed in Figures 2.3 and 2.5, range between 0.5 and 3 ps.

In Figure 2.6, we plot the average electron energy within GaN as a function of the the time elapsed since the electric field was initially applied, for the same applied electric field strength selections made in Figure 2.4; the same Monte Carlo simulations of the electron transport within GaN are employed for the purposes of this analysis. As with the case of GaAs, for zero-time, all the results coincide at the thermal equilibrium result, i.e., (3/2) $k_b T$. Unlike the case of GaAs, however, a peak average electron energy is found for the particular case of the applied electric field strength being set to 560 kV/cm; all the other average electron energy dependencies appear to exhibit a monotonic dependence on the applied electric field strength, as was the case for bulk zinc blende GaAs. It is seen that the same apparent strong correlation in ‘‘settling times’’ found for the case of GaAs is also found for the case of GaN. All of the ‘‘settling times’’ associated with bulk wurtzite GaN, observed in Figures. 2.4 and 2.6, range between 0.1 and 0.3 ps.

Finally, we plot the dependence of the transient electron drift velocity on the applied electric field strength for a fixed selection of the time elapsed since the onset of the applied electric field. In Figure 2.7, we plot this dependence for the case of bulk zinc blende GaAs. The time elapsed since the onset of the applied electric field is set to 1 ps

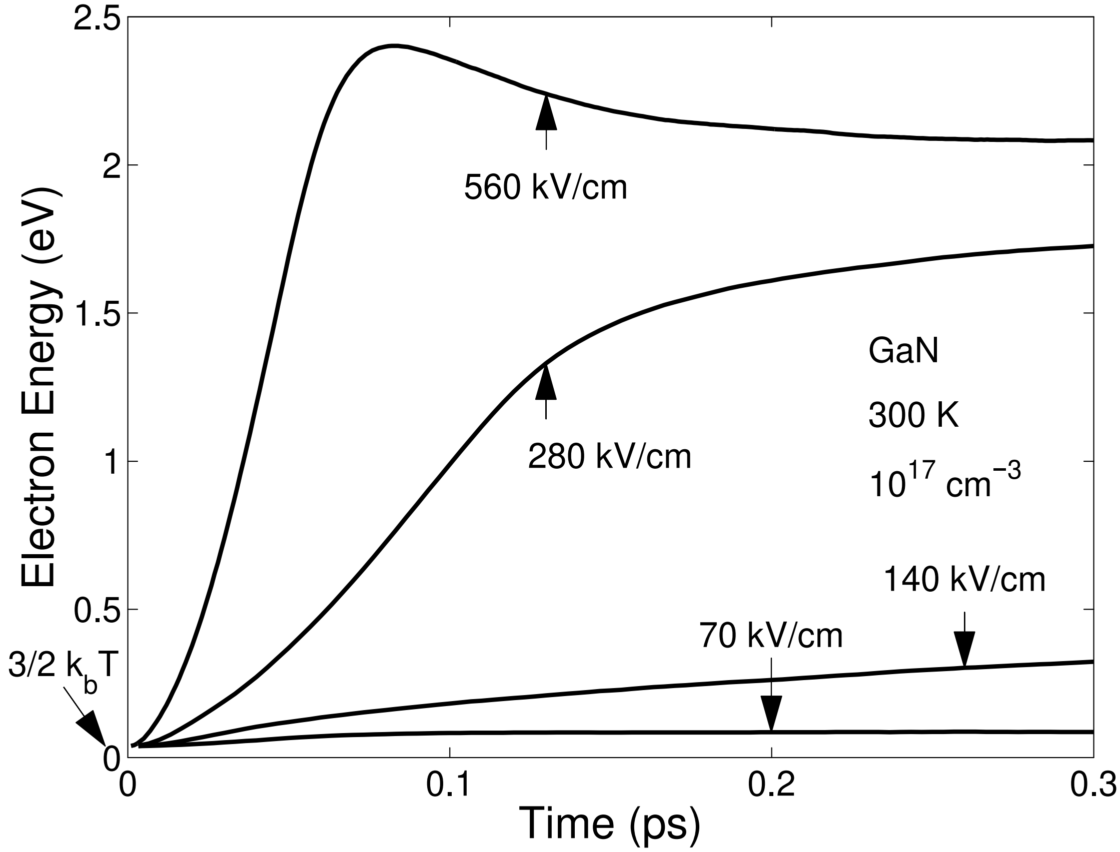

Figure 2.6: The dependence of the average electron energy on the time elapsed since the onset of the applied electric field for the case of bulk wurtzite GaN. The various selections of the applied electric field strength are indicated. These results were determined from Monte Carlo simulations of the electron transport within this material; the same simulations as those employed to determine Figure 2.4. For the purposes of these simulations, the crystal temperature is set to 300 K and the doping concentration is set to 10^{17} cm^{-3}.

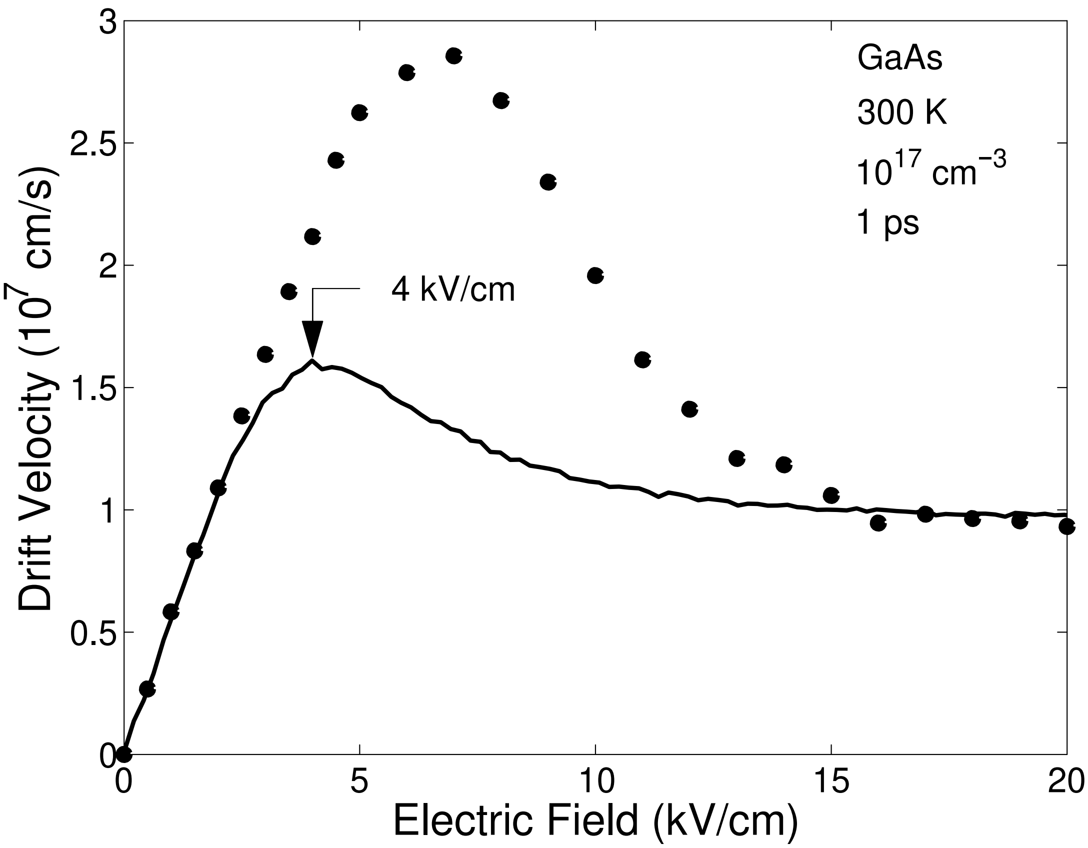

Figure 2.7: The dependence of the electron drift velocity on the applied electric field strength for the case of bulk zinc blende GaAs. Steady-state results are depicted with the solid line. The transient electron transport results are indicated with the solid points. These transient electron transport results are determined for 1 ps following the onset of the applied electric field. For the purposes of these simulations, the crystal temperature is set to 300 K and the doping concentration is set to 10^{17} cm^{-3}.

for all cases, this being the time over which transient electron transport effects occur for the case of bulk zinc blende GaAs; recall Figures 2.3 and 2.5. The corresponding steady-state electron drift velocity dependence on the applied electric field strength is also depicted in this figure. As was noted previously, transient electron transport effects are particularly evident for applied electric field strength selections beyond the peak field. Indeed, for the time elapsed since the onset of the applied electric field being set to 1 ps, transient electron drift velocities as high as 2.9×10^7 cm/s (for an applied electric field strength selection of around 7 kV/cm) may be achieved while the corresponding steady-state electron drift velocity is found to be only around 1.3×10^7 cm/s. For the case of bulk wurtzite GaN, shown in Figure 2.8, the enhancement is even greater, i.e., transient electron drift velocities as high as 6.8×10^7 cm/s (for an applied electric field selection of around 300 kV/cm) may be achieved while the corresponding steady-state electron drift velocity is found to be only around 1.7×10^7 cm/s; the time elapsed since the onset of the applied electric field is set to 0.1 ps for this particular case, this being the time over which transient electron transport effects occur for the case of bulk wurtzite GaN; recall Figures 2.4 and 2.6.

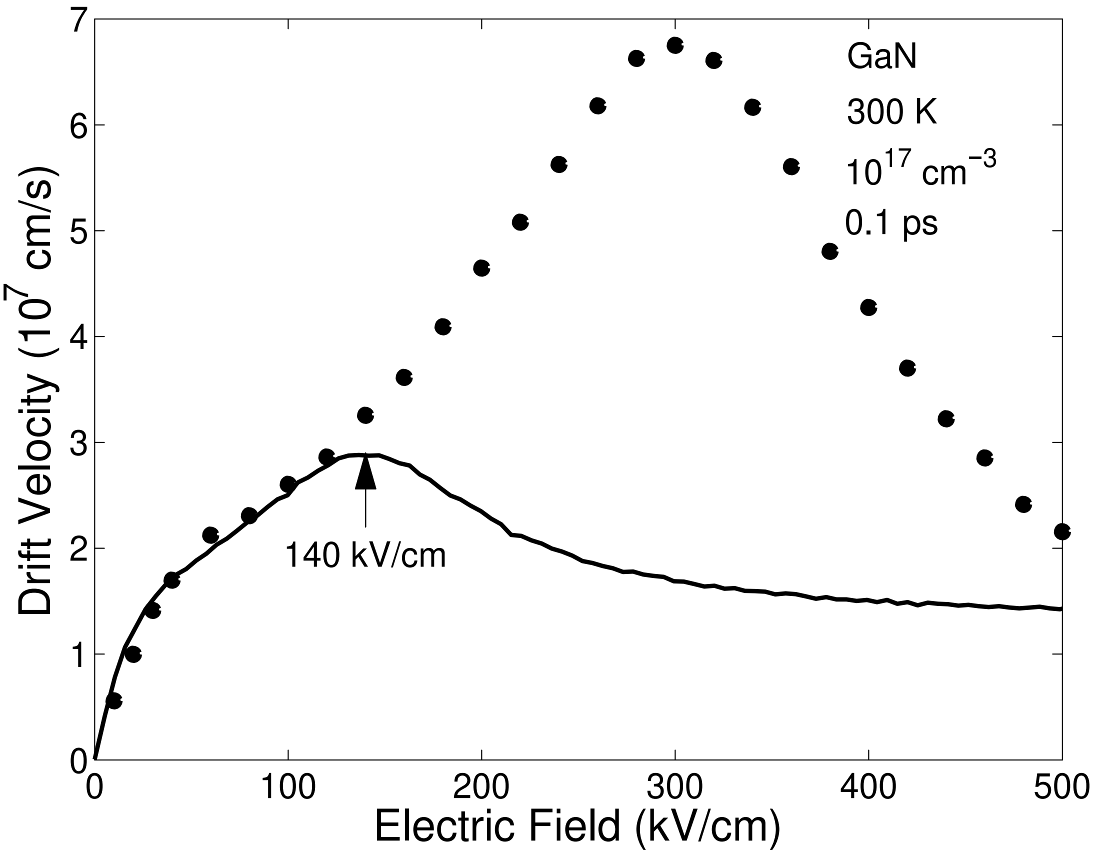

Figure 2.8: The dependence of the electron drift velocity on the applied electric field strength for the case of bulk wurtzite GaN. Steady-state results are depicted with the solid line. The transient electron transport results are indicated with the solid points. These transient electron transport results are determined for 0.1 ps following the onset of the applied electric field. For the purposes of these simulations, the crystal temperature is set to 300 K and the doping concentration is set to 10^{17} cm^{-3}.

2.4 Device implications

These results have important implications in terms of the performance of electron devices. Noting that the cut-off frequency for a device

$$f_T = \frac{1}{2\pi\tau}, \tag{2.1}$$

where τ represents the transit-time across the device, we can use our results to suggest the device length required in order to satisfy a desired cut-off frequency requirement. Figure 2.7, for example, suggests that for the case of zinc-blende GaAs that cut-off frequencies of around 160 GHz may be achieved for device lengths of at most 290 nm; for a set transit-time of 1 ps, i.e., $f_T \sim$160 GHz, a rough estimate for the maximum electron range, i.e., the maximum device length, may be obtained by multiplying the peak transient electron drift velocity by this transit-time. Figure 2.8 suggests that for the case of wurtzite GaN cut-off frequencies of around 1.6 THz may be achieved with device lengths of at most 70 nm. Focussing on the specific case of wurtzite GaN, it is seen that for a set device length of 70 nm, assuming a uniform field distribution within the device, the application of 2 V across the device, i.e., an applied electric field of 300 kV/cm, this being the applied electric field at which the peak transient electron drift velocity is achieved for the case of wurtzite GaN (recall Figure 2.8), will ensure that the transit-time is around 0.1 ps, i.e., $f_T \sim$1.6 THz. The non-idealities of an actual device, such as non-uniformities in the electric field distribution, must be considered when evaluating the performance of any particular device configuration, of course.

2.5 Conclusions

In conclusion, we have presented a detailed comparative analysis of the transient electron transport that occurs within bulk zinc-blende GaAs and bulk wurtzite GaN. A three-valley Monte Carlo simulation approach was used for the purposes of this analysis. We found that in both cases that the electron drift velocity and the average electron energy ‘‘settling times’’ are strongly correlated. We also devised a new means of rendering transparent the electron drift velocity enhancement offered by transient electron transport. Finally, the device implications of these results were commented upon.

Acknowledgments: The authors would like to acknowledge the assistance of Dr. Thomas Johnson, of The University of British Columbia, for his important contributions to this manuscript. The authors also gratefully acknowledge financial support from the Natural Sciences and Engineering Research Council of Canada. The work at Rensselaer Polytechnic Institute (M. S. Shur) was supported primarily through the Engineering Research Centers program of the National Science Foundation under the NSF Cooperative Agreement No. EEC-0812056 and in part by New York State under NYSTAR contract C090145.

References

[1] H. P. Markusa and J. J. Tietjen, "The preparation and properties of vapor-deposited single-crystalline GaN," *Applied Physics Letters*, vol. 15, no. 10, pp. 327-329, 1969.

[2] Y. Li, Y. Lu, H. Shen, M. Wraback, M. G. Brown, M. Schurman, L. Koszi, and R. A. Stall, "Temperature dependence of energy gap in GaN thin film studied by thermo-modulation," *Applied Physics Letters*, vol. 70, no. 18, pp. 2458-2460, 1997.

[3] Y. Dora, A. Chakraborty, L. McCarthy, S. Keller, S. P. DenBaars, and U. K. Mishra, "High breakdown voltage achieved on AlGaN/GaN HEMTs with integrated slant field plates," *IEEE Electron Device Letters*, vol. 27, no. 9, pp. 713-715, 2006.

[4] Z. Dong, J. Wang, C. P. Wen, D. Gong, Y. Li, M. Yu, Y. Hao, F. Xu, B. Shen, and Y. Wang, "High breakdown AlGaN/GaN MOSHEMT with thermal oxidized Ni/Ti as gate insulator," *Solid State Electronics*, vol. 54, no. 11, pp. 1339-1342, 2010.

[5] I. B. Rowena, S. L. Selvaraj, and T. Egawa, "Buffer thickness contribution to suppress vertical leakage current with high breakdown field (2.3 MV/cm) for GaN on Si," *IEEE Electron Device Letters*, vol. 32, no. 11, pp. 1534-1536, 2011.

[6] M. D. Kamatagi, N. S. Sankeshwar, and B. G. Mulimani, "Thermal conductivity of GaN," *Diamond and Related Materials*, vol. 16, no. 1, pp. 98-106, 2007.

[7] S. K. O'Leary, B. E. Foutz, M. S. Shur, and L. F. Eastman, "Steady-state electron transport in the III–V nitride semiconductors: A sensitivity analysis," *Journal of Electronic Materials*, vol. 32, no. 5, pp. 327-334, 2003.

[8] S. K. O'Leary, B. E. Foutz, M. S. Shur, and L. F. Eastman, "Steady-state and transient electron transport within the III–V Nitride semiconductors, GaN, AlN, and InN: A review," *Journal of Electronic Materials*, vol. 17, no. 2, pp. 87-126, 2006.

[9] B. Wang , N. Tipirneni , M. Riva , A. Monti , G. Simin, and E. Santi "An efficient, high-frequency drive circuit for GaN power HFETs," *IEEE Transactions on Industry Applications*, vol. 45, no. 2, pp. 843 -853, 2009.

[10] G. Meneghesso, M. Meneghini, A. Tazzoli, N. Ronchi, A. Stocco, A. Chini, and E. Zanoni, "Reliability issues of Gallium Nitride High Electron Mobility Transistors," *International Journal of Microwave and Wireless Technologies*, vol. 2, no. 1, pp. 39-50, 2010.

[11] J. H. Leach, and H. Morkoç, "Status of reliability of GaN-based hetero-junction field effect transistors," *Proceedings of the IEEE*, vol. 98, no. 7, pp. 1127-1139, 2010.

[12] W. Dongfang, Y. Tingting, W. Ke, C. Xiaojuan, and L. Xinyu, "Gate-structure optimization for high frequency power AlGaN/GaN HEMTs," *Journal of Semiconductors,* vol. 31, no. 5, 054003, 2010.

[13] A. Akselrad, "The optoelectronic technology of gallium nitride: the 2002 Benjamin Franklin medal in engineering presented to Shuji Nakamura," *Journal of the Franklin Institute*, vol. 340, no. 3, pp. 249-261, 2003.

[14] S. Fündling, U. Jahn, A. Trampert, H. Riechert, H. -H. Wehmann, and A. Waag, "Metal-organic vapour-phase epitaxy of gallium nitride nanostructures for optoelectronic applications," *Microelectronics Journal*, vol. 40, no. 2, pp. 333-335, 2009.

[15] E. Monroy, F. Guillot, S. Leconte, L. Nevou, L. Doyennette, M. Tchernycheva, F. H. Julien, E. Baumann, F. R. Giorgetta, and D. Hofstetter, "Latest developments in GaN-based quantum devices for infrared optoelectronics," *Journal of Materials Science: Materials in Electronics,* vol. 19, no. 8, pp. 821-827, 2008.

[16] F. G. Kalaitzakis, E. Iliopoulos, G. Konstantinidis, and N. T. Pelekanos, "Monolitihic integration of nitride-based transistor with light emitting diode for sensing applications," *Microelectronic Engineering*, vol. 90, pp. 33-36, 2012.

[17] S. Strite, and H. Morkoç, "GaN, AlN, and InN: A review," *Journal of Vacuum Science and Technology B*, vol. 10, no. 4, pp. 1237-1266, 1992.

[18] H. Morkoç, S. Strite, G. B. Gao, M. E. Lin, B. Sverdlov, and M. Burns, "Large-band-gap SiC, III-V nitride, and II-VI ZnSe-based semiconductor device technologies," *Journal of Applied Physics*, vol. 76, no. 3, pp. 1363-1398, 1994.

[19] S. J. Pearton, J. C. Zolper, R. J. Shul, and F. Ren, "GaN: Processing, defects, and devices," *Journal of Applied Physics*, vol. 86, no. 1, pp. 1-78, 1999.

[20] D. Zhuang, and J. H. Edgar, "Wet etching of GaN, AlN, and SiC: a review," *Materials Science and Engineering: R: Reports*, vol. 48, no. 1, pp. 1-46, 2005.

[21] M. A. Littlejohn, J. R. Hauser, and T. H. Glisson, "Monte Carlo calculation of the velocity-field relationship for gallium nitride," *Applied Physics Letters*, vol. 26, no. 11, pp. 625-627, 1975.

[22] D. K. Ferry, "High-field transport in wide-band-gap semiconductors," *Physics Review B*, vol. 12, no. , pp. 2361-2369, 1975.

[23] P. Das, and D. K. Ferry, "Hot electron microwave conductivity of wide bandgap semiconductors," *Solid State Electronics*, vol. 19, no. 10, pp. 851-855, 1976.

[24] B. Gelmont, K. Kim, and M. Shur, "Monte Carlo simulation of electron transport in gallium nitride," *Journal of Applied Physics*, vol. 74, no. 3, pp. 1818-1821, 1993.

[25] V. W. L. Chin, T. L. Tansley, and T. Osotchan, "Electron mobilities in gallium, indium, and aluminum nitrides," *Journal of Applied Physics*, vol. 75, no. 11, pp. 7365-7372, 1994.

[26] N. S. Mansour, K. W. Kim, and M. A. Littlejohn, "Theoretical study of electron transport in gallium nitride," *Journal of Applied Physics*, vol. 77, no. 6, pp. 2834-2836, 1995.

[27] J. Kolník, İ. H. Oğuzman, K. F. Brennan, R. Wang, P. P. Ruden, and Y. Wang, "Electronic transport studies of bulk zincblende and wurtzite phases of GaN based on an ensemble Monte Carlo calculation including a full zone band structure," *Journal of Applied Physics*, vol. 78, no. 2, pp. 1033-1038, 1995.

[28] M. Shur, B. Gelmont, and M. A. Khan, "Electron mobility in two-dimensional electron gas in AIGaN/GaN heterostructures and in bulk GaN," *Journal of Electronic Materials*, vol. 25, no. 5, pp. 777-785.

[29] B. E. Foutz, L. F. Eastman, U. V. Bhapkar, and M. S. Shur, "Comparison of high field electron transport in GaN and GaAs," *Applied Physics Letters*, vol. 70, no. 21, pp. 2849-2851, 1997.

[30] U. V. Bhapkar and M. S. Shur, "Monte Carlo calculation of velocity-field characteristics of wurtzite GaN," *Journal of Applied Physics*, vol. 82, no. 4, pp. 1649-1655, 1997.

[31] B. E. Foutz, S. K. O'Leary, M. S. Shur, and L. F. Eastman, "Transient Electron Transport in Wurtzite GaN, InN and AlN," *Journal of Applied Physics*, vol. 85, no. 11, pp. 7727-7734, 1999.

[32] S. K. O'Leary, B. E. Foutz, M. S. Shur, and L. F. Eastman, "Polar optical phonon instability and intervalley transfer in III-V semiconductors," *Solid State Communications*, vol. 118, no. 2, pp. 79-83, 2001.

[33] R. Brazis and R. Raguotis, "Additional phonon modes and close satellite valleys crucial for electron transport in hexagonal gallium nitride," *Applied Physics Letters*, vol. 85, no. 4, pp. 609-611, 2004.

[34] F. Bertazzi, M. Moresco, and E. Bellotti, "Theory of high field carrier transport and impact ionization in wurtzite GaN. Part I: A full band Monte Carlo model," *Journal of Applied Physics*, vol. 106, no. 6, 063718, 2009.

[35] J. G. Ruch, "Electron dynamics in short-channel field-effect transistors," *IEEE Transactions on Electron Devices*, vol. 19, no. 5, pp. 652-654, 1972.

[36] M. S. Shur, "Influence of non-uniform field distribution on frequency limits of GaAs field-effect transistors," *Electronics Letters*, vol. 12, no. 23, pp. 615-616, 1976.

[37] W. Fawcett, A. D. Boardman, and S. Swain, "Monte Carlo determination of electron transport properties in gallium arsenide," *Journal of Physics and Chemistry of Solids*, vol. 31, no. 9, pp. 1963-1990, 1970.

[38] P. Lugli and D. K. Ferry, "Degeneracy in the ensemble Monte Carlo method for high-field transport in semiconductors," *IEEE Transactions on Electron Devices*, vol. 32, no. 11, pp. 2431-2437, 1985.

[39] K. Seeger, *Semiconductor Physics: An Introduction*, 9th ed. Berlin, Germany: Springer, 2004.

[40] S. K. O'Leary, B. E. Foutz, M. S. Shur, U. V. Bhapkar, and L. F. Eastman, "Electron Transport in Wurtzite Indium Nitride," *Journal of Applied Physics*, vol. 83, no. 2, pp. 826-829, 1998.

[41] S. K. O'Leary, B. E. Foutz, M. S. Shur, U. V. Bhapkar, and L. F. Eastman, "Monte Carlo simulation of electron transport in wurtzite aluminum nitride," *Solid State Communications*, vol. 105, no. 10, pp. 621-626, 1998.

[42] S. K. O'Leary, B. E. Foutz, M. S. Shur, and L. F. Eastman, "Steady-state and transient electron transport within bulk wurtzite indium nitride: An updated semiclassical three-valley Monte Carlo simulation analysis," *Applied Physics Letters*, vol. 87, no. 22, pp. 222103-1-3, 2005.

[43] S. K. O'Leary, B. E. Foutz, M. S. Shur, and L. F. Eastman, "Potential performance of indium-nitride-based devices," *Applied Physics Letters*, vol. 88, no. 15, pp. 152113-1-3, 2006.

[44] S. K. O'Leary, B. E. Foutz, M. S. Shur, and L. F. Eastman, "The sensitivity of the electron transport within bulk wurtzite indium nitride to variations in the crystal temperature, the doping concentration, and the non-parabolicity coefficient: an updated Monte Carlo analysis," *Journal of Materials Science: Materials in Electronics,* vol. 21, no. 3, pp. 218-230, 2010.

[45] S. K. O'Leary, B. E. Foutz, M. S. Shur, and L. F. Eastman, "Steady-state and transient electron transport within bulk wurtzite zinc oxide," *Solid State Communications*, vol. 150, no. 43, pp. 2182-2185, 2010.

[46] W. A. Hadi, S. K. O'Leary, M. S. Shur, and L.F. Eastman, "The sensitivity of the steady-state electron transport within bulk wurtzite zinc oxide to variations in the non-parabolicity coefficient," *Solid State Communications*, vol. 151, no. 12, pp. 874-878, 2011.

CHAPTER 3

On the applicability of a semi-analytical approach to determining the transient electron transport response of gallium arsenide, gallium nitride, and zinc oxide

A version of this manuscript was published in the Journal of Material Science: Materials in Electronics.

3.1 Introduction

The wide energy gap semiconductors, GaN and ZnO, are a focus of considerable current interest [1-7]. This interest has been fuelled, in large measure, by the considerable promise that these materials offer for novel electronic and optoelectronic device applications [8, 9]. GaN, with its wide and direct energy gap, i.e., 3.39 eV at room temperature [10], offers a high breakdown field [11, 12], high thermal conductivity [13, 14], and favorable electron transport characteristics [15-18], making it ideally suited for high-power and high-frequency electron device applications. On the optoelectronics front, the direct nature of the energy gap associated with GaN also make it well suited for optoelectronic device applications in the ultraviolet frequency range [19]. ZnO, while currently finding applications as a material for low-field thin-film transistor electron device structures [20] and as a potential material for transparent conducting electrodes [21], also possesses a direct energy gap [22, 23] with a magnitude that is very similar to that of GaN [24]. Thus, it might be expected that, with some further improvements in its material quality, ZnO may also be employed for some of the device roles currently implemented or envisaged for GaN.

In order to analyze the performance and further improve on the design of compound semiconductor electron devices, an understanding of the electron transport that occurs within the underlying electronic materials is necessary. With its wide energy gap, large polar optical phonon energy, and wide intervalley energy separation, GaN is expected to exhibit favorable electron transport characteristics [25]. ZnO, with a similar energy gap to that possessed by GaN, a slightly lower polar optical phonon energy, and a much wider intervalley energy separation, is also expected to exhibit favorable electron transport characteristics. Studies of both the steady-state and transient electron transport that occurs within bulk wurtzite GaN [16-18, 25-37] and bulk wurtzite ZnO [23, 38-44] have been pursued through the years. From these studies, key conclusions, regarding the nature of the electron transport within these materials, have been drawn. In addition, insights into means of properly designing electron devices fabricated with these materials have been gleaned.

Steady-state electron transport is the dominant electron transport mechanism in devices with larger dimensions. For devices with smaller dimensions, however, transient electron transport must also be considered when evaluating device performance. Ruch [45] demonstrated, for both silicon and GaAs, that the transient electron drift velocity may exceed the corresponding steady-state electron drift velocity, by a considerable margin, for appropriate selections of the applied electric field strength. This overshoot has been observed for many compound semiconductors, including GaN [15] and ZnO [42]. Shur and Eastman [46] explored the device implications of transient electron transport, and demonstrated that substantial improvements in the device performance can be achieved as a consequence of the transient electron transport. The benefits of transient electron transport were further extolled by Foutz *et al.* [15] in 1999 and O'Leary *et al.* [47] in 2006.

Fundamentally, the transient electron transport response of a semiconductor may be characterized through the solution of the Boltzmann transport equation. The ensemble Monte Carlo simulation technique offers an effective means of solving this equation. Unfortunately, transient Monte Carlo solutions to the Boltzmann equation have a number of drawbacks. First, and perhaps most significantly, the computations demanded of the

Monte Carlo technique are quite intensive, with individual runs taking a long time to execute, even on powerful machines. Secondly, many Monte Carlo simulators only consider the electron transport within the bulk. The results obtained, thus, can not be applied directly to actual electron device structures, where the fields may be highly non-uniform and time-varying. Accordingly, the development of an alternate means of characterizing the transient electron transport within a compound semiconductor, that allows for the rapid evaluation of the transient electron transport response, and allows for the treatment of non-uniform and time-varying electric fields, is a priority.

In 1976, Shur [48] developed a semi-analytical technique for determining the transient electron transport response within compound semiconductors, and applied it to the specific case of GaAs, the most significant compound semiconductor at the time. Stemming from the application of momentum conservation and energy conservation principles, the semi-analytical approach of Shur [48] cast its analysis of the transient electron transport within compound semiconductors in terms of the momentum and energy relaxation times. These relaxation times were determined from Monte Carlo generated steady-state results for the electron drift velocity as a function of the applied electric field strength, the average electron energy as a function of the applied electric field strength, and the occupancy of the valleys as a function of the applied electric field strength, coupled with knowledge of the electron effective mass associated with each valley at the respective valley energy minimum.

In this paper, we aim to critically evaluate the validity of this semi-analytical technique of Shur [48]. In particular, we will solve the semi-analytical equations of Shur [48] and contrast the obtained results for the transient electron transport with results obtained using Monte Carlo simulations of the electron transport. Our approach will be to examine the response of an ensemble of electrons to the application of a constant and uniform applied electric field. For the purposes of this analysis, three aspects of the transient electron transport will be considered: (1) the dependence of the electron drift velocity on the time elapsed since the onset of the applied electric field, (2) the dependence of the average electron energy on the time elapsed since the onset of the applied electric field, and (3) the dependence of the average electron displacement on the time elapsed since the onset of the applied electric field. The materials considered in this analysis include zinc-blende GaAs, albeit primarily for benchmarking purposes, wurtzite GaN, and wurtzite ZnO. In order to simplify matters, we will focus solely on the bulk response for the purposes of this analysis.

This paper is organized in the following manner. In Section 3.2, we describe the Monte Carlo simulations of the electron transport that we employ for the purposes of this analysis. Then, in Section 3.3, the semi-analytical approach of Shur [48] is briefly described. The results of this analysis are then presented in Section 3.4, results determined using this semi-analytical approach being contrasted with those obtained through Monte Carlo simulations. A possible explanation for the closeness of the semi-analytical results and the Monte Carlo simulation results, for the specific case of wurtzite ZnO, is then provided in Section 3.5. The device implications of these results are briefly discussed in Section 3.6. Finally, the conclusions of this analysis are summarized in Section 3.7.

3.2 Monte Carlo electron transport simulations

For this analysis of the transient electron transport within bulk zinc-blende GaAs, bulk wurtzite GaN, and bulk wurtzite ZnO, we employ ensemble semi-classical three-valley Monte Carlo simulations. The scattering mechanisms considered are: (1) ionized impurity, (2) polar optical phonon, (3) piezoelectric, and (4) acoustic deformation potential. Intervalley scattering is also considered, each valley being treated through the application of the Kane model [49][1]. We assume that all donors are ionized and that the free electron concentration is equal to the dopant concentration. For these transient electron transport simulations, thermal equilibrium is assumed prior to the application of the electric field. Our approach will be to examine the response of an ensemble of electrons to the application of a constant and uniform applied electric field. The motion of 10,000 electrons is considered during the course of each simulation. Electron degeneracy effects are accounted for by means of the rejection technique of Lugli and Ferry [50]. Electron screening is also accounted for following the Brooks-Herring method [51]. Further details of our Monte Carlo simulation approach are presented in the literature [15-18, 33, 42, 44, 52-57].

Most of the material and band structural parameter selections, used for our simulations of the transient electron transport within bulk wurtzite ZnO, are from Albrecht *et al.* [23]; we adopt the same material and band structural parameter selections as O'Leary *et al.* [42] and Hadi *et al.* [43, 44]. Unfortunately, as Albrecht *et al.* [23] did not provide an exhaustive list of all of the material parameters needed for our Monte

---

[1] In the Kane model, the energy bands are assumed to be non-parabolic, spherical, and of the form $E(1+\alpha E) = \frac{\hbar^2 k^2}{2m^*}$, where $\hbar k$ denotes the crystal momentum, E represents the energy, m^* is the effective mass of the electrons within this valley, and α is the non-parabolicity coefficient [49].

Carlo simulations, some of the material parameters employed by us are drawn from other sources in the literature [58], or through a direct fit with the results of Albrecht *et al.* [23], i.e., we tweaked the material parameters until the resultant velocity-field characteristic corresponded with that found by Albrecht *et al.* [23]. With the exception of the second order non-parabolicity factor, which we neglect for the purposes of our analysis [49], we employ the same three-valley band model for the conduction band as that employed by Albrecht *et al.* [23]. The lowest energy conduction band valley electron effective mass selection, 0.17 m_e, where m_e denotes the free electron mass, while smaller than the selections of Adachi *et al.* [58] (0.234 m_e), Guo *et al.* [39] (0.54 m_e), and Furno *et al.* [41] (0.21 m_e perpendicular and 0.23 m_e parallel), is in keeping with the relation between the electron effective mass and the direct energy gap found for other III–V and II–VI semiconductors, as was shown in Figure 1 of O'Leary *et al.* [42]; given the considerable overlap in authorship between Bertazzi *et al.* [40] and Furno *et al.* [41], it will be assumed that the choice of electron effective mass is similar. As with Albrecht *et al.* [23], anisotropy in the bands is neglected, the simulations of Bertazzi *et al.* [40] and Furno *et al.* [41] demonstrating that the anisotropy that is present only leads to a slight correction in the results. The material and band structural parameter selections, employed for the purposes this analysis of the transient electron transport within bulk wurtzite ZnO, are tabulated in Tables 3.1 and 3.2, respectively. The material and band structural parameters, corresponding to bulk wurtzite GaN and bulk zinc-blende GaAs, are as specified by O'Leary *et al.* [18] and Foutz *et al.* [33].

Table 3.1: The material parameter selections corresponding to bulk wurtzite ZnO that are employed for the purposes of this analysis. The source of each parameter is identified.

Parameter	**ZnO**	**Reference**
Mass density (g/cm^3)	5.68	[58]
Longitudinal sound velocity(cm/s)	4.00×10^5	determined through fit
Transverse sound velocity (cm/s)	2.7×10^5	[39]
Acoustic deformation potential (eV)	3.83	[23]
Static dielectric constant	8.2	[23]
High frequency dielectric constant	3.7	[23]
Effective mass (Γ_1 valley)	0.17 m_e	[23]
Piezoelectric constant, e_{14} (C/cm^2)	3.75×10^{-5}	determined through fit
Direct energy gap (eV)	3.4	[23]
Polar optical phonon energy (meV)	72	[23]
Intervalley deformation potentials (eV/cm)	10^9	[23]
Intervalley phonon energies (meV)	72	[23]

Table 3.2: The band structure parameter selections corresponding to bulk wurtzite ZnO. These band structure parameter selections are mostly from Albrecht *et al.* [23].

	Valley number	**1**	**2**	**3**
ZnO	Valley location	Γ_1 [23]	Γ_1 [23]	L-M [23]
	Valley degeneracy	1	1	6
	Effective mass	0.17 m_e [23]	0.42 m_e [23]	0.7 m_e [23]
	Intervalley energy separation (eV)	_	4.4 [23]	4.6 [23]
	Energy gap (eV)	3.4 [23]	7.8 [23]	8.0 [23]
	Non-parabolicity (eV^{-1})	0.66 [23]	0.15 [23]	0.0 [23]

3.3 The semi-analytical approach

Fundamentally, the semi-analytical approach of Shur *et al.* [48] draws upon the principles of momentum and energy conservation. The approach involves the solution of two coupled one-dimensional differential equations, one for the electron momentum, the other for the electron energy. For the case of momentum, under the action of an applied electric field, for the one-dimensional case, it can be shown that,

$$\frac{d[m^*(\varepsilon)v]}{dt} = q\xi - \frac{m^*(\varepsilon)v}{\tau_m(\varepsilon)}, \tag{3.1}$$

where q denotes the charge of an electron, v represents the average electron drift velocity, ε is the electron energy, $\tau_m(\varepsilon)$ is the momentum relaxation time, ξ is the strength of the electric field, and $m^*(\varepsilon)$ is the energy dependent effective mass, the effective mass being dependent upon the particular valleys that the electrons occupy; Eq. (3.1) corresponds to a one-dimensional projection of electron transport in the direction of the applied electric field. For the case of energy, it can be shown that

$$\frac{d\varepsilon}{dt} = q\xi v - \frac{\varepsilon - \varepsilon_o}{\tau_\varepsilon(\varepsilon)}, \tag{3.2}$$

where $\tau_\varepsilon(\varepsilon)$ denotes the energy relaxation time and ε_o represents the thermal equilibrium energy, i.e., $\varepsilon_o = \left(\frac{3}{2}\right)k_b T$, where k_b is Boltzmann's constant and T is the temperature. The entire analysis is cast with respect to the electron energy, ε.

Expressions for the momentum and energy relaxation times, i.e., $\tau_m(\varepsilon)$ and $\tau_\varepsilon(\varepsilon)$, may be obtained from steady-state Monte Carlo results. Setting the derivatives of Eqs. (3.1) and (3.2) to zero, the momentum relaxation time,

$$\tau_m(\varepsilon) = \frac{m^*(\varepsilon) v_{ss}(\varepsilon)}{q\xi_{ss}(\varepsilon)}, \tag{3.3}$$

while the energy relaxation time,

$$\tau_\varepsilon(\varepsilon) = \frac{\varepsilon - \varepsilon_o}{q\xi_{ss}(\varepsilon) v_{ss}(\varepsilon)}, \tag{3.4}$$

where v_{ss} (ε) is the steady-state electron drift velocity as a function of the electron energy and $\xi_{ss}(\varepsilon)$ is the electric field strength as a function of the electron energy. The electron energy dependent electron drift velocity, v_{ss} (ε), is found through a substitution of $\xi_{ss}(\varepsilon)$ into the corresponding steady-state velocity-field characteristic.

3.4 Results

In Figure 3.1, we plot the electron drift velocity associated with bulk zinc-blende GaAs as a function of the time elapsed since the onset of the applied electric field. For all cases considered, the crystal temperature is set to 300 K and the doping concentration is set to 10^{17} cm^{-3}. Electric field strength selections of 2, 4, 6, and 8 kV/cm are chosen, these corresponding to half-multiples of the peak field associated with zinc-blende GaAs; the peak field, i.e., the applied electric field at which point the steady-state velocity-field characteristic achieves its peak, is found to be 4 kV/cm for the case of zinc-blende GaAs. The results corresponding to the Monte Carlo simulations are depicted with the solid lines while the results of the semi-analytical technique are depicted with the dashed lines. We first note that for the electric field strength selections 2 and 4 kV/cm, that very little velocity overshoot occurs. In contrast, for electric field strength selections in excess of 4 kV/cm, considerable velocity overshoot occurs. As was observed before, 4 kV/cm corresponds to the peak in the velocity-field characteristic associated with zinc-blende GaAs. This suggests that the velocity overshoot is related to the peak in the velocity-field characteristic associated with this material. In terms of how the Monte Carlo results contrast with their semi-analytical counterparts, we note that, in all cases, the Monte Carlo results form an upper bound on the corresponding semi-analytical results. This bound, however, is noted to be quite tight for the lower applied electric field strength selections, i.e., for the cases of 2 and 4 kV/cm. For the higher applied electric field strength selections, the deviations noted were found to be more substantive, although not such as to invalidate the utility of the semi-analytical approach.

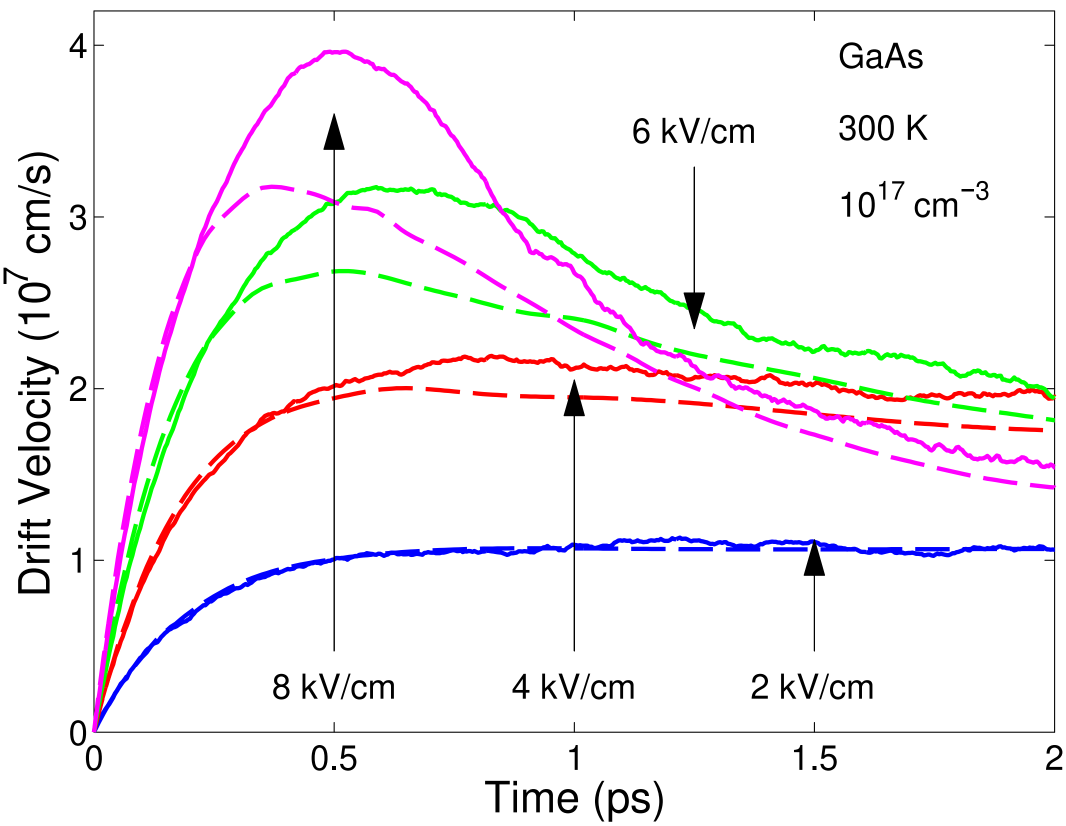

Figure 3.1: The electron drift velocity associated with bulk zinc-blende GaAs as a function of the time elapsed since the onset of the applied electric field. For all cases, we have assumed an initial zero-field electron distribution, a crystal temperature of 300 K, and a doping concentration of 10^{17} cm^{-3}. The Monte Carlo results are depicted with the solid lines and the semi-analytical results are represented with the dashed lines. The online version is depicted in color.

In Figure 3.2, we plot the electron drift velocity associated with bulk wurtzite GaN as a function of the time elapsed since the onset of the applied electric field. For all cases considered, the crystal temperature is set to 300 K and the doping concentration is set to 10^{17} cm^{-3}. Electric field strength selections of 70, 140, 210, and 280 kV/cm are chosen, these corresponding to half-multiples of the peak field associated with wurtzite GaN; the peak field associated with wurtzite GaN is 140 kV/cm. The results corresponding to the Monte Carlo simulations are depicted with the solid lines while the results of the semi-analytical technique are depicted with the dashed lines. We first note that, as before, for the lower electric field strength selections, i.e., 70 and 140 kV/cm, that very little velocity overshoot occurs. In contrast, for electric field strength selections in excess of 140 kV/cm, considerable velocity overshoot occurs. As was mentioned earlier, 140 kV/cm corresponds to the peak in the velocity-field characteristic associated with wurtzite GaN. Thus, as with the case of zinc-blende GaAs, this suggests that the velocity overshoot associated with wurtzite GaN is related to the peak in the velocity-field characteristic associated with this material. In terms of how the Monte Carlo results contrast with their semi-analytical counterparts, we note that, for many cases, the Monte Carlo results form an upper bound on the corresponding semi-analytical results; unlike the case of zinc-blende GaAs, however, this bound is not exact, as there are cases for which the semi-analytical results exceed the corresponding Monte Carlo results. This bound is noted to be quite tight for the lower applied electric field strength selections, i.e., the cases of 70 and 140 kV/cm. For the higher applied electric field strength selections, however, the deviations noted were found to be more substantive, although, as with the

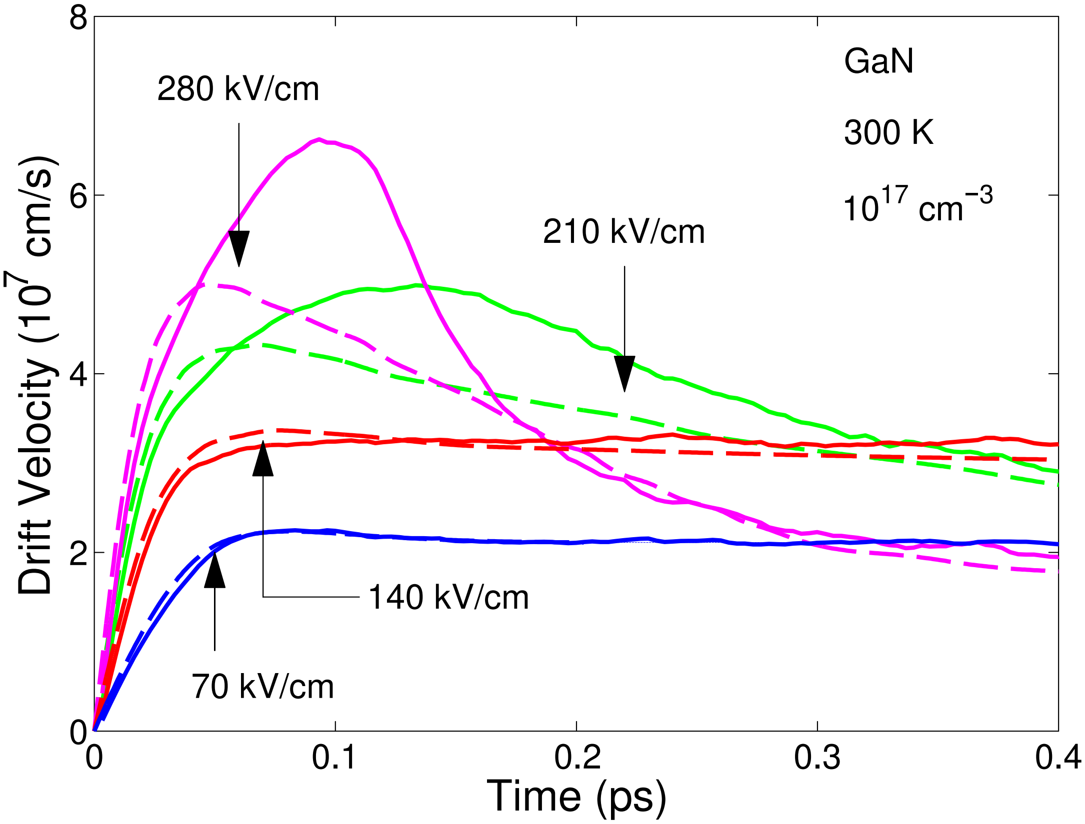

Figure 3.2: The electron drift velocity associated with bulk wurtzite GaN as a function of the time elapsed since the onset of the applied electric field. For all cases, we have assumed an initial zero-field electron distribution, a crystal temperature of 300 K, and a doping concentration of 10^{17} cm^{-3}. The Monte Carlo results are depicted with the solid lines and the semi-analytical results are represented with the dashed lines. The online version is depicted in color.

case of zinc-blende GaAs, not such as to invalidate the utility of the semi-analytical approach.

In Figure 3.3, we plot the electron drift velocity associated with bulk wurtzite ZnO as a function of the time elapsed since the onset of the applied electric field. For all cases considered, the crystal temperature is set to 300 K and the doping concentration is set to 10^{17} cm^{-3}. Electric field strength selections of 135, 270, 405, and 540 kV/cm are chosen, these corresponding to half-multiples of the peak field associated with wurtzite ZnO; the peak field associated with wurtzite ZnO is 270 kV/cm. The results corresponding to the Monte Carlo simulations are depicted with the solid lines while the results of the semi-analytical technique are depicted with the dashed lines. We first note that, as before, for the lower electric field strength selections, i.e., 135 and 270 kV/cm, that very little velocity overshoot occurs. In contrast, for electric field strength selections in excess of 270 kV/cm, considerable velocity overshoot occurs. As was mentioned earlier, 270 kV/cm corresponds to the peak in the velocity-field characteristic associated with wurtzite ZnO. Thus, as with the cases of zinc-blende GaAs and wurtzite GaN, this suggests that the velocity overshoot associated with wurtzite ZnO is related to the peak in the velocity-field characteristic associated with this material. In terms of how the Monte Carlo results contrast with their semi-analytical counterparts, we note that, for most cases, the semi-analytical results form an upper bound on the corresponding Monte Carlo results; this bound is not exact, however, as there are cases for which the Monte Carlo results exceed the corresponding semi-analytical results. This bound is noted to be quite tight for the lower applied electric field strength selections, i.e., the cases of 135 and 270 kV/cm. For the higher applied electric field strength selections, however, the

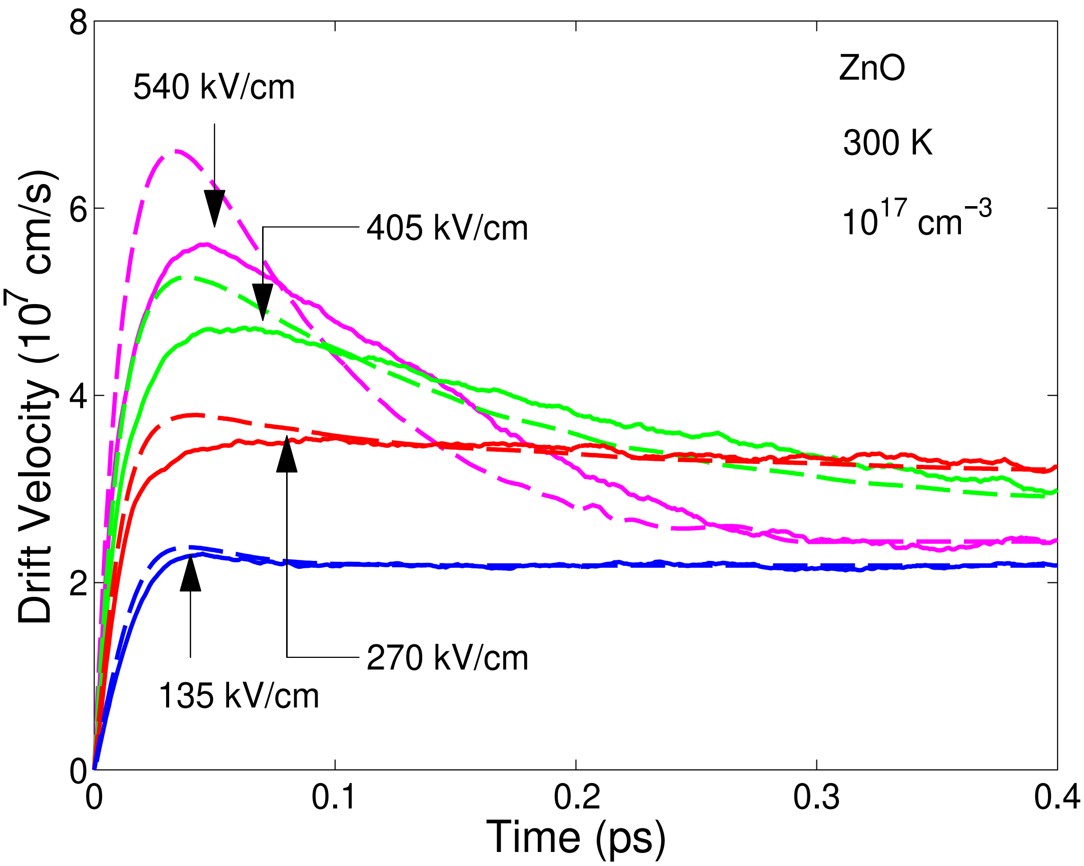

Figure 3.3: The electron drift velocity associated with bulk wurtzite ZnO as a function of the time elapsed since the onset of the applied electric field. For all cases, we have assumed an initial zero-field electron distribution, a crystal temperature of 300 K, and a doping concentration of 10^{17} cm^{-3}. The Monte Carlo results are depicted with the solid lines and the semi-analytical results are represented with the dashed lines. The online version is depicted in color.

deviations noted were found to be more substantive, although, as with the cases of zinc-blende GaAs and wurtzite GaN, not such as to invalidate the utility of the semi-analytical approach. We speculate that the uniqueness of the wurtzite ZnO case, i.e., the closeness of the semi-analytical results to the results of our Monte Carlo simulations, arises as a consequence of the fact that very few upper valley transitions occur for the case of this material, primarily on account of its large non-parabolicity coefficient [43]. Further analysis in support of this supposition is provided in Section 3.5.

In Figure 3.4, we plot the average electron energy associated with bulk zinc-blende GaAs as a function of the time elapsed since the onset of the applied electric field. For all cases considered, the crystal temperature is set to 300 K and the doping concentration is set to 10^{17} cm^{-3}. Electric field strength selections of 2, 4, 6, and 8 kV/cm are chosen, these corresponding to half-multiples of the peak field associated with zinc-blende GaAs. The results corresponding to the Monte Carlo simulations are depicted with the solid lines while the results of the semi-analytical technique are depicted with the dashed lines. The same Monte Carlo simulations and semi-analytical computations, employed in the determination of Figure 3.1, are used in order to determine these plots. We note that for all the applied electric field strength selections considered, the semi-analytical results form an upper bound on the Monte Carlo results. This bound is observed to be quite tight for most cases, the deviation between these results being greatest for the applied electric field strength being set to 4 kV/cm, i.e., the peak field.

In Figure 3.5, we plot the average electron energy associated with bulk wurtzite GaN as a function of the time elapsed since the onset of the applied electric field. For all cases considered, the crystal temperature is set to 300 K and the doping concentration is

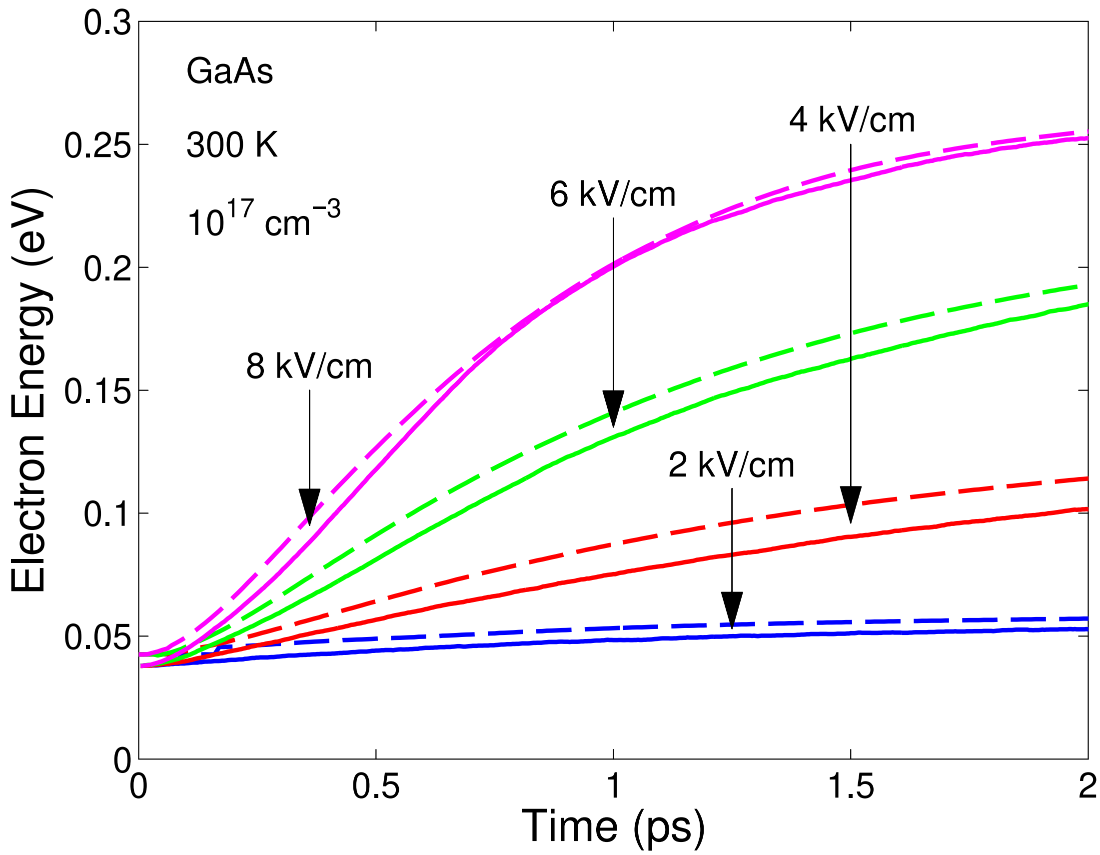

Figure 3.4: The average electron energy associated with bulk zinc-blende GaAs as a function of the time elapsed since the onset of the applied electric field. For all cases, we have assumed an initial zero-field electron distribution, a crystal temperature of 300 K, and a doping concentration of 10^{17} cm^{-3}. The Monte Carlo results are depicted with the solid lines and the semi-analytical results are represented with the dashed lines. The online version is depicted in color.

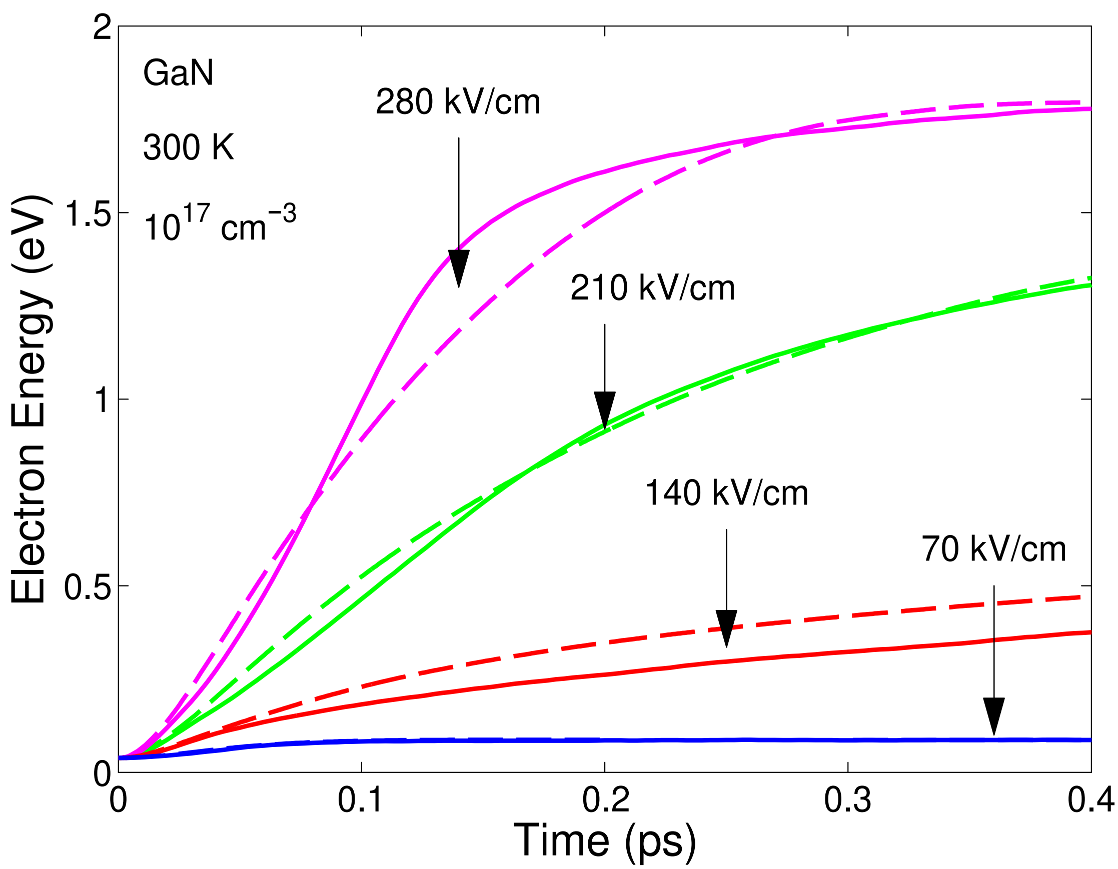

Figure 3.5: The average electron energy associated with bulk wurtzite GaN as a function of the time elapsed since the onset of the applied electric field. For all cases, we have assumed an initial zero-field electron distribution, a crystal temperature of 300 K, and a doping concentration of 10^{17} cm^{-3}. The Monte Carlo results are depicted with the solid lines and the semi-analytical results are represented with the dashed lines. The online version is depicted in color.

set to 10^{17} cm^{-3}. Electric field strength selections of 70, 140, 210, and 280 kV/cm are chosen, these corresponding to half-multiples of the peak field associated with wurtzite GaN. The results corresponding to the Monte Carlo simulations are depicted with the solid lines while the results of the semi-analytical technique are depicted with the dashed lines. The same Monte Carlo simulations and semi-analytical computations, employed in the determination of Figure 3.2, are used in order to determine these plots. We note that for the applied electric field strength selections 70, 140, and 210 kV/cm, the semi-analytical results form an upper bound on the Monte Carlo simulation results; this bound is not exact, as the 210 kV/cm case shows ranges of time for which the semi-analytical result is less than that obtained for the Monte Carlo simulation result, albeit slightly. This bound is observed to be quite tight for most cases, the deviation between these results being greatest for the applied electric field strength being set to 140 kV/cm, i.e., the peak field. The opposite effect is observed when the applied electric field strength is set to 280 kV/cm, however. For this case, the Monte Carlo result forms an upper bound on the semi-analytical result, except for times long after the onset of the applied electric field, i.e., beyond 0.25 ps following the onset of the applied electric field; this bound is not exact, however, as is seen for times less than 0.07 ps. It is noted that the deviation between the Monte Carlo results and that of the semi-analytical approach appears to become greatest at about 0.15 ps following the onset of the applied electric field. The exact reasons for this behaviour are unknown at the present time.

In Figure 3.6, we plot the average electron energy associated with bulk wurtzite ZnO as a function of the time elapsed since the onset of the applied electric field. For all cases considered, the crystal temperature is set to 300 K and the doping concentration is

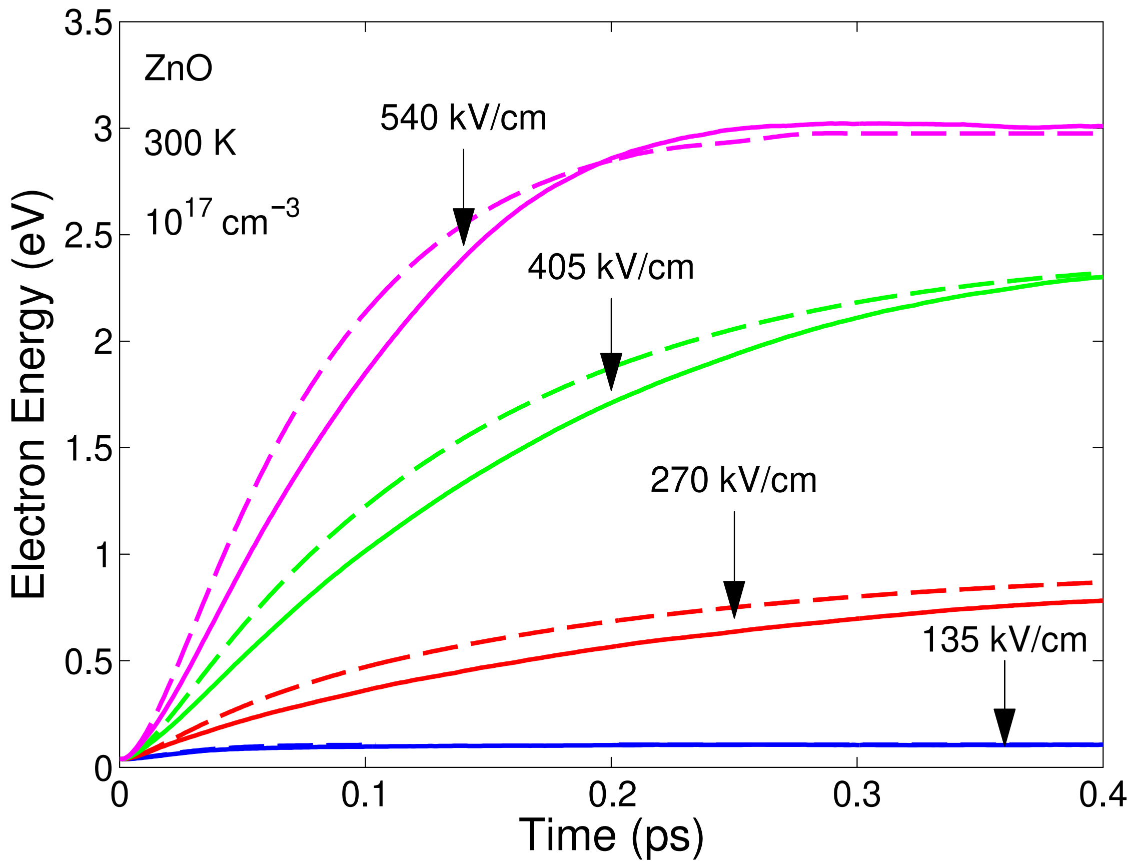

Figure 3.6: The average electron energy associated with bulk wurtzite ZnO as a function of the time elapsed since the onset of the applied electric field. For all cases, we have assumed an initial zero-field electron distribution, a crystal temperature of 300 K, and a doping concentration of 10^{17} cm^{-3}. The Monte Carlo results are depicted with the solid lines and the semi-analytical results are represented with the dashed lines. The online version is depicted in color.

set to 10^{17} cm^{-3}. Electric field strength selections of 135, 270, 405, and 540 kV/cm are chosen, these corresponding to half-multiples of the peak field associated with wurtzite ZnO. The results corresponding to the Monte Carlo simulations are depicted with the solid lines while the results of the semi-analytical technique are depicted with the dashed lines. The same Monte Carlo simulations and semi-analytical computations, employed in the determination of Figure 3.3, are used in order to determine these plots. We note that for all the applied electric field strength selections considered, the semi-analytical results form an upper bound on the Monte Carlo results. It is noted, however, that this bound is not exact for the case of the applied electric field strength set to 540 kV/cm, for times in excess of 0.2 ps following the onset of the applied electric field. Nevertheless, the deviations between the Monte Carlo results and those of the semi-analytical approach are found to be relatively small.

Integrating the electron drift velocity with respect to time one obtains the average electron displacement as a function of time; for the purposes of brevity, we henceforth refer to the average electron displacement as simply the electron displacement. In Figure 3.7, we plot the electron displacement associated with bulk zinc-blende GaAs as a function of the time elapsed since the onset of the applied electric field. For all cases considered, the crystal temperature is set to 300 K and the doping concentration is set to 10^{17} cm^{-3}. Electric field strength selections of 2, 4, 6, and 8 kV/cm are chosen, these corresponding to half-multiples of the peak field associated with zinc-blende GaAs. The results corresponding to the Monte Carlo simulations are depicted with the solid lines while the results of the semi-analytical technique are depicted with the dashed lines. The same Monte Carlo simulations and semi-analytical computations,

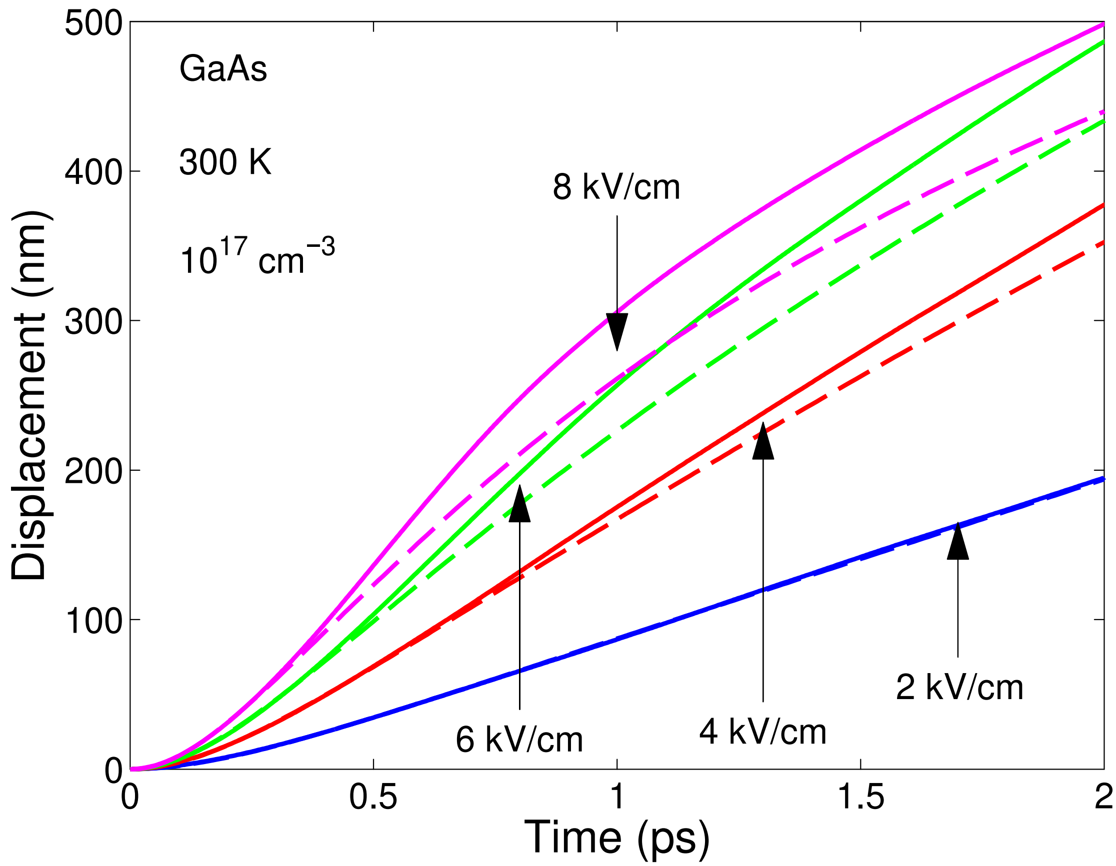

Figure 3.7: The electron displacement associated with bulk zinc-blende GaAs as a function of the time elapsed since the onset of the applied electric field. For all cases, we have assumed an initial zero-field electron distribution, a crystal temperature of 300 K, and a doping concentration of 10^{17} cm^{-3}. The Monte Carlo results are depicted with the solid lines and the semi-analytical results are represented with the dashed lines. The online version is depicted in color.

employed in the determination of Figures 3.1 and 3.4, are used in order to determine these plots. We note that for all the applied electric field strength selections considered, the Monte Carlo results form an upper bound on the semi-analytical results. The difference between the Monte Carlo results and those of the semi-analytical approach become larger as the applied electric field strength is increased.

In Figure 3.8, we plot the electron displacement associated with bulk wurtzite GaN as a function of the time elapsed since the onset of the applied electric field. For all cases considered, the crystal temperature is set to 300 K and the doping concentration is set to 10^{17} cm^{-3}. Electric field strength selections of 70, 140, 210, and 280 kV/cm are chosen, these corresponding to half-multiples of the peak field associated with zinc-blende GaN. The results corresponding to the Monte Carlo simulations are depicted with the solid lines while the results of the semi-analytical technique are depicted with the dashed lines. The same Monte Carlo simulations and semi-analytical computations, employed in the determination of Figures 3.2 and 3.5, are used in order to determine these plots. We note that for all the applied electric field strength selections considered, the Monte Carlo results form an upper bound on the semi-analytical results; this bound is not exact, as is seen for the case of the electric field set to 140 kV/cm. The difference between the Monte Carlo results and those of the semi-analytical approach become larger as the applied electric field strength is increased.

Finally, in Figure 3.9, we plot the electron displacement associated with bulk wurtzite ZnO as a function of the time elapsed since the onset of the applied electric field. For all cases considered, the crystal temperature is set to 300 K and the doping concentration is set to 10^{17} cm^{-3}. Electric field strength selections of 135, 270, 405, and

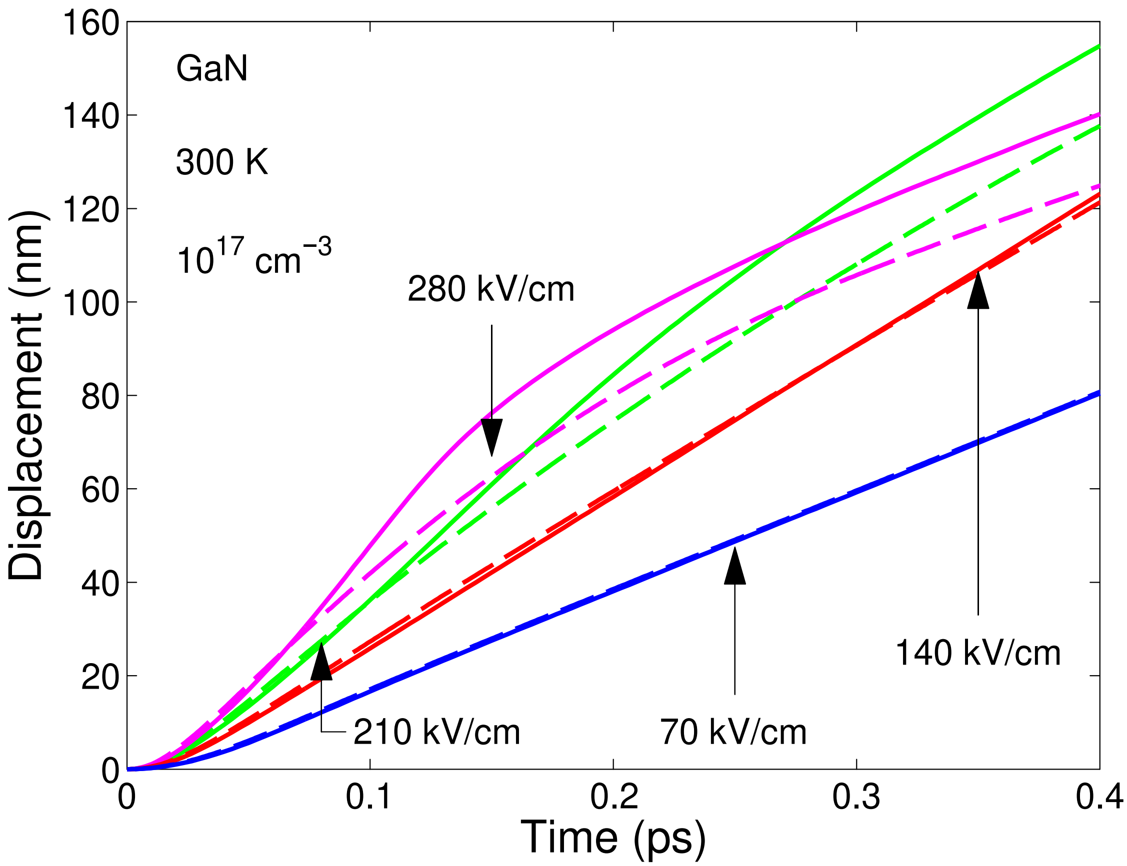

Figure 3.8: The electron displacement associated with bulk wurtzite GaN as a function of the time elapsed since the onset of the applied electric field. For all cases, we have assumed an initial zero-field electron distribution, a crystal temperature of 300 K, and a doping concentration of 10^{17} cm^{-3}. The Monte Carlo results are depicted with the solid lines and the semi-analytical results are represented with the dashed lines. The online version is depicted in color.

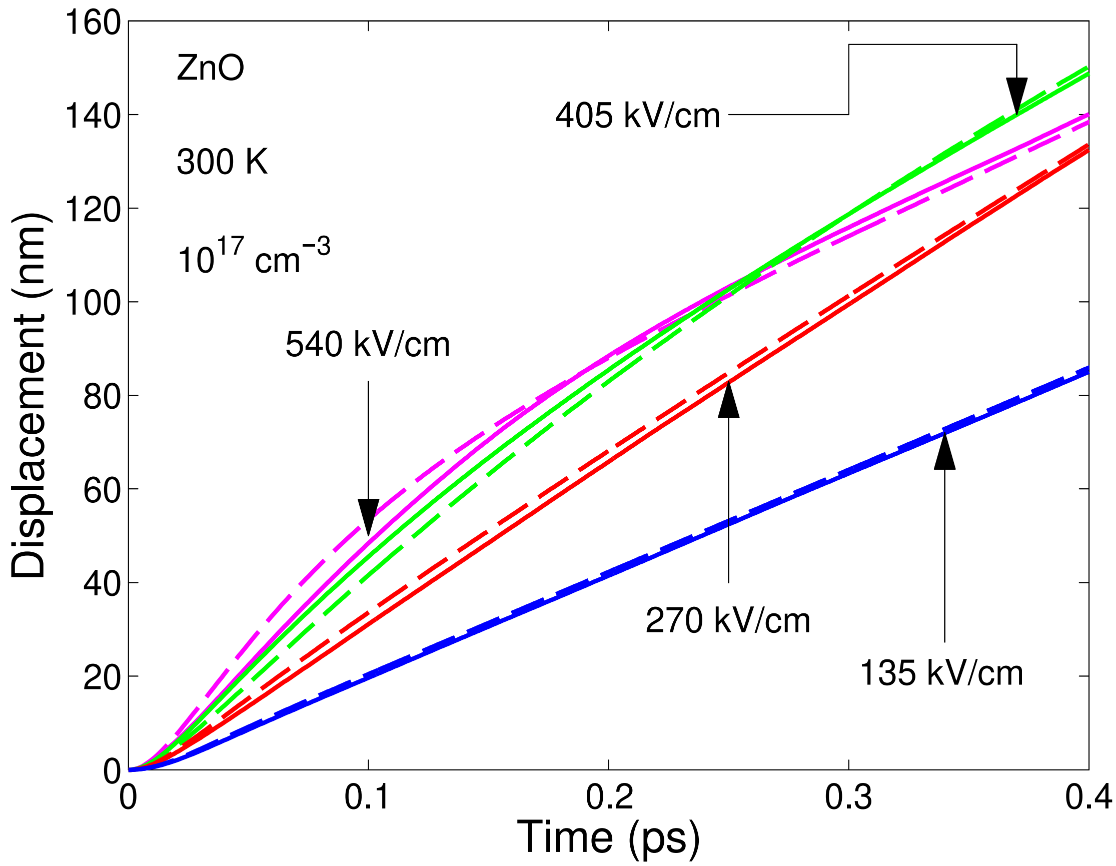

Figure 3.9: The electron displacement associated with bulk wurtzite ZnO as a function of the time elapsed since the onset of the applied electric field. For all cases, we have assumed an initial zero-field electron distribution, a crystal temperature of 300 K, and a doping concentration of 10^{17} cm^{-3}. The Monte Carlo results are depicted with the solid lines and the semi-analytical results are represented with the dashed lines. The online version is depicted in color.

540 kV/cm are chosen, these corresponding to half-multiples of the peak field associated with wurtzite ZnO. The results corresponding to the Monte Carlo simulations are depicted with the solid lines while the results of the semi-analytical technique are depicted with the dashed lines. The same Monte Carlo simulations and semi-analytical computations, employed in the determination of Figures 3.3 and 3.6, are used in order to determine these plots. We note that for most of the applied electric field strength selections considered, the semi-analytical results form an upper bound on the Monte Carlo results, although the case of 540 kV/cm seems to counter this trend for times beyond 0.2 ps. The differences between the Monte Carlo results and those of the semi-analytical approach are noted to be quite small for the case of this material. We speculate that the closeness of the semi-analytical results to those of our Monte Carlo simulations is probably related to the limited upper valley occupancy that occurs for the case of wurtzite ZnO, as opposed to the cases of zinc-blende GaAs and wurtzite GaN. Further work will be performed in Section 3.5 in order to buttress this supposition.

3.5 Upper valley occupancy and the agreement between the semi-analytical approach and that of our Monte Carlo simulations

One could speculate that the lack of upper valley occupancy that occurs for the specific case of wurtzite ZnO is what might be responsible for the closeness of the Monte Carlo simulation results with those of our semi-analytical approach. In order to put this conjecture to the test, in this section, with all other material parameters being set to their nominal bulk wurtzite ZnO values, i.e., those values set in Table 3.1 and 3.2, we examine the impact that variations in the non-parabolicity coefficient, α, have on the closeness between the semi-analytical results and those of our Monte Carlo simulations; the non-parabolicity coefficient, α, is nominally set to 0.66 eV^{-1} for the case of wurtzite ZnO, as is seen in Table 3.2. In Figure 3.10, we plot the electron drift velocity associated with bulk wurtzite ZnO as a function of the time elapsed since the onset of the applied electric field for a number of non-parabolicity coefficient selections. For all cases considered, the crystal temperature is set to 300 K and the doping concentration is set to 10^{17} cm^{-3}. The electric field strength selections are set to twice the peak field of the corresponding steady-state velocity-field characteristic for each case; the peak fields are found to be 160, 200, and 270 kV/cm, for the cases of the non-parabolicity coefficient, α, set to 0.0, 0.2, and 0.66 eV^{-1}, respectively. It is noted that the closeness between the semi-analytical results and that of our Monte Carlo simulations seems to improve as the non-parabolicity coefficient increases. As was mentioned by Hadi *et al.* [43], greater non-parabolicity inhibits upper energy conduction band valley occupancy. This may be seen in Figure 3.11, in which we plot the occupancy of the lowest energy conduction band valley, Γ_1, within wurtzite ZnO, as a function of time for the same non-parabolicity

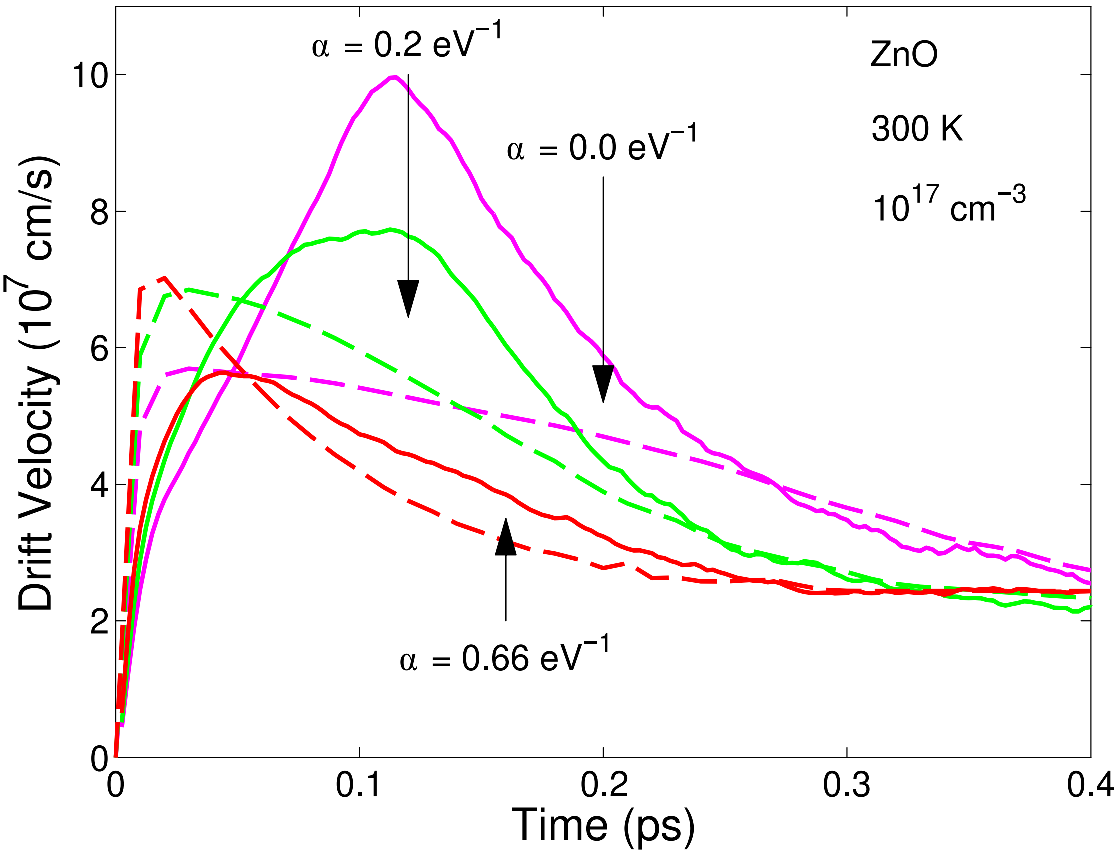

Figure 3.10: The electron drift velocity associated with bulk wurtzite ZnO as a function of the time elapsed since the onset of the applied electric field for a number of selections of the non-parabolicity coefficient, α. The other bulk wurtzite ZnO material values are set to their nominal values, i.e., those set in Tables 3.1 and 3.2. The applied electric field strength is set to twice the peak field for each case. For all cases, we have assumed an initial zero-field electron distribution, a crystal temperature of 300 K, and a doping concentration of 10^{17} cm^{-3}. The Monte Carlo results are depicted with the solid lines and the semi-analytical results are represented with the dashed lines. The online version is depicted in color.

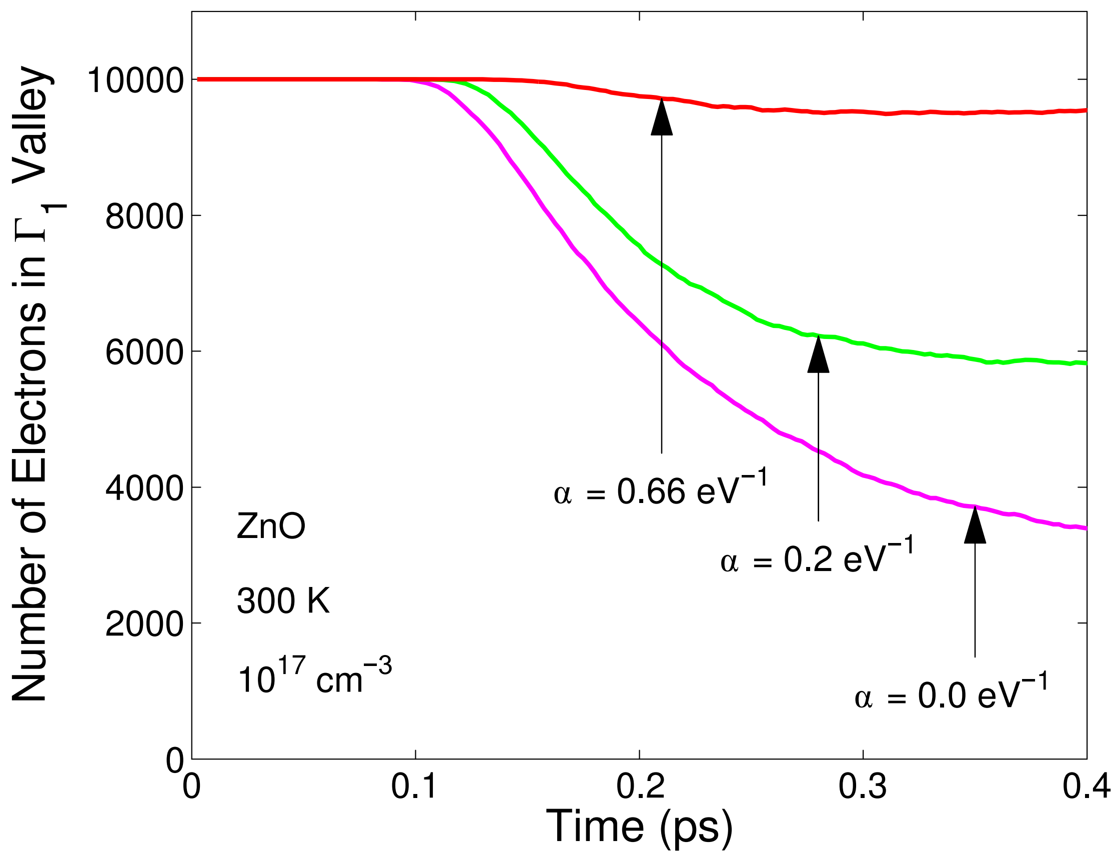

Figure 3.11: The number of electrons in the lowest energy conduction band valley, Γ_1, as a function of the time elapsed since the onset of the applied electric field for a number of selections of the non-parabolicity coefficient, α, for the case of bulk wurtzite ZnO. The other bulk wurtzite ZnO material values are set to their nominal values, i.e., those set in Tables 3.1 and 3.2. The applied electric field strength is set to twice the peak field for each case. For all cases, we have assumed an initial zero-field electron distribution, a crystal temperature of 300 K, and a doping concentration of 10^{17} cm^{-3}. These results correspond to Monte Carlo simulations of the electron transport; the same simulations used to determine the results presented in Figure 3.10. The motion of 10,000 electrons is considered during each simulation. The online version is depicted in color.

coefficient selections as those considered in Figure 3.10; these results were obtained using the same electron transport simulations as those used to determine the results presented in Figure 3.10. Thus, less upper energy conduction band valley occupancy seems to be correlated with a greater closeness between the semi-analytical results and those of our Monte Carlo simulations.

3.6 Device Implications

The transient electron transport response of a material plays an important role in defining the limits on the device performance of electron devices fabricated from such materials. Noting that the cut-off frequency for an electron device

$$f_T = \frac{1}{2\pi\tau}, \tag{3.5}$$

where τ represents the transit-time across the device, a rough estimate for the dependence of the cut-off frequency on the device length may be obtained using the previously determined relationship between the electron displacement on the time elapsed since the onset of the applied electric field. This relationship, instead cast in terms of the cut-off frequency as a function of the device length, i.e., electron displacement, is depicted in Figure 3.12 for the cases of zinc-blende GaAs, wurtzite GaN, and wurtzite ZnO. In all cases, the electric field strength is set twice the peak field, i.e., 8 kV/cm for the case of zinc-blende GaAs, 280 kV/cm for the case of wurtzite GaN, and 540 kV/cm for the case of wurtzite ZnO; it should be noted, however, that optimal applied electric field strengths,

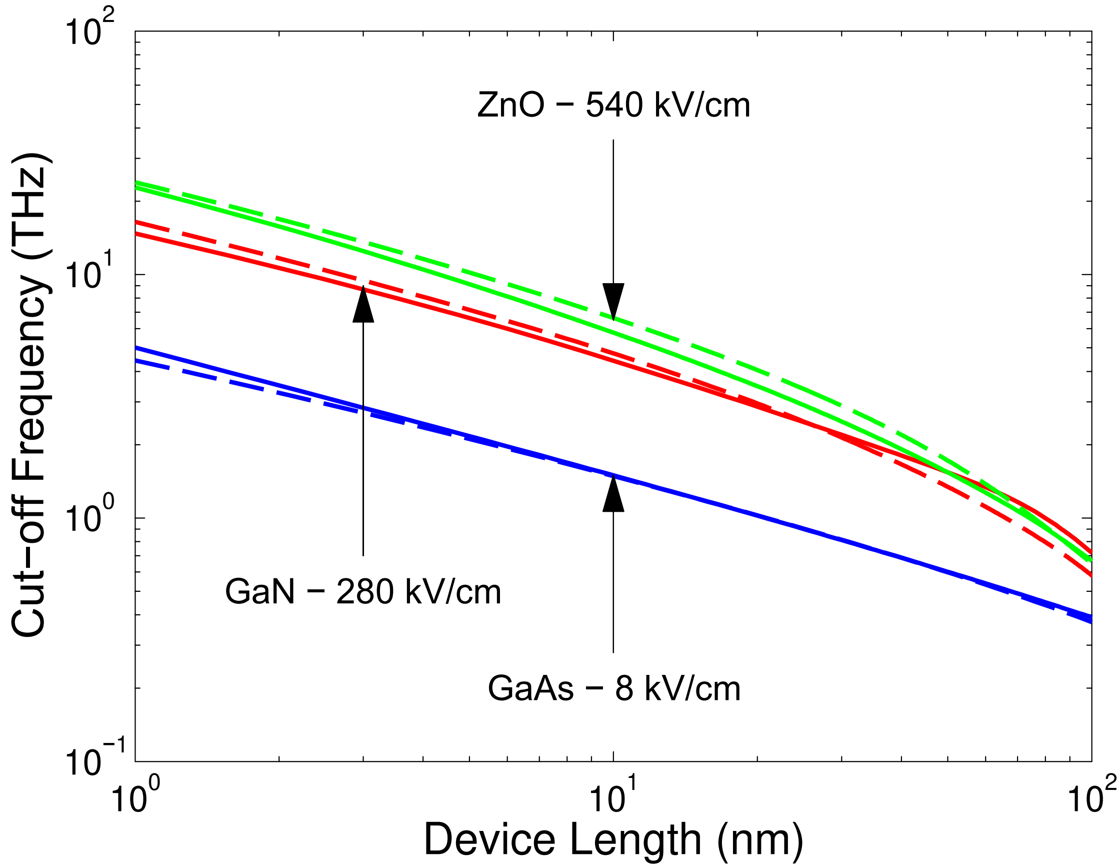

Figure 3.12: The cut-off frequency, f_T, determined from Eq. (3.5), as a function of the electron device length, L, for the cases of zinc-blende GaAs, wurtzite GaN, and wurtzite ZnO. For all cases, the applied electric field strength is set to twice the peak field, i.e., 8 kV/cm for the case of zinc-blende GaAs, 280 kV/cm for the case of wurtzite GaN, and 540 kV/cm for the case of wurtzite ZnO. The Monte Carlo results are depicted with the solid lines and the semi-analytical results are represented with the dashed lines. The online version is depicted in color.

i.e., those required in order to achieve the minimal transit-time for a given device length, may be greatly in excess of these field strengths. In all cases, results obtained through the use of Monte Carlo simulations are depicted with the solid curves while those obtained using the semi-analytical approach are shown with the dashed lines. It is seen that the results obtained from our Monte Carlo simulations are very close to those produced through the semi-analytical approach of Shur [48]. This suggests that this semi-analytical approach of Shur [48] may be used in order to assess the performance of electron device structures, offering a distinct advantage over Monte Carlo simulation, especially in cases where the fields are highly non-uniform or potentially time-varying.

3.7 Conclusions

We critically examined the applicability of the semi-analytical approach of Shur [48] in evaluating the transient electron transport response of zinc-blende GaAs, wurtzite GaN, and wurtzite ZnO. In particular, we contrasted results obtained from Monte Carlo simulations of the electron transport with those obtained using the semi-analytical approach of Shur [48]. Our approach was to examine the response of an ensemble of electrons to the application of a constant and uniform applied electric field. For the purposes of this analysis, three aspects of the transient electron transport were considered: (1) the dependence of the electron drift velocity on the time elapsed since the onset of the applied electric field, (2) the dependence of the average electron energy on the time elapsed since the onset of the applied electric field, and (3) the dependence of the average electron displacement on the time elapsed since the onset of the applied electric field. The results obtained showed that this semi-analytical approach of Shur [48] produces results that are very similar to those produced using Monte Carlo simulations. Thus, this semi-analytical approach of Shur [48] should be applicable for the treatment of non-uniform and time-varying electric fields, making it a useful tool for the treatment of the transient electron transport response within electron device configurations.

Acknowledgments: The authors gratefully acknowledge financial support from the Natural Sciences and Engineering Research Council of Canada. The work at Rensselaer Polytechnic Institute (M. S. Shur) was supported primarily through the Engineering Research Centers program of the National Science Foundation under the NSF Cooperative Agreement No. EEC-0812056 and in part by New York State under NYSTAR contract C090145.

References

[1] C. Liu, F. Yun and H. Morkoç, "Ferromagnetism of ZnO and GaN: a review," *Journal of Materials Science: Materials in Electronics*, vol. 16, no. 9, pp. 555-597, 2005.

[2] Ü. Özgür, Ya. I. Alivov, C. Liu, A. Teke, M. A. Reshchikov, S. Doğan, V. Avrutin, S.-J. Cho, and H. Morkoç, "A comprehensive review of ZnO materials and devices," *Journal of Applied Physics*, vol. 98, no. 4, pp. 041301-1-103, 2005.

[3] A. Ashrafi and C. Jagadish, "Review of zincblende ZnO: stability of metastable ZnO phases," *Journal of Applied Physics*, vol. 102, no. 7, pp. 071101-1-12, 2007.

[4] R. P. Davies, C. R. Abernathy, S. J. Pearton, D. P. Norton, M. P. Ivill, and F. Ren, "review of recent advances in transition and lanthanide metal-doped GaN and ZnO," *Chemical Engineering Communications*, vol. 196, no. 9, pp. 1030-1053, 2009.

[5] Ü. Özgür, D. Hofstetter, and H. Morkoç, "ZnO devices and applications: a review of current status and future prospects," *Proceedings of the IEEE*, vol. 98, no. 7, pp. 1255-1268, 2010.

[6] F. Scholz, "Semipolar GaN grown on foreign substrates: a review," *Semiconductor Science and Technology*, vol. 27, no. 2, pp. 024002-1-15, 2012.

[7] R.S. Pengelly, S.M. Wood, J.W. Milligan, S.T. Sheppard, and W.L. Pribble, "A Review of GaN on SiC High Electron-Mobility Power Transistors and MMICs," *IEEE Transactions on Microwave Theory and Techniques*, vol. 60, no. 6, pp. 1764-1783, 2012.

[8] S. Strite and H. Morkoç, "GaN, AlN, and InN: A review," *Journal of Vacuum Science and Technology B*, vol. 10, no. 4, pp. 1237-1266, 1992.

[9] H. Morkoç and Ü. Özgür, *Zinc oxide*: *Fundamentals, Materials and Device Technology*. Weinheim, Germany: Wiley-VCH, 2009.

[10] H. P. Markusa and J. J. Tietjen, "The preparation and properties of vapor-deposited single-crystalline GaN," *Applied Physics Letters*, vol. 15, no. 10, pp. 327-329, 1969.

[11] D. Visalli, M. Van Hove, P. Srivastava, J. Derluyn, J. Das, M. Leys, S. Degroote, K. Cheng, M. Germain, and G. Borghs, "Experimental and simulation study of breakdown voltage enhancement of AlGaN/GaN heterostructures by Si substrate removal," *Applied Physics Letters*, vol. 97, no. 11, pp. 113501-1-3, 2010.

[12] I. B. Rowena, S. L. Selvaraj, and T. Egawa, "Buffer Thickness Contribution to Suppress Vertical Leakage Current With High Breakdown Field (2.3 MV/cm) for GaN on Si," *IEEE Electron Device Letters,* vol. 32, no. 11, pp. 1534-1536, 2011.

[13] B. A. Danilchenko, I. A. Obukhov, T. Paskiewicz, S. Wolski, and A. Jeżowski, "On the upper limit of thermal conductivity GaN crystals," *Solid State Communications*, vol. 144, no. 3-4, pp. 114-117, 2007.

[14] K. Jagannadham, E.A. Berkman, and N. Elmasry, "Thermal conductivity of semi insulating, *p*-type, and *n*-type GaN films on sapphire," *Journal of Vacuum Science and Technology A*, vol. 26, no. 3, pp. 375-379, 2008.

[15] B. E. Foutz, S. K. O'Leary, M. S. Shur and L. F. Eastman, "Transient electron transport in wurtzite GaN, InN and AlN," *Journal of Applied Physics*, vol. 85, no. 11, pp. 7727-7734, 1999.

[16] S. K. O'Leary, B. E. Foutz, M. S. Shur, and L. F. Eastman, "Polar optical phonon instability and intervalley transfer in III-V semiconductors," *Solid State Communications*, vol. 118, no. 2, pp. 79-83, 2001.

[17] S. K. O'Leary, B. E. Foutz, M. S. Shur, and L. F. Eastman, "Steady-state electron transport in the III–V nitride semiconductors: A sensitivity analysis," *Journal of Electronic Materials*, vol. 32, no. 5, pp. 327-334, 2003.

[18] S. K. O'Leary, B. E. Foutz, M. S. Shur, and L. F. Eastman, "Steady-state and transient electron transport within the III–V Nitride semiconductors, GaN, AlN, and InN: A review," *Journal of Electronic Materials*, vol. 17, no. 2, pp. 87-126, 2006.

[19] M. Shur, M. Shatalov, A. Dobrinsky, and R. Gaska, "Deep UV LEDs," in *Advances in GaN and ZnO-based Thin Film, Bulk, and Nanostructured Materials and Devices* (Series in Materials Science), edited by S. Pearton. Berlin, Germany: Springer-Verlag, pp. 83-120, 2012.

[20] D. H. Levy and S. F. Nelson, "Thin-film electronics by atomic layer deposition," *Journal of Vacuum Science and Technology A*, vol. 30, no. 1, pp. 018501-1-9, 2012.

[21] H. Liu, V. Avrutin, N. Izyumskaya, Ü. Özgür, and H. Morkoç, "Transparent conducting oxides for electrode applications in light emitting and absorbing devices," *Superlattices and Microstructures* , vol. 48, no. 5, pp. 458-484, 2010.

[22] C. -K. Yang and K. S. Dy, "Band structure of ZnO using the LMTO method," *Solid State Communications*, vol. 88, no. 6, pp. 491-494, 1993.

[23] J. D. Albrecht, P. P. Ruden, S. Limpijumnong, W. R. L. Lambrecht, and K. F. Brennan, "High field electron transport properties of bulk ZnO," *Journal of Applied Physics,* vol. 86, no. 12, pp. 6864-6867, 1999.

[24] J. F. Muth, R. M. Kolbas, A. K. Sharma, S. Oktyabrsky, and J. Narayan, "Excitonic structure and absorption coefficient measurements of ZnO single crystal epitaxial films deposited by pulsed laser deposition," *Journal of Applied Physics,* vol. 85, no. 11, pp. 7884-7887, 1999

[25] D. K. Ferry, "High-field transport in wide-band-gap semiconductors," *Physical Review B*, vol. 12, no. 6, pp. 2361-2369, 1975.

[26] M. A. Littlejohn, J. R. Hauser, and T. H. Glisson, "Monte Carlo calculation of the velocity-field relationship for gallium nitride," *Applied Physics Letters*, vol. 26, no. 11, pp. 625-627, 1975.

[27] P. Das and D. K. Ferry, "Hot electron microwave conductivity of wide bandgap semiconductors," *Solid State Electronics*, vol. 19, no. 10, pp. 851-855, 1976.

[28] B. Gelmont, K. Kim, and M. Shur, "Monte Carlo simulation of electron transport in gallium nitride," *Journal of Applied Physics*, vol. 74, no. 3, pp. 1818-1821, 1993.

[29] V. W. L. Chin, T. L. Tansley, and T. Osotchan, "Electron mobilities in gallium, indium, and aluminum nitrides," *Journal of Applied Physics*, vol. 75, no. 11, pp. 7365-7372, 1994.

[30] N. S. Mansour, K. W. Kim, and M. A. Littlejohn, "Theoretical study of electron transport in gallium nitride," *Journal of Applied Physics*, vol. 77, no. 6, pp. 2834-2836, 1995.

[31] J. Kolník, İ. H. Oğuzman, K. F. Brennan, R. Wang, P. P. Ruden, and Y. Wang, "Electronic transport studies of bulk zincblende and wurtzite phases of GaN based on an ensemble Monte Carlo calculation including a full zone band structure," *Journal of Applied Physics*, vol. 78, no. 2, pp. 1033-1038, 1995.

[32] M. Shur, B. Gelmont, and M. A. Khan, "Electron mobility in two-dimensional electron gas in AIGaN/GaN heterostructures and in bulk GaN," *Journal of Electronic Materials*, vol. 25, no. 5, pp. 777-785, 1996.

[33] B. E. Foutz, L. F. Eastman, U. V. Bhapkar, and M. S. Shur, "Comparison of high field electron transport in GaN and GaAs," *Applied Physics Letters*, vol. 70, no. 21, pp. 2849-2851, 1997.

[34] U. V. Bhapkar and M. S. Shur, "Monte Carlo calculation of velocity-field characteristics of wurtzite GaN," *Journal of Applied Physics*, vol. 82, no. 4, pp. 1649-1655, 1997.

[35] J. D. Albrecht, R. P. Wang, P. P. Ruden, M. Farahmand, and K. F. Brennan, "Monte Carlo calculation of electron transport properties of bulk AlN," *Journal of Applied Physics*, vol. 83, no. 3, pp. 1446-1449, 1998.

[36] N. G. Weimann, L. F. Eastman, D. Doppalapudi, H. M. Ng, and T. D. Moustakas, "Scattering of electrons at threading dislocations in GaN," *Journal of Applied Physics*, vol. 83, no. 7, pp. 3656-3659, 1998.

[37] J. D. Albrecht, R. P. Wang, P. P. Ruden, M. Farahmand, and K. F. Brennan, "Electron transport characteristics of GaN for high temperature device modeling," *Journal of Applied Physics*, vol. 83, no. 9, pp. 4777-4781, 1998.

[38] D. C. Look, D. C. Reynolds, J. R. Sizelove, R. L. Jones, C. W. Litton, G. Cantwell, and W. C. Harsch, "Electrical properties of bulk ZnO," *Solid State Communications*, vol. 105, no. 6, pp. 399-401, 1998.

[39] B. Guo, U. Ravaioli, and M. Staedele, "Full band Monte Carlo calculations of velocity-field characteristics of wurtzite ZnO," *Computer Physics Communications*, vol. 175, no. 7, pp. 482-486, 2006.

[40] F. Bertazzi, M. Goano, and E. Bellotti, "Electron and Hole Transport in Bulk ZnO: A Full Band Monte Carlo Study," *Journal of Electronic Materials*, vol. 36, no. 8, pp. 857-863, 2007.

[41] E. Furno, F. Bertazzi, M. Goano, G. Ghione, and E. Bellotti, "Hydrodynamic transport parameters of wurtzite ZnO from analytic and full-band Monte Carlo simulation," *Solid-State Electronics*, vol. 52, no. 11, pp. 1796-1801, 2008.

[42] S. K. O'Leary, B. E. Foutz, M. S. Shur, and L. F. Eastman, "Steady-state and transient electron transport within bulk wurtzite zinc oxide," *Solid State Communications*, vol. 150, no. 43, pp. 2182-2185, 2010.

[43] W. A. Hadi, S. K. O'Leary, M. S. Shur, and L.F. Eastman, "The sensitivity of the steady-state electron transport within bulk wurtzite zinc oxide to variations in the non-parabolicity coefficient," *Solid State Communications*, vol. 151, no. 12, pp. 874-878, 2011.

[44] W. A. Hadi, M. S. Shur, and S. K. O'Leary, "A transient electron transport analysis of bulk wurtzite zinc oxide," *Journal of Applied Physics*, vol. 112, no. 3, pp. 033720-1-5, 2012.

[45] J. G. Ruch, "Electron dynamics in short-channel field-effect transistors," *IEEE Transactions on Electron Devices*, vol. 19, no. 5, pp. 652-654, 1972.

[46] M. S. Shur and L. F. Eastman, “Ballistic transport in semiconductor at low temperatures for low-power high-speed logic,” *IEEE Transactions on Electron Devices*, vol. 26, no. 11, pp. 1677-1683, 1979.

[47] S. K. O'Leary, B. E. Foutz, M. S. Shur, and L. F. Eastman, “Potential performance of indium-nitride-based devices,” *Applied Physics letters*, vol. 88, no. 15, pp. 152113-1-3, 2006.

[48] M. S. Shur, “Influence of non-uniform field distribution on frequency limits of GaAs field-effect transistors,” *Electronics Letters*, vol. 12, no. 23, pp. 615-616, 1976.

[49] W. Fawcett, A. D. Boardman, and S. Swain, “Monte Carlo determination of electron transport properties in gallium arsenide,” *Journal of Physics and Chemistry of Solids*, vol. 31, no. 9, pp. 1963-1990, 1970.

[50] P. Lugli and D. K. Ferry, “Degeneracy in the ensemble Monte Carlo method for high-field transport in semiconductors,” *IEEE Transactions on Electron Devices*, vol. 32, no. 11, pp. 2431-2437, 1985.

[51] K. Seeger, *Semiconductor Physics*: *An Introduction*, 9th ed. Berlin, Germany: Springer, 2004.

[52] S. K. O’Leary, B. E. Foutz, M. S. Shur, U. V. Bhapkar, and L. F. Eastman, “Electron transport in wurtzite indium nitride,” *Journal of Applied Physics*, vol. 83, no. 2, pp. 826-829, 1998.

[53] S. K. O’Leary, B. E. Foutz, M. S. Shur, U. V. Bhapkar, and L. F. Eastman, “Monte Carlo simulation of electron transport in wurtzite aluminum nitride,” *Solid State Communications*, vol. 105, no. 10, pp. 621-626, 1998.

[54] S. K. O’Leary, B. E. Foutz, M. S. Shur, and L. F. Eastman, “Steady-state and transient electron transport within bulk wurtzite indium nitride: An updated semiclassical three-valley Monte Carlo simulation analysis,” *Applied Physics Letters*, vol. 87, no. 22, 222103, 2005.

[55] S. K. O’Leary, B. E. Foutz, M. S. Shur, and L. F. Eastman, “The sensitivity of the electron transport within bulk wurtzite indium nitride to variations in the crystal temperature, the doping concentration, and the non-parabolicity coefficient: an updated Monte Carlo analysis,” *Journal of Materials Science: Materials in Electronics,* vol. 21, no. 3, pp. 218-230, 2010.

[56] W. A. Hadi, M. S. Shur, and S. K. O'Leary, “The sensitivity of the steady-state and transient electron transport within bulk wurtzite zinc oxide to variations in the crystal temperature, the doping concentration, and the non-parabolicity coefficient,” *Journal of Materials Science: Materials in Electronics*, vol. 24, no. 1, pp. 2-12, 2013.

[57] W. A. Hadi, R. Cheekoori, M. S. Shur, and S. K. O'Leary, “Transient electron transport in the III-V compound semiconductors gallium arsenide and gallium nitride,” *Journal of Materials Science: Materials in Electronics*, vol. 24, no. 2, pp. 807-813, 2013.

[58] S. Adachi, *Properties of Group-IV, III-V and II-VI Semiconductors*. Chichester, England: John Wiley and Sons, 2005.

CHAPTER 4

Determining the optimal applied electric field strength for a given electron displacement for the case of bulk wurtzite zinc oxide: A transient Monte Carlo analysis

A version of this manuscript was submitted to the Journal of Applied Physics. It is co-authored with Dr. M. S. Shur and my supervisor, Dr. S. K. O'Leary.

4.1 Introduction

ZnO is a II-VI semiconductor that has attracted a considerable amount of attention in recent years [1-4]. With its small effective mass, large intervalley energy separation, and large polar optical phonon energy, ZnO is expected to exhibit favourable electron transport characteristics [5]. A number of studies of the electron transport that occurs within this material have been reported over the years. Experimental measurements of the low-field mobility associated with ZnO were reported by Hutson [6] in 1957 and Look *et al*. [7] in 1998. Then, in 1999, Albrecht *et al*. [8] reported on Monte Carlo simulations of the steady-state electron transport that occurs within bulk wurtzite ZnO. Their analysis was pursued within the framework of a three-valley model for the conduction band. The primary goal of their analysis was the determination of the velocity-field characteristics associated with this material, i.e., how the electron drift velocity varies as a function of the applied electric field strength. An evaluation of the steady-state distribution of electron energies within an ensemble of electrons associated with bulk wurtzite ZnO, for different applied electric field strength selections, was also pursued.

More recent Monte Carlo analyzes of the steady-state electron transport that occurs within bulk wurtzite ZnO have also been reported. In 2006, Guo *et al*. [9] reported on a full-band Monte Carlo simulation of the electrons within bulk wurtzite ZnO. They focused on how the velocity-field characteristics associated with this material vary with the crystal temperature. The dependence of the average electron energy on the applied electric field strength was also examined. Then, in 2007, Bertazzi *et al*. [10] employed a full-band Monte Carlo simulation approach in order to characterize the steady-state electron and hole transport that occurs within this material. The velocity field characteristics associated with both the electrons and the holes associated with bulk wurtzite ZnO were determined. In 2008, Furno *et al*. [11] employed Monte Carlo simulations in order to critically compare the steady-state results obtained using a full-band treatment of the conduction band with that obtained using a single analytical valley, Furno *et al*. [11] asserting that the upper energy valleys are so high above the conduction band minimum that their neglect is reasonable even for higher applied electric field strength selections. As with the other Monte Carlo analyzes, the velocity-field and energy-field characteristics associated with this material were the primary focus of this analysis. Key aspects of these steady-state analyzes were reviewed by Morkoç and Özgür [12].

Then, in 2010, O'Leary *et al.* [13] analyzed the transient electron transport that occurs within bulk wurtzite ZnO. Following Foutz *et al.* [14, 15], within the framework of a three-valley model for the conduction band, O'Leary *et al*. [13] studied how electrons, initially in thermal equilibrium, respond to the sudden application of a constant applied electric field. They found that ZnO exhibits a pronounced transient electron transport response for applied electric field strengths in excess of the peak applied electric field. In particular, it was found that the peak transient electron drift velocities exhibited by bulk wurtzite ZnO are higher than the corresponding steady-state electron drift velocities and that the accompanying velocity overshoot effects occur over distances of the order of 100 nm. These results of O'Leary *et al.* [13] suggest that ZnO holds great promise for high-speed electron device applications.

Another recent study on the transient electron transport that occurs within bulk wurtzite ZnO was that reported by Arabshahi *et al*. [16], also in 2010; in fact, Arabshahi *et al*. [16] reports on the steady-state and transient electron transport that occurs within bulk wurtzite ZnO, as well as that that occurs in a number of other wide energy gap semiconductors. For the purposes of their analysis of the transient electron transport within this material, a similar approach to that employed by O'Leary *et al*. [13] was employed. They find similar results to those found by O'Leary *et al*. [13], although differences between the results are noted. Differences in the material parameter selections, made by O'Leary *et al*. [13] and Arabshahi *et al*. [16], probably account for most of the differences between these results. Further studies into the nature of the electron transport within bulk wurtzite ZnO were performed by Hadi *et al*. [17-21].

In this paper, we determine the applied electric field strength required in order to minimize the transit-time, τ, for a given electron transit displacement, L, for the case of bulk wurtzite ZnO. We perform this analysis within the context of a transient analysis of the electron transport that occurs within this material. Our approach to modeling the transient electron transport of the electrons will follow the approach of Foutz *et al*. [14, 15] and O'Leary *et al.* [22, 23], i.e., we study how an ensemble of electrons, initially in thermal equilibrium, respond to the sudden application of a constant applied electric field strength, the point at which this field is applied corresponding to the moment when the electrons start their transit. A three-valley Monte Carlo simulation approach is employed for the purposes of this analysis. From this analysis, we aim to quantitatively estimate an upper bound on the ideal performance of a ZnO-based device, noting that the non-idealities found in real device structures will detract from these ideal estimates. A similar analysis was performed for the case of bulk wurtzite indium nitride (InN) by O'Leary *et al.* [23]. The present analysis parallels that of O'Leary *et al*. [23].

This paper is organized in the following manner. In Section 4.2, we present our view of wurtzite ZnO, as a potential future material for high-field electron device applications. Then, in Section 4.3, our three-valley Monte Carlo electron transport simulations are described. In Section 4.4, the results of our analysis are presented. Finally, in Section 4.5, the conclusions of this analysis are drawn.

4.2 ZnO for high-field electron device applications

At the outset, we would like to point out that the future electron devices that we are considering are ones that have yet to be realized, both in terms of the quality of the materials employed and in terms of the scale of the device features envisaged. At present, ZnO is predominantly being considered for use in thin-film transistor device applications [12]. Typically, the device applications contemplated for such transistors involve low-fields and materials that are deposited in thin-film form. Moreover, the scale of the device features considered are quite large by modern electron device standards, i.e., of the order of a micron. For the purposes of this analysis, however, we are instead interested in looking at the potential of this material for high-speed and high-frequency electron device applications where the ZnO material considered is of a high-quality crystalline form and the device features could potentially scale down to the tens of nanometres. Essentially, we view ZnO as a potential competitor to gallium nitride (GaN) for such device applications, and we are looking to critically assess the potential of ZnO in such device applications.

It should be pointed out that some have suggested a low breakdown field for the case of this material. Sasa *et al.* [24], for example, has suggested a breakdown field of below 100 kV/cm for the case of ZnO. If this were the case, transient electron transport effects would not be in evidence, as O'Leary *et al*. [13] demonstrated that transient electron transport effects only occur for applied electric field strengths in excess of 270 kV/cm for the case of bulk wurtzite ZnO. We would like to point out, however, that while breakdown is indeed in evidence in the experimental results of Sasa *et al.* [24], non-uniformities in the electric field distribution preclude the determination of its exact value; the particular structures employed by Sasa *et al*. [24] are known to exhibit large non-uniformities in their electric field distributions. Breakdown will initiate when the highest electric field in a given device structure exceeds the breakdown field. Thus, the determination of an average electric field strength corresponding to the onset of breakdown, determined simply by dividing the voltage difference between two points by the distance separating these points, provides a poor measure of the breakdown field. Li *et al.* [25] suggest breakdown fields that are even smaller, i.e., of the order of 1 kV/cm, albeit for ZnO that is polycrystalline in form. Clearly, the non-uniform nature of this particular form of ZnO is leading to this much lower breakdown field.

We assert that these values for the breakdown field are unrepresentative of pure intrinsic crystalline ZnO. A compelling argument in favour of a much higher breakdown field for this material may be achieved when one examines the breakdown fields exhibited by other semiconductors. In Figure 4.1, we plot the dependence of the breakdown field on the energy gap for a number of compound and elemental semiconductors, the values employed in this plot being drawn from a variety of references from the literature. While this dependence of the breakdown field on the energy gap is not without statistical scatter, the results presented compel one to conclude

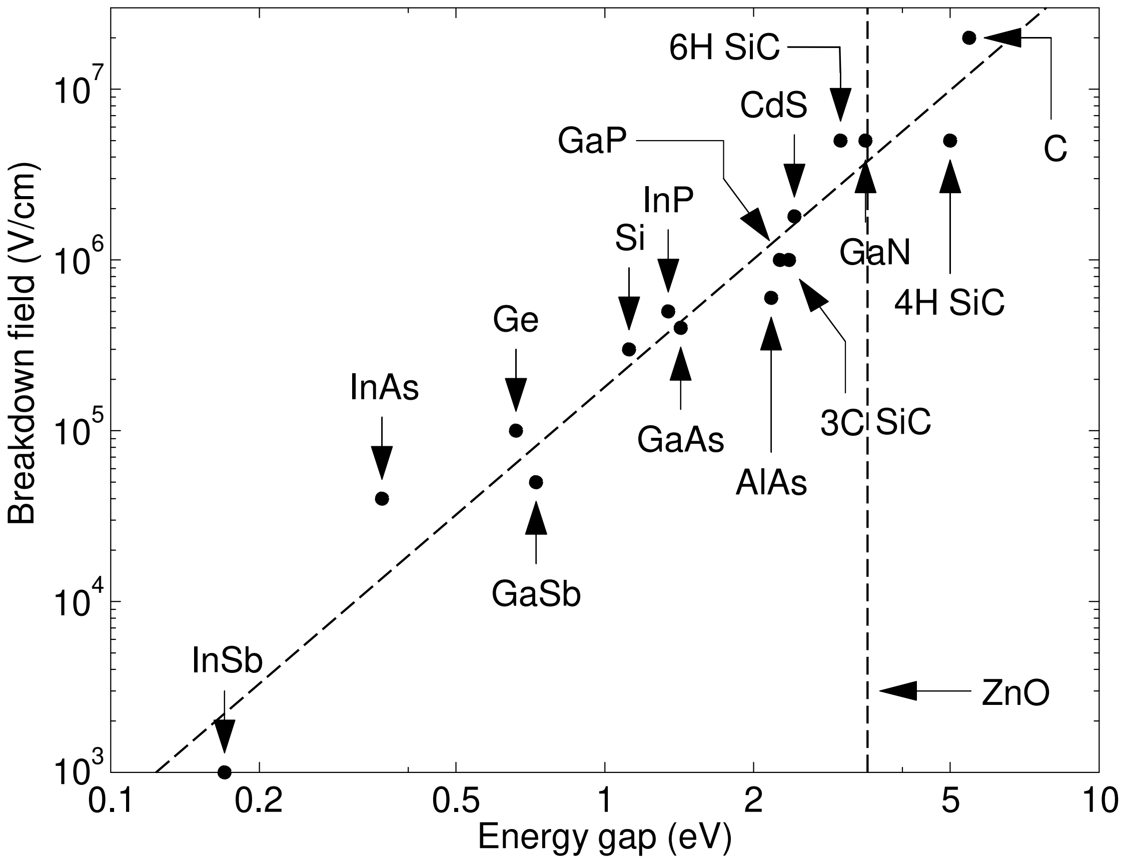

Figure 4.1: The breakdown electric field strength plotted as a function of the energy gap for selected elemental and compound semiconductors. This plot is depicted on a logarithmic scale.

that the breakdown field associated with crystalline ZnO, whose energy gap is around 3.4 eV, is at least 1 MV/cm, and most likely between 2 and 5 MV/cm. Adachi [26], for example, project a breakdown field of 3.5 MV/cm for the case of this material. Thus, transient electron transport is expected to make a significant impact upon the performance of ZnO-based electron devices when they are operated at high electric fields.

4.3 Monte Carlo simulations

We cast the entire analysis within the framework of a transient electron transport analysis. In particular, we employ ensemble semiclassical three-valley Monte Carlo simulations of the electron transport within bulk wurtzite ZnO. For all of these simulations, the motion of 10,000 electrons is examined. The scattering mechanisms considered are: (1) ionized impurity, (2) polar optical phonon, (3) piezoelectric, and (4) acoustic deformation potential. Intervalley scattering is also considered. The crystal temperature is set to 300 K and the doping concentration is set to 10^{17} cm^{-3} for all cases. Electron degeneracy effects are accounted for by means of the rejection technique of Lugli and Ferry [27]. Electron screening is also accounted for following the Brooks-Herring method [28]. The material and band structural parameter selections, employed for our simulations of the electron transport within bulk wurtzite ZnO, are from O'Leary *et al.* [13] and Hadi *et al.* [29, 30]; these material and band structural parameter selections are tabulated in Tables 4.1 and 4.2, respectively. Further details of our Monte Carlo simulation approach are presented in the literature [14, 15, 22, 23, 29, 31-36].

Table 4.1: The material parameter selections corresponding to bulk wurtzite ZnO that are employed for the purposes of this analysis. The source of each parameter is identified.

Parameter	ZnO	Reference
Mass density (g/cm^3)	5.68	[26]
Longitudinal sound velocity(cm/s)	4.00×10^5	determined through fit
Transverse sound velocity (cm/s)	2.7×10^5	[9]
Acoustic deformation potential (eV)	3.83	[8]
Static dielectric constant	8.2	[8]
High frequency dielectric constant	3.7	[8]
Effective mass (Γ_1 valley)	0.17 m_e	[8]
Piezoelectric constant, e_{14} (C/cm^2)	3.75×10^{-5}	determined through fit
Direct energy gap (eV)	3.4	[8]
Polar optical phonon energy (meV)	72	[8]
Intervalley deformation potentials (eV/cm)	10^9	[8]
Intervalley phonon energies (meV)	72	[8]

Table 4.2: The band structure parameter selections corresponding to bulk wurtzite ZnO. These band structure parameter selections are mostly from Albrecht *et al.* [8].

	Valley number	1	2	3
ZnO	Valley location	Γ_1 [8]	Γ_1 [8]	L-M [8]
	Valley degeneracy	1	1	6
	Effective mass	0.17 m_e [8]	0.42 m_e [8]	0.7 m_e [8]
	Intervalley energy separation (eV)	_	4.4 [8]	4.6 [8]
	Energy gap (eV)	3.4 [8]	7.8 [8]	8.0 [8]
	Non-parabolicity (eV^{-1})	0.66 [8]	0.15 [8]	0.0 [8]

4.4 Results

In Figure 4.2, we plot the electron drift velocity as a function of the time elapsed since the application of the electric field, for a number of different applied electric field strength selections, for the case of bulk wurtzite ZnO. For all cases, we assume an initial zero-field electron distribution, a crystal temperature of 300 K, and a doping concentration of 10^{17} cm^{-3} .We note that for the applied electric field strength selections 135 and 270 kV/cm, that the electron drift velocity reaches steady state very quickly, with little or no velocity overshoot. In contrast, for applied electric field strength selections in excess of 270 kV/cm, significant velocity overshoot occurs. This result suggests that in ZnO, for this particular selection of parameters and conditions, that 270 kV/cm is a critical applied electric field strength for the onset of velocity overshoot effects. O'Leary *et al*. [13] showed that 270 kV/cm also corresponds to the applied electric field strength at which point the peak in the steady-state velocity-field characteristic occurs for the case of bulk wurtzite ZnO for this particular selection of parameters and conditions (recall Figure 2a of O'Leary *et al*. [13]); we henceforth refer to this applied electric field strength as the peak field. This suggests that the velocity overshoot that occurs within bulk wurtzite ZnO is related to the presence of the peak in the steady-state velocity-field characteristic.

It is interesting to note that for all applied electric field strengths beyond 270 kV/cm, that a clear peak in the transient electron drift velocity is observed. In particular, peak transient electron drift velocities of around 4.7×10^7 cm/s at 0.062 ps, 5.6×10^7 cm/s at 0.045 ps, and 7.1×10^7 cm/s at 0.025 ps, are observed corresponding to the applied electric field strength selections 405, 540, and 1080 kV/cm, respectively. In

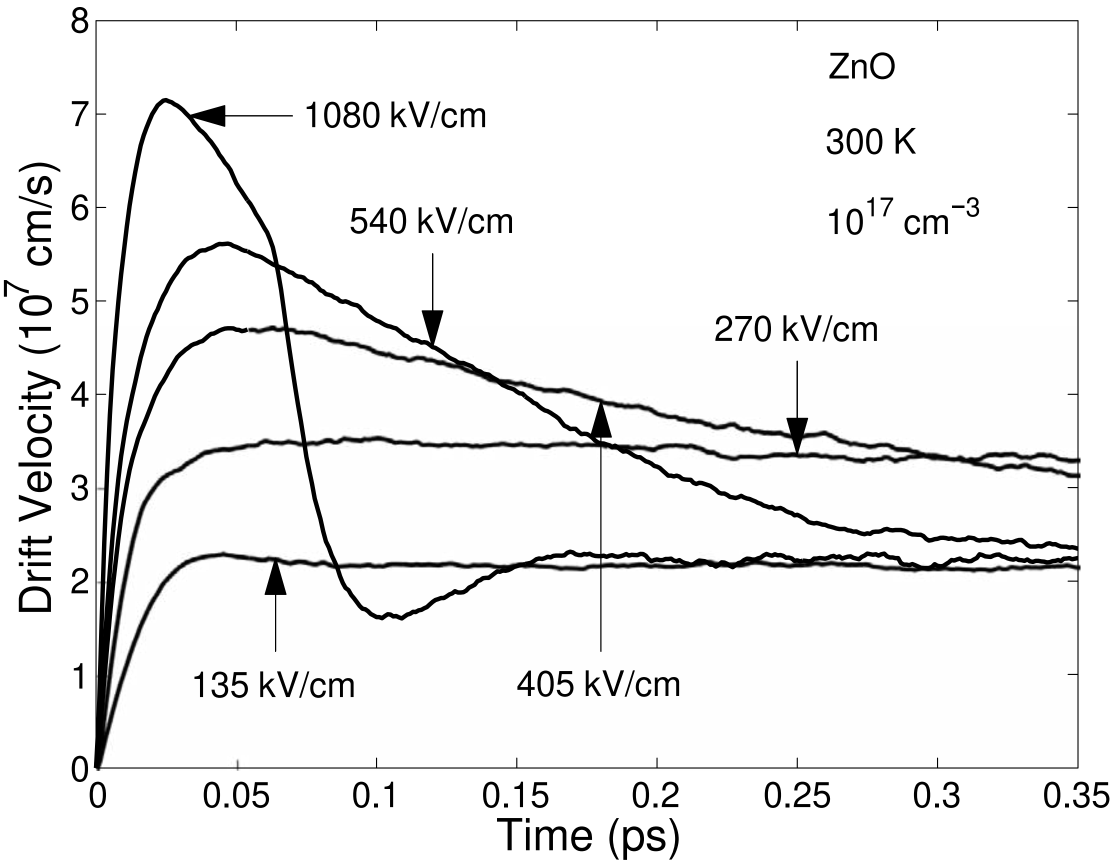

Figure 4.2: The electron drift velocity as a function of the time elapsed since the application of the electric field for the case of bulk wurtzite ZnO. We consider the applied electric field strength selections 135, 270, 405, 540, and 1080 kV/cm. For all cases, we have assumed an initial zero-field electron distribution, a crystal temperature of 300 K, and a doping concentration of 10^{17}cm^{-3}. A similar result was presented in Figure 4a of Hadi *et al.* [19] and Figure 1c of Hadi *et al.* [21].

Figure 4.3, we plot the peak transient electron drift velocity as a function of the applied electric field strength for a large number of applied field strengths, the peak transient electron drift velocity corresponding to each applied electric field strength relating to an individual Monte Carlo electron transport simulation; each Monte Carlo simulation is performed assuming an initial zero-field electron distribution, a crystal temperature of 300 K, and a doping concentration of 10^{17} cm^{-3}, as was assumed for the simulations used to determine the results depicted in Figure 4.2. For the cases in which a clear peak transient electron drift velocity was not easily discernible, we took the peak transient electron drift velocity to be the highest electron drift velocity between 0 and 0.4 ps. It is noted that the peak transient electron drift velocity monotonically increases with the applied electric field strength. The corresponding steady-state velocity-field characteristic associated with bulk wurtzite ZnO is also depicted in Figure 4.3. It is noted that the peak transient electron drift velocity appears to be essentially coincident with the steady-state velocity-field characteristic for applied electric field strengths less than the peak field, i.e., 270 kV/cm for the case of bulk wurtzite ZnO. Beyond this peak field, however, the transient electron drift velocity forms a loose upper bound on the steady-state velocity-field characteristic.

In Figure 4.4, we plot the distance displaced (electron transit displacement) since the application of the electric field as a function of the time elapsed, for a number of different applied electric field strength selections, for the case of bulk wurtzite ZnO. These plots are obtained through a numerical integration of the plots depicted in Figure 4.2. We note that the velocity overshoot that occurs substantially contributes to the initial rate of increase in the distance displaced. Eventually, however, steady-state

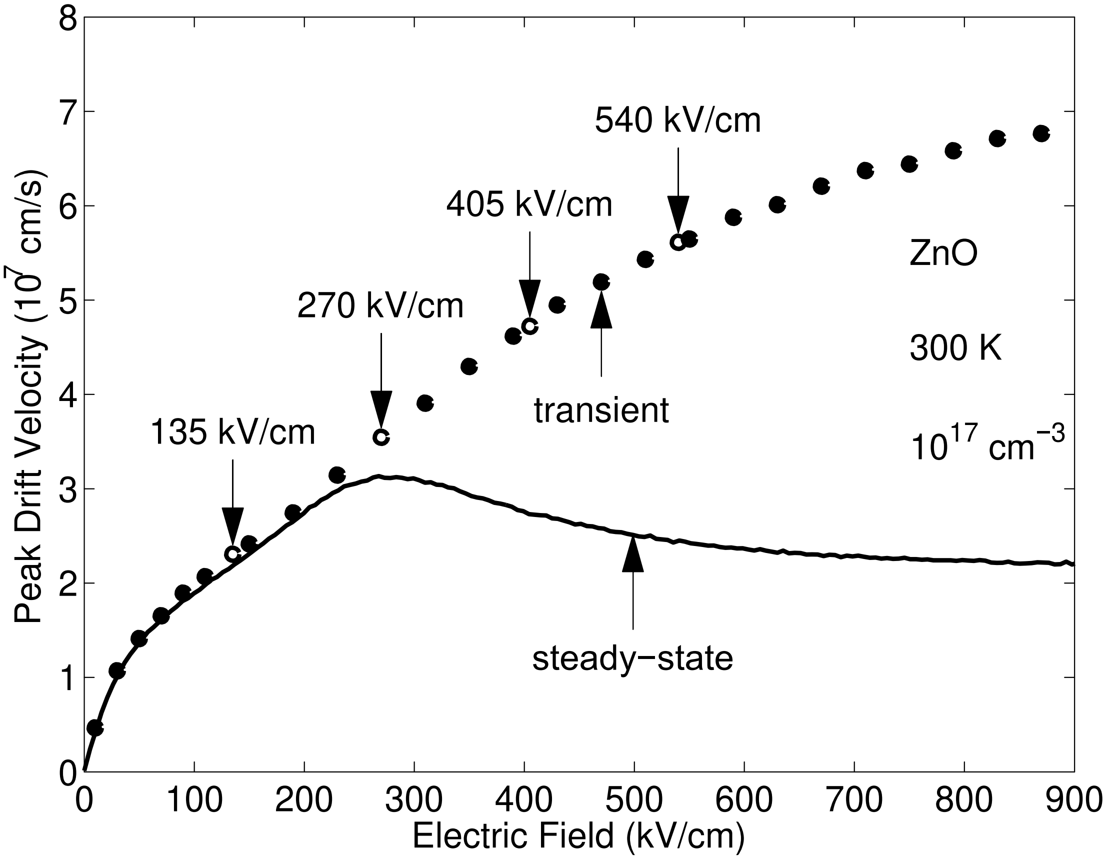

Figure 4.3: The peak transient electron drift velocity as a function of the applied electric field strength for the case of bulk wurtzite ZnO. These results are determined from Monte Carlo simulations of the electron transport, assuming an initial zero-field electron distribution, a crystal temperature of 300 K, and a doping concentration of 10^{17} cm^{-3}. The solid and open points depict results determined through the use of Monte Carlo simulations of the electron transport. The open points correspond to results depicted in Figure 4.2. The dependence of the steady-state electron drift velocity on the applied electric field strength, i.e., the velocity-field characteristic associated with bulk wurtzite ZnO, is also depicted with a solid line.

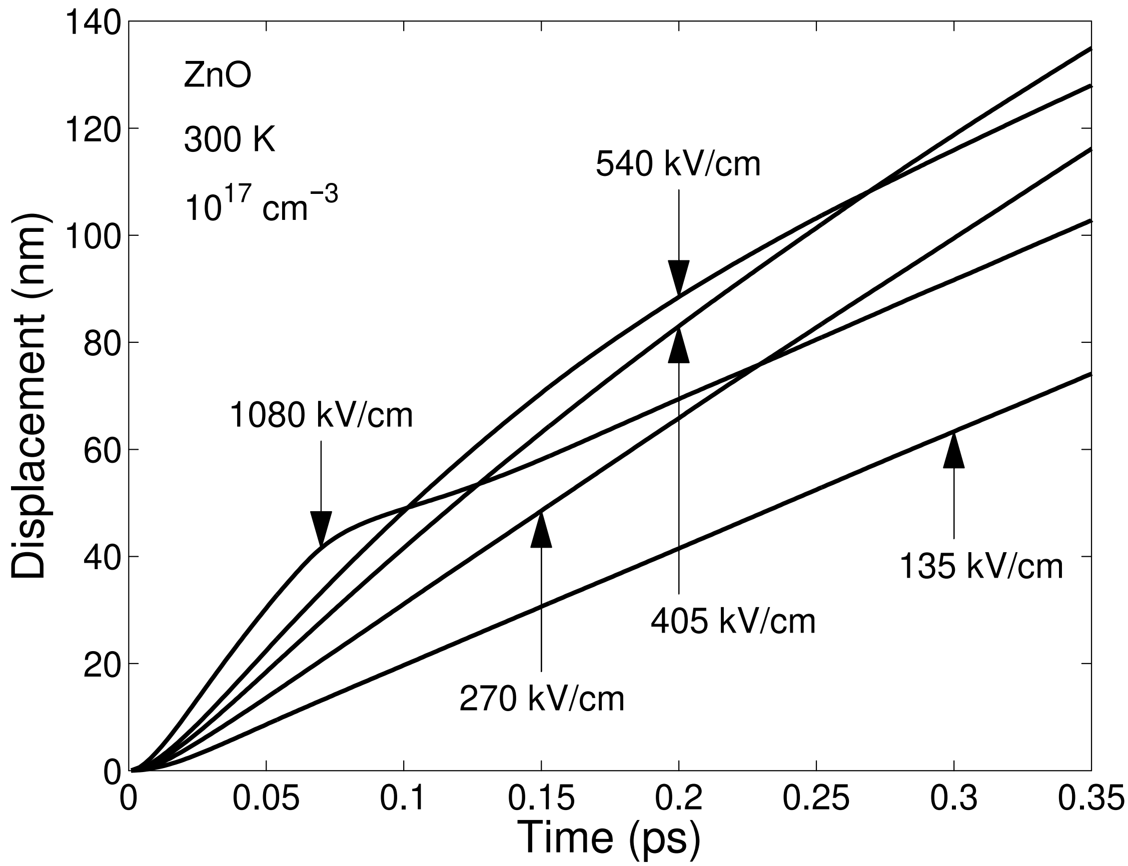

Figure 4.4: The distance displaced since the onset of the applied electric field as a function of the time elapsed for the case of bulk wurtzite ZnO. We consider the applied electric field strength selections 135, 270, 405, 540, and 1080 kV/cm. For all cases, we have assumed an initial zero-field electron distribution, a crystal temperature of 300 K, and a doping concentration of 10^{17}cm^{-3}. A similar result was presented in Figure 4b of Hadi *et al.* [19] and Figure 3c of Hadi *et al.* [21].

conditions are achieved, and the electron drift velocity settles to its corresponding steady-state value. It is noted that for a given displacement, *L*, that there exists an optimal applied electric field strength that will minimize the corresponding time-to-transit, τ . For *L* set to 100 nm, from Figure 4.4 it is seen that for the cases of the applied electric field strength selections set to 270, 405, 540, and 1080 kV/cm, that the corresponding times-to-transit, τ, are 0.302, 0.246, 0.239, and 0.338 ps, respectively; for the case of the applied electric field strength selection set to 135 kV/cm, the corresponding time-to-transit 100 nm is found to be 0.468 ps, beyond the range depicted in Figure 4.4. A detailed analysis, the results of which are presented in Figure 4.5, suggests that the time-to-transit across 100 nm, τ, is minimized when the applied electric field strength is between 450 and 500 kV/cm, τ being about 0.24 ps for this range of applied electric field strengths. We henceforth refer to the applied electric field strength that provides for the minimal time-to-transit as the optimal applied electric field strength.

We now determine the minimal time-to-transit, τ_{min}, corresponding to selections of *L* ranging between 10 and 1000 nm. For each selection of *L*, the optimal applied electric field strength is determined using the procedure illustrated in Figure 4.5. In Figure 4.6, we plot the optimal applied electric field strength as a function of *L*, noting that as *L* is increased that this optimal applied electric field strength monotonically decreases, eventually settling at the peak field; recall from Figure 2a of O'Leary *et al.* [13] that this peak field is about 270 kV/cm. This makes sense as the minimum time-to-transit across a long displacement will be achieved by the highest steady-state electron drift velocity, and this occurs at the peak field, 270 kV/cm, i.e., across a long distance, following an initial transient response, most of the electron transit

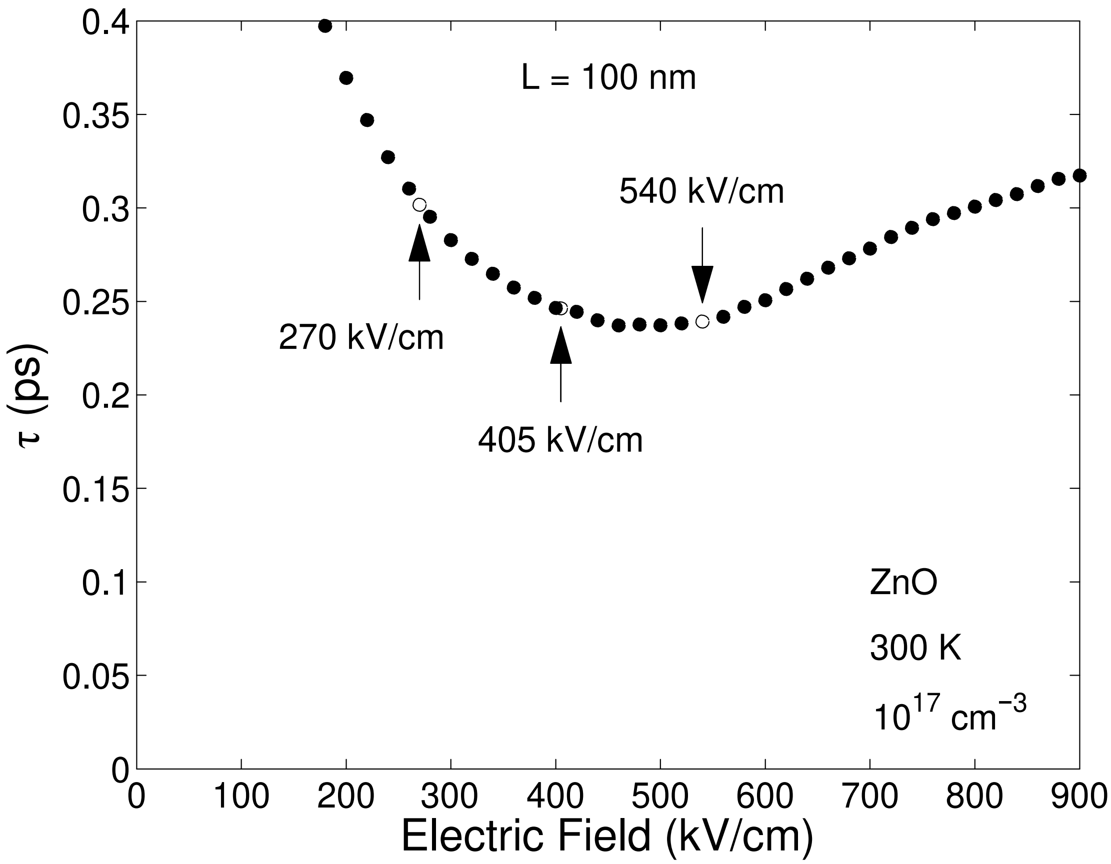

Figure 4.5: The time-to-transit as a function of the applied electric field strength for *L* set to 100 nm for the case of bulk wurtzite ZnO. The solid and open points depict results determined through the use of our Monte Carlo simulations of electron transport. The open points correspond to the results depicted in Figure 4.4. For all cases, we have assumed an initial zero-field electron distribution, a crystal temperature of 300 K, and a doping concentration of 10^{17} cm^{-3}.

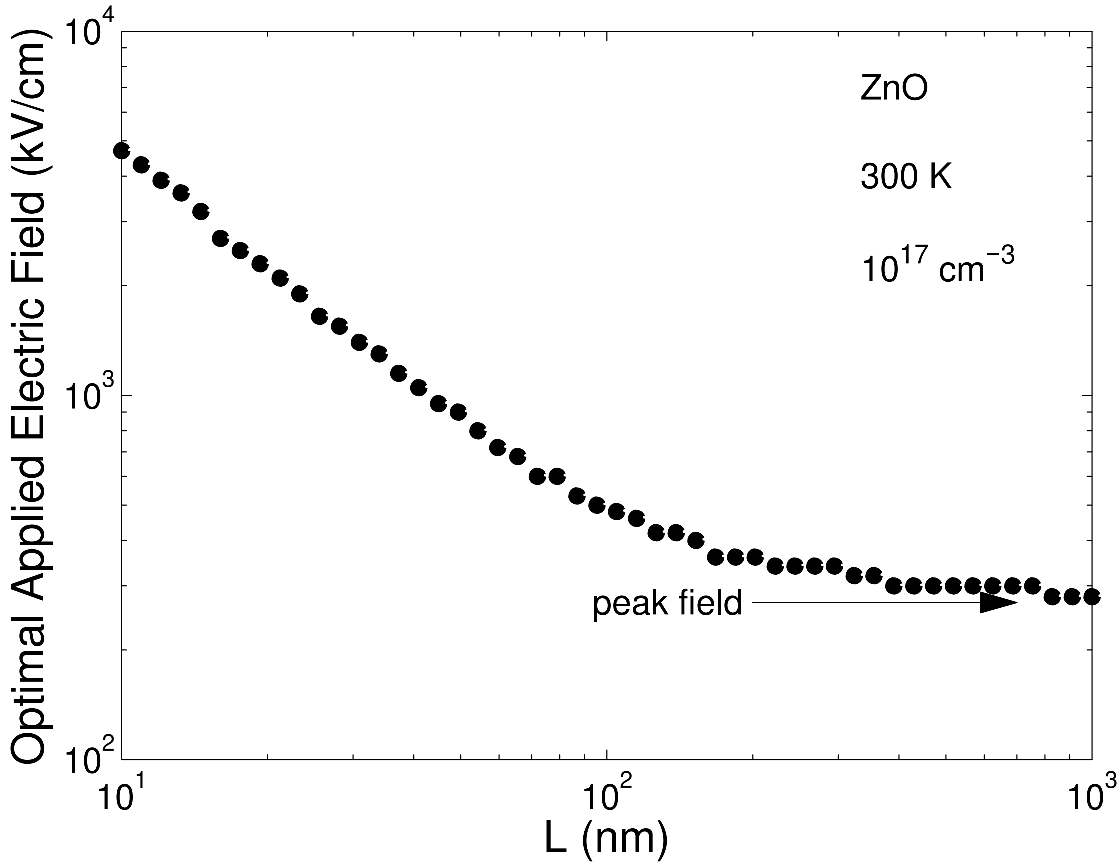

Figure 4.6: The optimal applied electric field strength plotted as a function of the electron displacement, *L*, for the case of bulk wurtzite ZnO. These results were obtained using the optimization procedure illustrated in Figure 4.5 for various displacement selections. As a point of reference, the peak field is depicted with the arrow. For all cases, we have assumed an initial zero-field electron distribution, a crystal temperature of 300 K, and a doping concentration of 10^{17} cm^{-3}.

will be steady-state in nature, the minimum time-to-transit in steady-state being achieved at the peak electron drift velocity.

We now employ these results in order to provide an upper bound on the performance of ZnO-based electron devices. Noting that the cut-off frequency for a device,

$$f_T = \frac{1}{2\pi\tau}, \tag{4.1}$$

it is seen that by setting τ to $\tau_{\min}$ that the optimal cut-off frequency for such a device may be obtained. In Figure 4.7, we plot the optimal cut-off frequency for an ideal ZnO-based device as a function of the device length, L, where we have assumed that the electron transport within such a device occurs only across its length, i.e., the device length corresponds to the displacement, L; our determination of the optimal cut-off frequency may be viewed as that corresponding to an ideal ZnO-based device operating at the optimal applied electric field strength, the non-idealities found in real device structures detracting from this estimate. We find that the optimal cut-off frequency of an ideal ZnO-based device ranges from around 50.3 GHz when the device length is set to 1000 nm to about 11.5 THz when the device length is set to 10 nm.

It is instructive to contrast the results obtained through our Monte Carlo simulations of the electron transport within bulk wurtzite ZnO, these taking into account the transient electron transport response of this material, with those obtained solely through steady-state considerations. We note that for steady-state electron transport, across a device of length L,

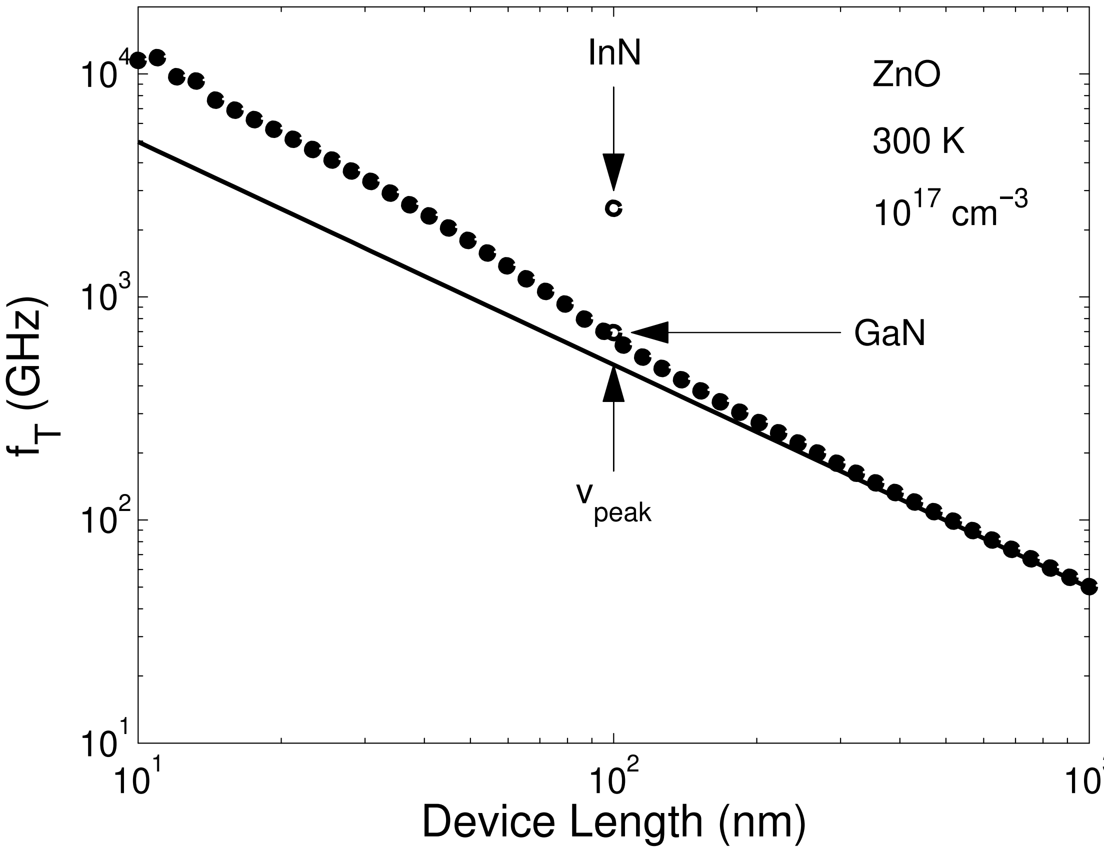

Figure 4.7: The optimal cut-off frequency plotted as a function of the device length for the case of an ideal ZnO-based electron device. The solid points depict results determined through the use of our Monte Carlo simulations of electron transport within bulk wurtzite ZnO; we employed the optimization procedure illustrated in Figure 4.5 for all the device length selections considered. For all cases, we have assumed an initial zero-field electron distribution, a crystal temperature of 300 K, and a doping concentration of 10^{17} cm^{-3}. The steady-state result, obtained through the use of Eqs. (4.1) and (4.2), is shown with the solid line. Results corresponding to the cases of bulk wurtzite GaN and bulk wurtzite InN, for the specific case of L set to 100 nm, are indicated with the open points. These results were also determined through similarly performed Monte Carlo electron transport simulations.

$$\tau = \frac{L}{v}, \tag{4.2}$$

where v denotes the corresponding steady-state electron drift velocity. By substituting the τ of Eq. (4.2) into Eq. (4.1), we can estimate the corresponding steady-state cut-off frequency. In Figure 4.7, we plot this steady-state cutoff frequency as a function of the device length, L, for v being set to the steady-state peak electron drift velocity, v_{peak}, for bulk wurtzite ZnO; Figure 2a of O'Leary *et al.* [13] suggests that v_{peak}, achieved at the peak field of about 270 kV/cm, is around 3.1×10^7 cm/s. We note that the optimized transient results asymptotically approach the peak electron drift velocity steady-state results in the long device limit. This arises as a consequence of the fact that in longer devices more of the transport is steady-state in character. This trend towards steady-state results as the device length is increased also explains why the optimal applied electric field strength asymptotically approaches the peak field in the long device limit; recall Figure 4.6.

4.5 Conclusions

In conclusion, we have studied how electrons, initially in thermal equilibrium, drift under the action of an applied electric field within bulk wurtzite ZnO. In particular, within the framework of a transient Monte Carlo analysis of the electron transport within this material, we determined the applied electric field strength that ensures the minimum time-to-transit for a given displacement. This analysis was performed for a range of displacements, and the optimal applied electric field strength was plotted as a function of the displacement. We then used these results in order to provide an upper bound on the potential performance of ZnO-based devices, assuming that the transit across a ZnO-based device occurs solely across the device length. We found that the optimal cut-off frequency ranges from around 50.3 GHz when the device length is set to 1000 nm to about 11.5 THz when the device length is set to 10 nm. This suggests that ZnO can be used as a potential material for terahertz radiation detection purposes, where the electromagnetic radiation and the electron drift are strongly coupled and parasitic reactive elements play an important role.

Acknowledgements: Two of the authors (W. A. H. and S. K. O.) gratefully acknowledge financial assistance from the Natural Sciences and Engineering Research Council of Canada. The work at Rensselaer Polytechnic Institute (M. S. Shur) was supported primarily through the Engineering Research Centers program of the National Science Foundation under the NSF Cooperative Agreement No. EEC-0812056 and in part by New York State under NYSTAR contract 17

References

[1] S. J. Pearton, D. P. Norton, K. Ip, Y. W. Heo, and T. Steiner, "Recent advances in processing of ZnO," *Journal of Vacuum Science and Technology B*, vol. 22, no. 3, pp. 932-938, 2004.

[2] Ü. Özgür, Ya. I. Alivov, C. Liu, A. Teke, M. A. Reshchikov, S. Doğan, V. Avrutin, S.-J. Cho, and H. Morkoç, "A comprehensive review of ZnO materials and devices," *Journal of Applied Physics*, vol. 98, no. 4, 041301, 2005.

[3] A. Ashrafi and C. Jagadish, "Review of zincblende ZnO: stability of metastable ZnO phases," *Journal of Applied Physics*, vol. 102, no. 7, pp. 071101-1-12, 2007.

[4] B. Wen, J. E. Sader, and J. J. Boland, "Mechanical properties of ZnO nanowires," *Physical Review Letters*, vol. 101, no. 17, pp. 175502-1-4, 2008.

[5] D. K. Ferry, "High-field transport in wide-band-gap semiconductors," *Physical Review B*, vol. 12, no. 6, pp. 2361-2369, 1975.

[6] A. R. Hutson, "Hall effect studies of doped zinc oxide single crystals," *Physical Review* , vol. 108, no. 2, pp. 222-230, 1957.

[7] D. C. Look, D. C. Reynolds, J. R. Sizelove, R. L. Jones, C. W. Litton, G. Cantwell, and W. C. Harsch, "Electrical properties of bulk ZnO," *Solid State Communications*, vol. 105, no. 6, pp. 399-401, 1998.

[8] J. D. Albrecht, P. P. Ruden, S. Limpijumnong, W. R. L. Lambrecht, and K. F. Brennan, "High field electron transport properties of bulk ZnO," *Journal of Applied Physics,* vol. 86, no. 12, pp. 6864-6867, 1999.

[9] B. Guo, U. Ravaioli, and M. Staedele, "Full band Monte Carlo calculations of velocity-field characteristics of wurtzite ZnO," *Computer Physics Communications*, vol. 175, no. 7, pp. 482-486, 2006.

[10] F. Bertazzi, M. Goano, and E. Bellotti, "Electron and Hole Transport in Bulk ZnO: A Full Band Monte Carlo Study," *Journal of Electronic Materials*, vol. 36, no. 8, pp. 857-863, 2007.

[11] E. Furno, F. Bertazzi, M. Goano, G. Ghione, and E. Bellotti, "Hydrodynamic transport parameters of wurtzite ZnO from analytic and full-band Monte Carlo simulation," *Solid-State Electronics*, vol. 52, no. 11, pp. 1796-1801, 2008.

[12] H. Morkoç and Ü. Özgür, *Zinc Oxide*: *Fundamentals, Materials and Device Technology*. Weinheim, Germany: Wiley-VCH, 2009.

[13] S. K. O'Leary, B. E. Foutz, M. S. Shur, and L. F. Eastman, "Steady-state and transient electron transport within bulk wurtzite zinc oxide," *Solid State Communications*, vol. 150, no. 43, pp. 2182-2185, 2010.

[14] B. E. Foutz, L. F. Eastman, U. V. Bhapkar, and M. S. Shur, "Comparison of high field electron transport in GaN and GaAs," *Applied Physics Letters*, vol. 70, no. 21, pp. 2849-2851, 1997.

[15] B. E. Foutz, S. K. O'Leary, M. S. Shur, and L. F. Eastman, "Transient Electron Transport in Wurtzite GaN, InN and AlN," *Journal of Applied Physics*, vol. 85, no. 11, pp. 7727-7734, 1999.

[16] H. Arabshahi, M. R. Ronki-Abadi, and F. B. Bagh-Siyahi, "Comparison of High Field Electron Transport Properties in Wurtzite Phase of ZnO, GaN and SiC," *Research Journal of Applied Sciences*, vol. 5, no. 3, pp. 215-220, 2010.

[17] W. A. Hadi, M. S. Shur, and S. K. O'Leary, "A transient electron transport analysis of bulk wurtzite zinc oxide," *Journal of Applied Physics*, vol. 112, no. 3, pp. 033720-1-5, 2012.

[18] W. A. Hadi, S. Chowdhury, M. S. Shur, and S. K. O'Leary, "A detailed characterization of the transient electron transport within zinc oxide, gallium nitride, and gallium arsenide," *Journal of Applied Physics*, vol. 112, no. 12, pp. 123722-1-6, 2012.

[19] W. A. Hadi, M. S. Shur, and S. K. O'Leary, "The sensitivity of the steady-state and transient electron transport within bulk wurtzite zinc oxide to variations in the crystal temperature, the doping concentration, and the non-parabolicity coefficient," *Journal of Materials Science: Materials in Electronics*, vol. 24, no. 1, pp. 2-12, 2013.

[20] W. A. Hadi, R. Cheekoori, M. S. Shur, and S. K. O'Leary, "Transient electron transport in the III-V compound semiconductors gallium arsenide and gallium nitride," *Journal of Materials Science: Materials in Electronics*, vol. 24, no. 2, pp. 807-813, 2013.

[21] W. A. Hadi, R. Cheekoori, M. S. Shur, and S. K. O'Leary, "On the applicability of a semi-analytical approach to determining the transient electron transport response of gallium arsenide, gallium nitride, and zinc oxide," *Journal of Materials Science: Materials in Electronics*, vol. 24, no. 5, pp. 1624-1634, 2013.

[22] S. K. O'Leary, B. E. Foutz, M. S. Shur, and L. F. Eastman, "Steady-state and transient electron transport within bulk wurtzite indium nitride: An updated semiclassical three-valley Monte Carlo simulation analysis," *Applied Physics Letters*, vol. 87, no. 22, pp. 222103-1-3, 2005.

[23] S. K. O'Leary, B. E. Foutz, M. S. Shur, and L. F. Eastman, "Potential performance of indium-nitride-based devices," *Applied Physics letters*, vol. 88, no. 15, pp. 152113-1-3, 2006.

[24] S. Sasa, T. Hayafuji, M. Kawasaki, A. Nakashima, K. Koike, M. Yano, and M. Inoue, "High-field characteristics of ZnO and ZnO/ZnMgO heterostructures," *Physica Status Solidi C*, vol. 5, no. 1, pp. 115-118, 2008.

[25] S. Li, J. Li, F. Liu, M. A. Alim, and G. Chen, "The dimensional effect of breakdown field in ZnO varistors," *Journal of Physics D: Applied Physics*, vol. 35, pp. 1884-1888, 2002.

[26] S. Adachi, *Properties of Group IV, III-V, and II-VI Semiconductors*. Chichester, England: John Wiley and Sons, 2005.

[27] P. Lugli and D. K. Ferry, "Degeneracy in the ensemble Monte Carlo method for high-field transport in semiconductors," *IEEE Transactions on Electron Devices*, vol. 32, no. 11, pp. 2431-2437, 1985.

[28] K. Seeger, *Semiconductor Physics*: *An Introduction*, 9th ed. Berlin, Germany: Springer, 2004.

[29] W. A. Hadi, S. K. O'Leary, M. S. Shur, and L.F. Eastman, "The sensitivity of the steady-state electron transport within bulk wurtzite zinc oxide to variations in the non-parabolicity coefficient," *Solid State Communications*, vol. 151, no. 12, pp. 874-878, 2011.

[30] Most of the material parameter selections used by O'Leary *et al.* [13] for their simulations of the electron transport within bulk wurtzite ZnO are actually from Albrecht *et al.* [8]. Unfortunately, as Albrecht *et al.* [8] did not provide an exhaustive list of all of the material parameters needed for their Monte Carlo simulations, some of the material parameters employed by O'Leary *et al.* [13] were drawn from other sources in the literature, or through a direct fit with the results of Albrecht *et al.* [8], i.e., the material parameters were tweaked until the resultant velocity-field characteristic corresponded with that found by Albrecht *et al.* [8]. With the exception of the second order non-parabolicity coefficient, which we neglect in our analysis, O'Leary *et al.* [13] employed the same three-valley band model as that employed by Albrecht *et al.* [8].

[31] S. K. O'Leary, B. E. Foutz, M. S. Shur, U. V. Bhapkar, and L. F. Eastman, "Electron transport in wurtzite indium nitride," *Journal of Applied Physics*, vol. 83, no. 2, pp. 826-829, 1998.

[32] S. K. O'Leary, B. E. Foutz, M. S. Shur, U. V. Bhapkar, and L. F. Eastman, "Monte Carlo simulation of electron transport in wurtzite aluminum nitride," *Solid State Communications*, vol. 105, no. 10, pp. 621-626, 1998.

[33] S. K. O'Leary, B. E. Foutz, M. S. Shur, and L. F. Eastman, "Polar optical phonon instability and intervalley transfer in III-V semiconductors," *Solid State Communications*, vol. 118, no. 2, pp. 79-83, 2001.

[34] S. K. O'Leary, B. E. Foutz, M. S. Shur, and L. F. Eastman, "Steady-state electron transport in the III–V nitride semiconductors: A sensitivity analysis," *Journal of Electronic Materials*, vol. 32, no. 5, pp. 327-334, 2003.

[35] S. K. O'Leary, B. E. Foutz, M. S. Shur, and L. F. Eastman, "Steady-state and transient electron transport within the III–V Nitride semiconductors, GaN, AlN, and InN: A review," *Journal of Materials Science: Materials in Electronics*, vol. 17, no. 2, pp. 87-126, 2006.

[36] S. K. O'Leary, B. E. Foutz, M. S. Shur, and L. F. Eastman, "The sensitivity of the electron transport within bulk wurtzite indium nitride to variations in the crystal temperature, the doping concentration, and the non-parabolicity coefficient: an updated Monte Carlo analysis," *Journal of Materials Science: Materials in Electronics,* vol. 21, no. 3, pp. 218-230, 2010.

CHAPTER 5

On the applicability of a semi-analytical approach in determining the optimal applied electric field strength for a given electron displacement for the case of bulk wurtzite zinc oxide

To be submitted to the Journal of Materials Science: Materials in Electronics. It is co-authored with Dr. M. Shur, and my supervisor, Dr. S. K. O'Leary.

5.1 Introduction

In recent years, the material properties of ZnO have become the focus of great interest. This interest is being fueled, in large measure, by the extraordinary potential of this material for device applications. A II-VI compound semiconductor, ZnO possesses material properties that makes it particularly suitable for a number of important electronic and optoelectronic device applications [1]. These properties include its wide and direct energy gap [2], wide inter-valley energy separation, and large polar optical phonon energy. These material properties suggest that bulk wurtzite ZnO will exhibit favorable electron transport characteristics, i.e., elevated steady-state electron drift velocities and a pronounced transient electron transport response [3].

While steady-state electron transport remains the primary focus of studies into the nature of the electron transport within compound semiconductors, with the trend towards smaller device dimensions, the transient component to the overall electron transport response is increasingly being considered as well. The benefits of transient electron transport, and how device performance may be enhanced as a consequence, has been studied, at length, by a number of researchers, and is well documented in the scientific literature [4-6]. In recent years, both the steady-state and the transient electron transport within ZnO have been examined through the use of Monte Carlo simulations of the electron transport [7-15]. These studies point to high steady-state electron drift velocities as well as substantial overshoot transient electron drift velocities within this material. This suggests that ZnO offers great potential as a material for possible future high-field electron device applications.

While Monte Carlo simulations offer a means of solving the Boltzmann transport equation, and thereby characterizing the nature of the electron transport that occurs within a given material, the intensive nature of the computations demanded of this technique are a drawback. In addition, it is often difficult to consider time-varying and non-uniform electric fields within the framework of a Monte Carlo simulation of the electron transport. The need for greater computational efficiency becomes particularly acute when one is aiming to optimize the performance of such a device, as a large number of simulations are demanded of such an optimization. An alternative approach to determining the transient electron transport response within a semiconductor material is that suggested by Shur in 1976 [5]. Drawing upon steady-state Monte Carlo electron transport results, this model uses a semi-analytical approach to determine the character of the transient electron transport response, based on the application of momentum and energy balance equations that analyzes transient electron transport in terms of the momentum and energy relaxation times [5]. This semi-analytical approach draws upon Monte Carlo steady-state data, comprising of the electron drift velocity, average electron energy, and the electron valley occupancy as functions of a range of electric fields considered. Only one set of steady-state Monte Carlo data is needed to run as many transient electron transport responses as needed. Given that each semi-analytical evaluation of the transient electron transport response takes only a fraction of the time required for a corresponding Monte Carlo simulation, the practicality and speed of the method becomes evident. This is particularly true when one wishes to examine how the performance of such a material can be optimized.

We have previously studied the applicability of the semi-analytical approach in determining the transient electron transport response of an ensemble of electrons within GaAs, GaN, and ZnO [16]. We compared the semi-analytical results with those obtained using the Monte Carlo method in order to probe the efficacy of the semi-analytical approach. In this paper, we apply the semi-analytical method further, critically examining its applicability in terms of determining the optimal performance of a ZnO-based high-field electron device. To accomplish our goal, we will solve the momentum/energy balance equations using the semi-analytical method of Shur [5], and then compare our results with those obtained using the Monte Carlo method. In both the Monte Carlo and the semi-analytical methods, we apply constant electric fields to an ensemble of electrons, and study its response. We shall look at the following aspects of the transient electron transport response: (1) the transient electron drift velocity as a function of the time elapsed since the application of the electric field, (2) the average electron displacement as a function of the time elapsed since the application of the electric field, (3) the optimal electric field strength required in order to minimize the electron transit-time as a function of the channel length, and (4) the upper bound optimal cut-off frequency as a function of the channel length. The principal focus of this particular analysis is the differences between the two methods.

This paper is organized in the following manner. In Section 5.2, we describe the Monte Carlo simulations of the electron transport that are used for the purposes of this analysis. Then, in Section 5.3, we describe the semi-analytical approach of Shur [5]. In Section 5.4, we present the results obtained using this semi-analytical approach, and we contrast these results with those obtained using the Monte Carlo method. The device implications of the semi-analytical approach, and a critical comparison with results obtained using the Monte Carlo simulations, are then presented in Section 5.5. The limitations of the semi-analytical method, for the case of very high electric field strengths, are then presented in Section 5.6. Finally, the conclusions of this analysis are presented in Section 5.7.

5.2 Monte Carlo electron transport simulations

For the purposes of this analysis, results from Monte Carlo simulations of the electron transport are required. They will be used both as an input to our semi-analytical computations and in order to facilitate a comparison between the results obtained from these computations and those obtained through Monte Carlo simulations. Accordingly, both steady-state and transient electron transport results are required; the steady-state Monte Carlo electron transport results will be used as an input to our semi-analytical computations, while the transient Monte Carlo electron transport results will be used for the purposes of comparison with the corresponding results produced using the semi-analytical approach. We employ an ensemble semi-classical three-valley Monte Carlo electron transport simulation approach and study the motion of an ensemble of electrons under the action of an applied electric field within bulk wurtzite ZnO. For the purposes of our steady-state electron transport simulations, the motion of 3,000 electrons is considered, while for our transient electron transport simulations, the motion of 10,000 electrons, in a constant applied electric field, is considered. For our transient electron transport simulations, the time interval of interest is the one elapsed since the onset of the electric field up to the point where the electron ensemble reaches steady-state conditions.

The scattering mechanisms considered in this analysis are: (1) ionized impurity, (2) polar optical phonon, (3) piezoelectric, and (4) acoustic deformation potential. Intervalley scattering is also considered. The crystal temperature is set to 300 K and the doping concentration is set to 10^{17} cm^{-3} for all cases. We assume that all donors are ionized and that the free electron concentration is equal to the dopant concentration. We use the Kane model in order to account for the non-parablicity of each valley[1] [17,18]. In order to account for electron degeneracy effects, we use the rejection technique of Lugli and Ferry [19]. Electron screening is also accounted for following the Brooks-Herring method [20]. The material and band structural parameter selections are tabulated in Tables 5.1 and 5.2, respectively. Further details of our Monte Carlo electron transport simulation approach are presented in the literature [21-31].

---

[1] In the Kane model, the energy bands are assumed to be non-parabolic, spherical, and of the form

$$E(1+\alpha E) = \frac{\hbar^2 k^2}{2m^*},$$

where $\hbar k$ denotes the crystal momentum, E represents the energy, m^* is the effective mass of the electrons within this valley, and the non-parabolicity coefficient, α, is given by

$$\alpha = \frac{1}{E_g}\left(1-\frac{m^*}{m_e}\right)^2,$$

where m_e and E_g denote the free electron mass and the energy gap, respectively [18].

Table 5.1: The material parameter selections corresponding to bulk wurtzite ZnO that are employed for the purposes of this analysis. The source of each parameter is identified.

Parameter	ZnO	Reference
Mass density (g/cm^3)	5.68	[32]
Longitudinal sound velocity(cm/s)	4.00×10^5	determined through fit
Transverse sound velocity (cm/s)	2.7×10^5	[9]
Acoustic deformation potential (eV)	3.83	[8]
Static dielectric constant	8.2	[8]
High frequency dielectric constant	3.7	[8]
Effective mass (Γ_1 valley)	0.17 m_e	[8]
Piezoelectric constant, e_{14} (C/cm^2)	3.75×10^{-5}	determined through fit
Direct energy gap (eV)	3.4	[8]
Polar optical phonon energy (meV)	72	[8]
Intervalley deformation potentials (eV/cm)	10^9	[8]
Intervalley phonon energies(meV)	72	[8]

Table 5.2: The band structure parameter selections corresponding to bulk wurtzite ZnO. These band structure parameter selections are mostly from Albrecht *et al*. [8].

	Valley number	1	2	3
ZnO	Valley location	Γ_1 [8]	Γ_1 [8]	L-M [8]
	Valley degeneracy	1	1	6
	Effective mass	0.17m_e [8]	0.42m_e [8]	0.7m_e [8]
	Intervalley energy separation (eV)	_	4.4 [8]	4.6 [8]
	Energy gap (eV)	3.4 [8]	7.8 [8]	8.0 [8]
	Non-parabolicity (eV^{-1})	0.66 [8]	0.15 [8]	0.0 [8]

5.3 The semi-analytical approach

The semi-analytical approach, originally conceived by Shur [5] in 1976, and later employed by others, allows for the rapid evaluation of the transient electron transport response [4, 31]. In this approach, steady-state Monte Carlo data, comprising of the dependence of the electron drift velocity on the applied electric field strength (the velocity-field characteristic), the dependence of the average electron energy on the applied electric field strength, and the dependence of the conduction valley occupancy on the applied electric field strength, are used to determine the corresponding transient electron transport response through applying the principles of momentum and energy conservation. In particular, we solve for the following coupled differential equations

$$\frac{d[m^*(\varepsilon)v]}{dt} = q\xi - \frac{m^*(\varepsilon)v}{\tau_m(\varepsilon)}, \tag{5.1}$$

$$\frac{d\varepsilon}{dt} = q\xi v - \frac{\varepsilon - \varepsilon_o}{\tau_\varepsilon(\varepsilon)}, \tag{5.2}$$

where the first equation represents the conservation of momentum and the second equation represents the conservation of energy. In these equations, q represents the charge of an electron, v is the average electron drift velocity, ε is the electron energy, $\tau_m(\varepsilon)$ is the momentum relaxation time, $\tau_\varepsilon(\varepsilon)$ is the energy relaxation time, ξ is the strength of the electric field, $m^*(\varepsilon)$ is the effective mass, and ε_o represents the thermal equilibrium energy, i.e., $\varepsilon_o = (3/2)\ k_bT$, where k_b is Boltzmann's constant, and T is the temperature.

The momentum relaxation time is determined under steady-state conditions, where the derivative of the momentum with respect to time in Eq. (5.1) is set to zero. The energy relaxation time is also determined at steady-state conditions, by setting the derivative of the energy with respect to time in Eq. (5.2) to zero. We thus have

$$\tau_m(\varepsilon) = \frac{m^*(\varepsilon) v_{ss}(\varepsilon)}{q\xi_{ss}(\varepsilon)}, \tag{5.3}$$

and

$$\tau_\varepsilon(\varepsilon) = \frac{\varepsilon - \varepsilon_o}{q\xi_{ss}(\varepsilon) v_{ss}(\varepsilon)}, \tag{5.4}$$

where $v_{ss}(\varepsilon)$ and $\xi_{ss}(\varepsilon)$ denote the steady-state velocity and steady-state electric field strength at a given electron energy, respectively. The effective mass is measured by mapping the energy to the steady-state electron occupancy in the different valleys and then calculating the average mass. For the purposes of simplification, the electron effective mass in a given valley is considered to be the electron effective mass at the bottom of the valley. This particular point becomes important when we discuss the limitations of the semi-analytical model in studying transient transport within ZnO at very high electric field strengths, as we shall see later. In 2013, the applicability of this approach was critically assessed by Hadi *et al*. [16] in an examination of the transient electron transport within GaAs, GaN, and ZnO.

5.4 Results

In Figure 5.1, we plot the electron drift velocity as a function of the time elapsed since the application of the constant electric field, for a number of different applied electric field strength selections. Results obtained, from both Monte Carlo simulations of the electron transport and the corresponding semi-analytical approach, are depicted. We note that these results are almost identical for the applied electric field strength selections 200 and 400 kV/cm. For applied electric field strength selections in excess of 400 kV/cm, however, a significant difference between the results becomes apparent, this difference between results becoming greater as the applied electric field strength is increased. A particularly pronounced difference between the results is noted for the electric field strength selection 800 kV/cm.

We now consider how the electrons displace in response to the application of an electric field. We do this by integrating, with respect to time, the transient electron drift velocity. The electron displacement is plotted as a function of the time elapsed since the application of the constant electric field strength in Figure 5.2, these results corresponding to the results depicted in Figure 5.1. As with Figure 5.1, results obtained, from both Monte Carlo simulations of the electron transport and the corresponding semi-analytical approach, are depicted. We find satisfactory agreement between the two methods for the 200 and 400 kV/cm electric field selections. For the case of the 800 kV/cm applied electric field strength selection, however, we note a clear upper bound formed by the semi-analytical result over that obtained through Monte Carlo simulation for times less than 0.08 ps, and a convergence in the results thereafter. This is the time interval during which the velocity overshoot occurs and the semi-analytical upper bound

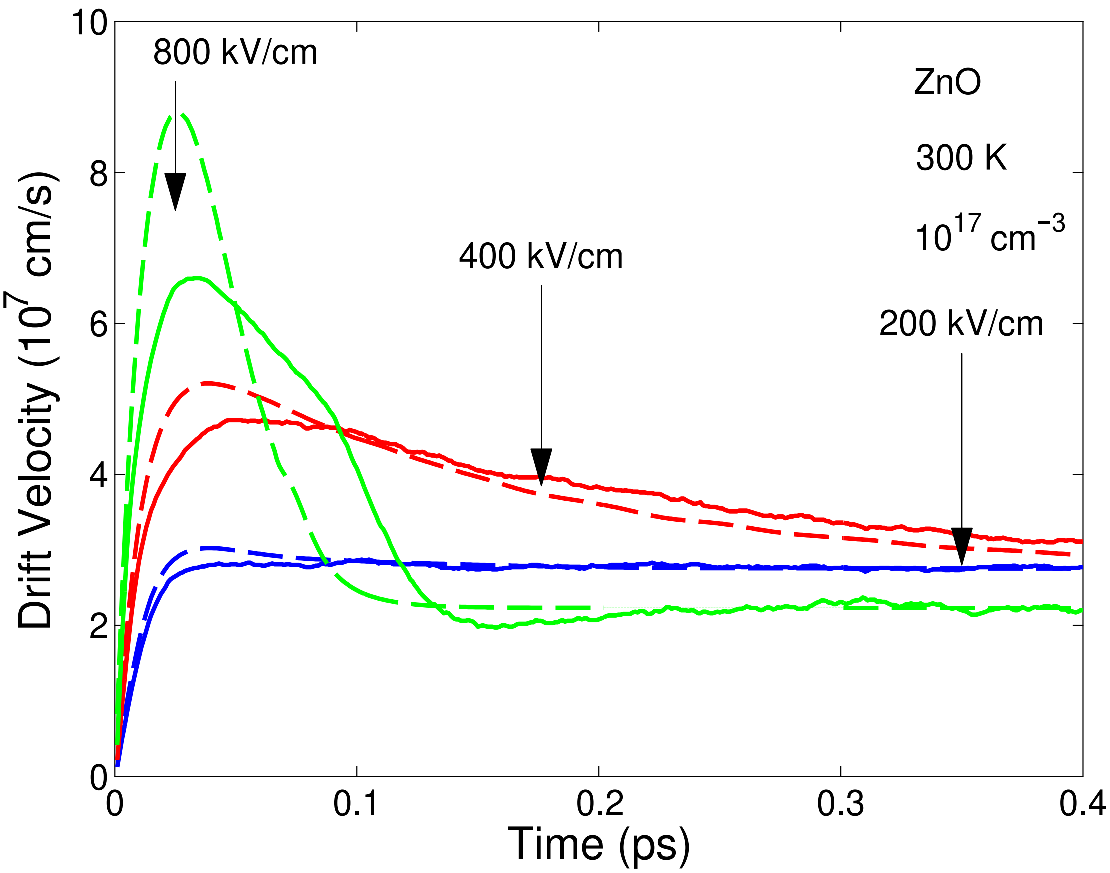

Figure 5.1: The electron drift velocity associated with bulk wurtzite ZnO as a function of the time elapsed since the onset of the applied electric field. We consider the applied electric field strength selections 200, 400, and 800 kV/cm. For all cases, we have assumed an initial zero-field electron distribution, a crystal temperature of 300 K, and a doping concentration of 10^{17} cm^{-3}. The Monte Carlo results are depicted with the solid lines and the semi-analytical results are represented with the dashed lines. The online version is depicted in color.

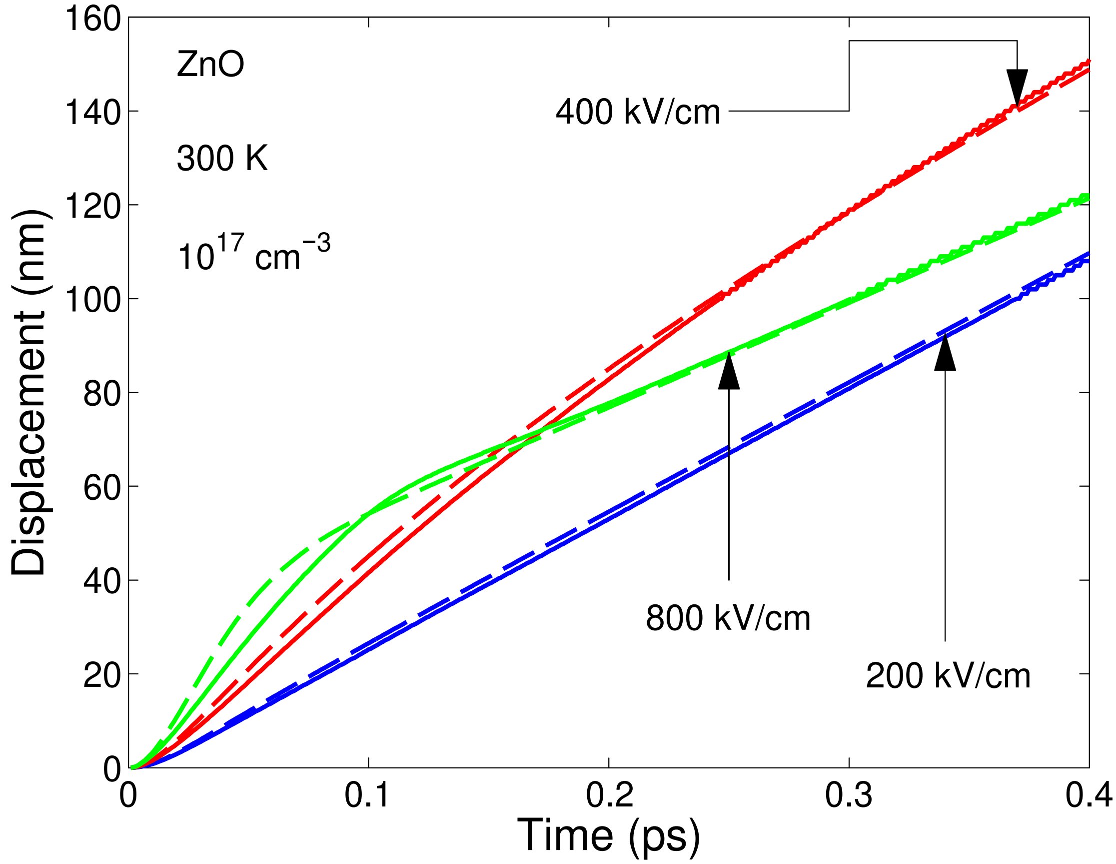

Figure 5.2: The electron displacement associated with bulk wurtzite ZnO as a function of the time elapsed since the onset of the applied electric field. We consider the applied electric field strength selections 200, 400, and 800 kV/cm. For all cases, we have assumed an initial zero-field electron distribution, a crystal temperature of 300 K, and a doping concentration of 10^{17} cm^{-3}. The Monte Carlo results are depicted with the solid lines and the semi-analytical results are represented with the dashed lines. The online version is depicted in color.

is due to its higher overshoot velocity as compared with that arising from Monte Carlo simulation; recall Figure 5.1.

With the electron displacement as a function of the time elapsed known, we can now determine how to minimize the transit-time, τ, across a given electron displacement. If we take this minimum transit-time across a certain displacement as a proxy for the minimum time it will take for an electron to transit a device of the same dimension, this will allow us to estimate the corresponding device performance. In order to optimize the device performance, i.e., minimize the transit-time for a given device length, this analysis must be performed repeatedly, over a wide range of electric field strength selections, thereby allowing us to determine which applied electric field strength selection provides for the shortest time for a given fixed electron displacement. In Figure 5.3, we plot the electron transit-time across a 100 nm channel length for a range of electric field strength selections. The objective of this exercise is to find the electric field strength in order to obtain the minimal electron transit time across a channel, $\tau_{\min}$. A similar analysis was done with the Monte Carlo approach, and we plot the results from this Monte Carlo analysis for the purposes of critical comparison. Despite the differences in the underlying transient electron drift velocity results, we find that the results of the semi-analytical method are very similar to those produced from Monte Carlo simulations for this set of conditions, both approaches predicting 465 kV/cm as the optimal applied electric field strength for this particular channel length selection. This should not be surprising, as there is little divergence between the results of both methods in terms of the transient electron drift velocity response around this electric field level strength; recall Figure 5.1. As such, we would expect a different outcome if the channel length chosen is much

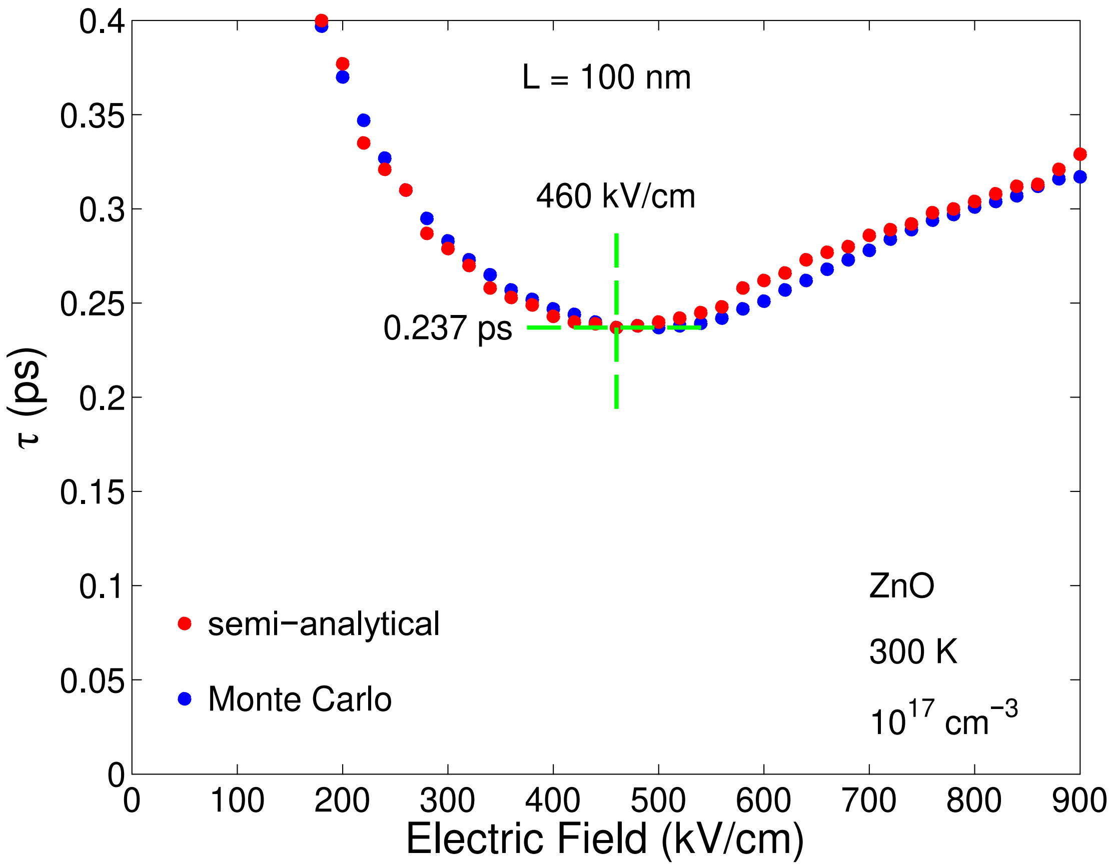

Figure 5.3: The time-to-transit as a function of the applied electric field strength for *L* set to 100 nm for the case of bulk wurtzite ZnO. For all cases, we have assumed an initial zero-field electron distribution, a crystal temperature of 300 K, and a doping concentration of 10^{17} cm^{-3}. The Monte Carlo results are depicted with blue solid circles and the semi-analytical results are represented with the red solid circles. The minimum time-to-transit, 0.237 ps, and the corresponding optimal electric field strength, 460 kV/cm, are depicted with the dashed green cross. For this selection of *L*, the minimum time-to-transit Monte Carlo results and the semi-analytical results are essentially coincident. The online version is depicted in color.

smaller than the 100 nm considered in Figure 5.3. We would expect a lower optimal electric field strength prediction in the semi-analytical method in that scenario, due to the higher velocity overshoot that it allows as opposed to its Monte Carlo counterpart.

In order to further investigate this point, in Figure 5.4 we plot the optimal applied electric field strength as a function of the device length determined from the semi-analytical and Monte Carlo approaches for a 10-1000 nm device length range using a similar approach to that used in Figure 5.3, i.e., for each device length considered, we found the electric field strength that produces the minimum electron transit-time across the given device length. The results obtained by the two methods are virtually coincident for channel lengths greater than 40 nm. At the 40 nm channel length, we obtain a 850 kV/cm optimal electric field using the semi-analytical approach as compared to 1050 kV/cm obtained using the Monte Carlo approach. The results of both methods start to diverge for channel lengths shorter than 40 nm. As an example, for a device length of 20 nm we get an optimal applied electric field of 2100 kV/cm using the semi-analytical method compared to 1700 kV/cm from the Monte Carlo method. For a device length of 10 nm, however, we get an optimal applied electric field of 3400 kV/cm using the semi-analytical approach compared to 4700 kV/cm from the Monte Carlo approach. The lower optimal electric field strength predictions using the semi-analytical model for short channel lengths is due to its exaggerated predictions of the drift velocity overshoots at high electric fields, as we have seen in Figure 5.1. Those velocity overshoots occur over very short periods of time, and therefore, their effect is most visible when examining optimization for very short channel lengths. Despite the gap in the results reported between the two methods for the shorter device channel lengths, however, the utility and

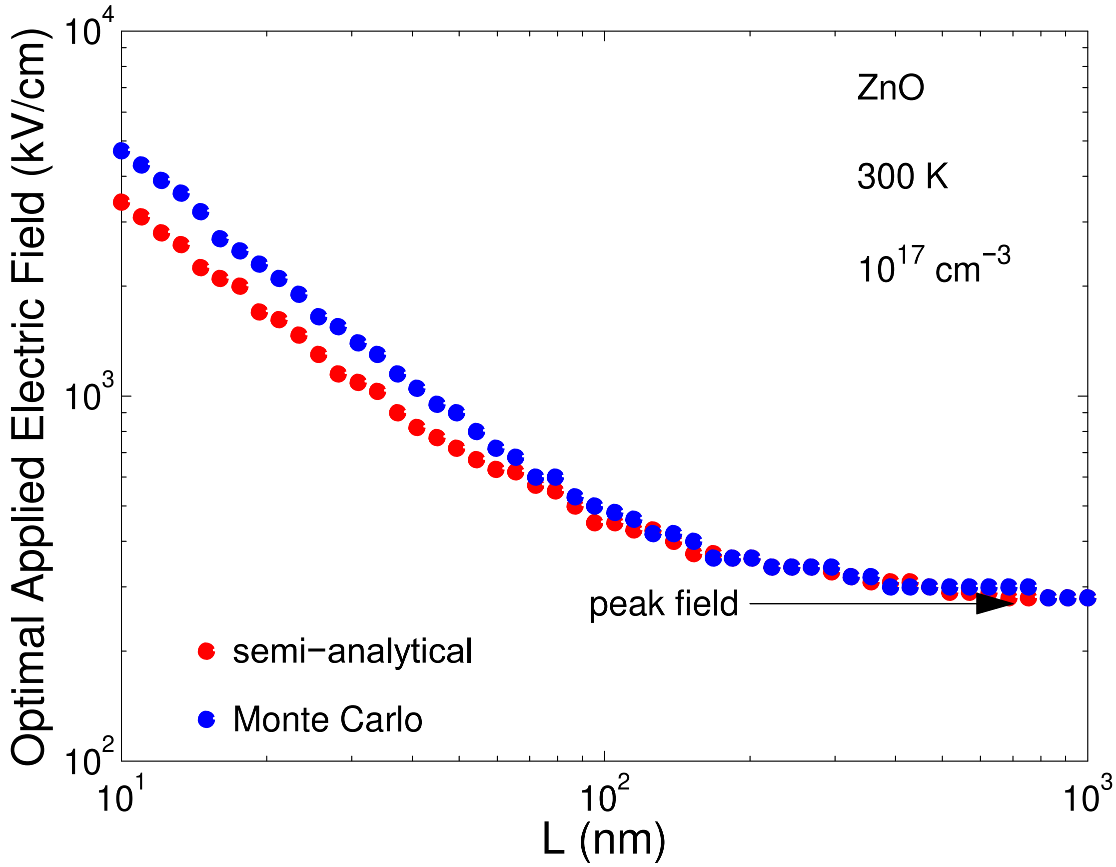

Figure 5.4: The optimal applied electric field strength plotted as a function of the electron displacement, *L*, for the case of bulk wurtzite ZnO. These results were obtained using the optimization procedure illustrated in Figure 5.3 for various displacement selections. As a point of reference, the peak field is depicted with the arrow. For all cases, we have assumed an initial zero-field electron distribution, a crystal temperature of 300 K, and a doping concentration of 10^{17} cm^{-3}. The Monte Carlo results are depicted with blue solid circles and the semi-analytical results are represented with the red solid circles. The online version is depicted in color.

value of the semi-analytical approach remains quite evident in the reported field optimization results presented in Figure 5.4.

5.5 Device implications

The device implications of this analysis may now be considered. In particular, we will focus upon determining an upper bound for the cut-off frequency within ZnO based electron devices. The optimal cut-off frequency is given by

$$f_{T_{\max}} = \frac{1}{2\pi\tau_{\min}}. \tag{5.5}$$

We have already used the semi-analytical method to determine the minimum possible electron transit-times and their corresponding optimal applied electric field strength values; recall Figure 5.4. We therefore substitute the obtained electron minimum transit-times, $\tau_{\min}$, into Eq. (5.5) to obtain the pertinent optimal cut-off frequencies. In Figure 5.5, we plot the corresponding cut-off frequencies for the 10-1000 nm device length range obtained using the semi-analytical approach. We also plot the corresponding Monte Carlo results for purposes of critical comparison.

We note that for device lengths in excess of 40 nm, the cut-off frequencies predicted by both approaches are virtually coincident. For a channel length of 40 nm, we obtain a 2.8 THz cut-off frequency using the semi-analytical method as compared to 2.3 THz obtained using the Monte Carlo approach. For a channel length of 20 nm, however, we obtain a cutoff frequency of 8.8 THz using the semi-analytical method

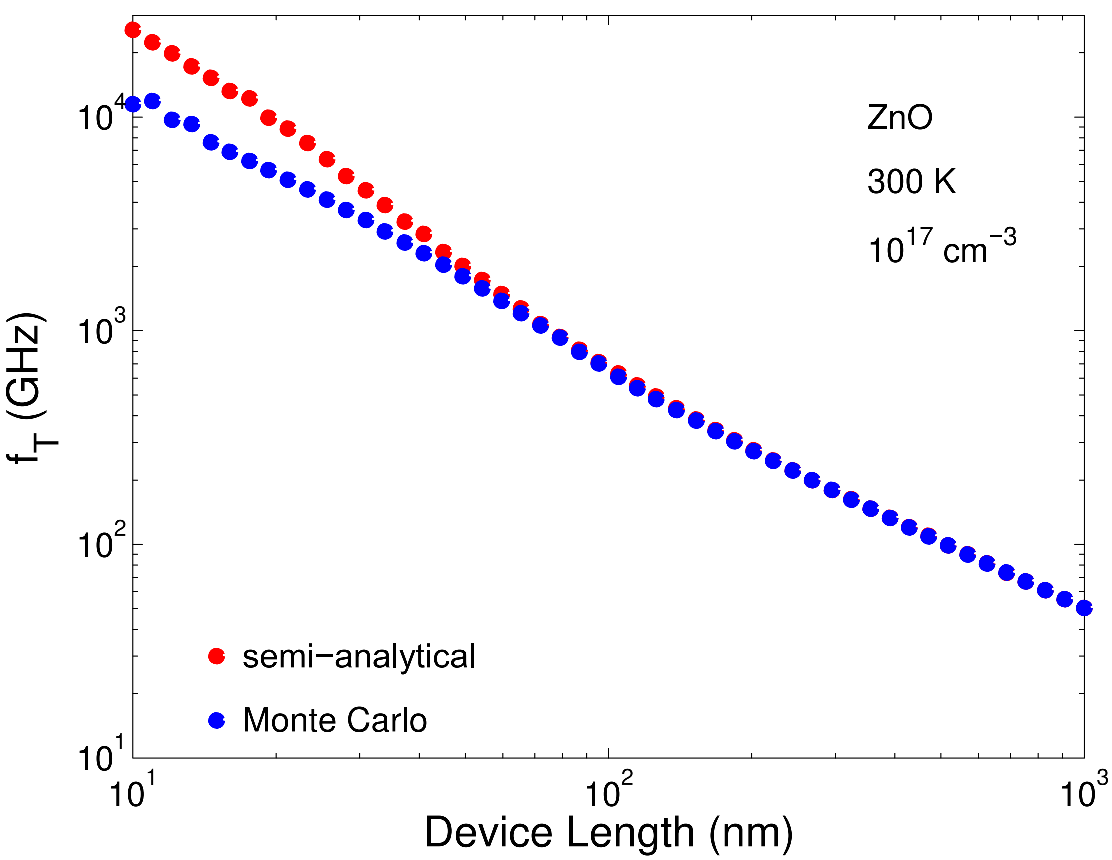

Figure 5.5: The optimal cut-off frequency plotted as a function of the device length for the case of an ideal ZnO-based electron device. We employed the optimization procedure illustrated in Figure 5.3 for all the device length selections considered. For all cases, we have assumed an initial zero-field electron distribution, a crystal temperature of 300 K, and a doping concentration of 10^{17} cm^{-3}. The Monte Carlo results are depicted with blue solid circles and the semi-analytical results are represented with the red solid circles. The online version is depicted in color.

compared to the Monte Carlo's 5.5 THz. For a channel length of 10 nm, a significant gap is reported, however, as we see a cut-off frequency of 25.6 THz obtained through the semi-analytical method compared to the Monte Carlo's 11.5 THz. Despite the gap between both methods at very short channel lengths, as with the case when discussing the field optimization of Figure 5.4, the reported results of Figure 5.5 clearly show the utility of the semi-analytical approach in predicting the cut-off frequencies of ZnO based devices.

5.6. High-field limitations

We have noticed a high-field limitation on the semi-analytical model, these results drifting away from those of their Monte Carlo counterparts. Exaggerated velocity overshoot predictions are reported at very high field strengths; recall Figures 5.1. This shortcoming of the semi-analytical approach is also in evidence when the device lengths considered for electric field strength optimization and device implications are smaller than 40 nm; recall Figures 5.4 and 5.5. A possible explanation for this gap in the reported results between both methods at very high-field strengths might lie in the way the semi-analytical model accounts for the electron effective mass in the lower valley. The model considers the electron effective mass in each valley to be determined by its value at the valley minimum. This assumption works well in materials like GaN and GaAs, that have low non-parabolicity in these valleys. Wurtzite ZnO, however, possesses a pronounced non-parabolicity coefficient in its central conduction band valley; consider Figure 5.6a. As a result, the electron effective mass within such a valley can dramatically change, especially as the electrons become highly energized at very high electric field strengths.

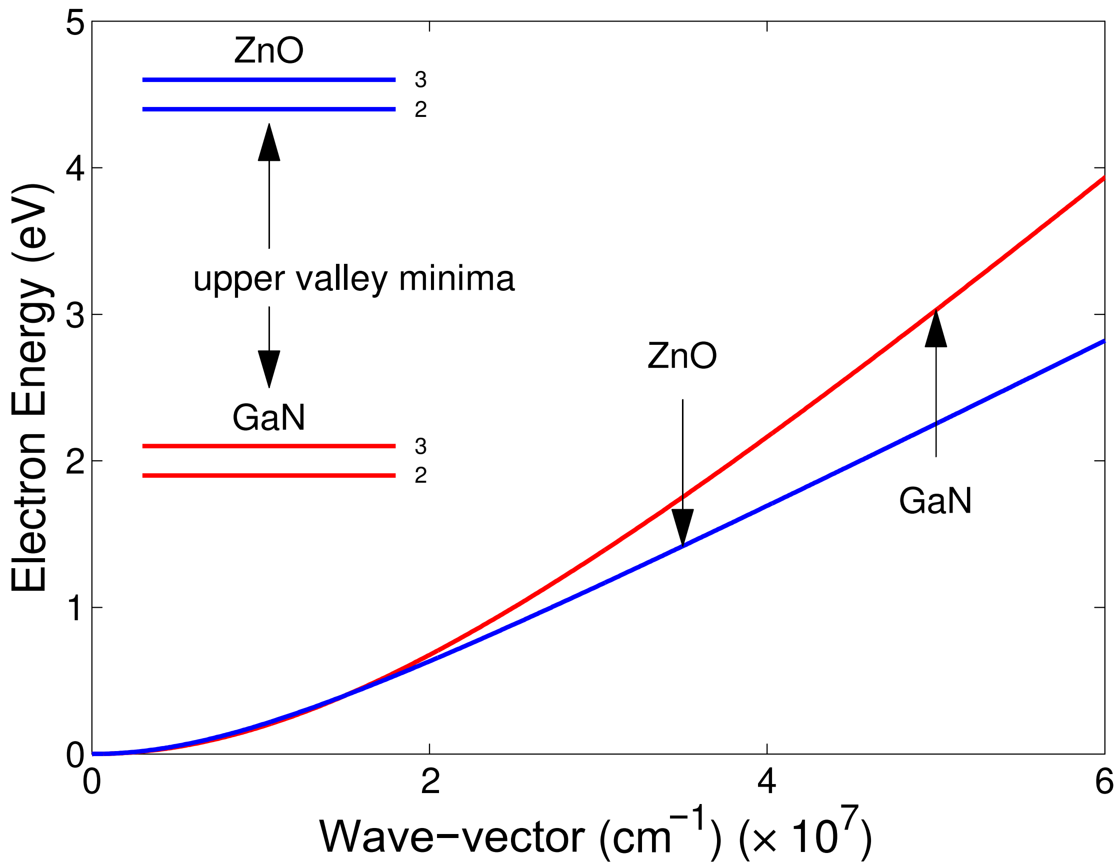

Figure 5.6a: The electron energy as a function of the electron wave-vector for the cases of wurtzite GaN and wurtzite ZnO. The GaN result is depicted with the red line and the ZnO result is represented with the blue line. The corresponding upper valley minima, corresponding to the 2nd and 3rd valley minima for each material, are also indicated using the corresponding colors. The online version is depicted in color.

To illustrate this point, in Figure 5.6b we plot the electron effective mass as a function of energy within bulk wurtzite ZnO. For the purposes of comparison, we also plot the electron effective mass as a function of energy within GaN. Since there is very little inter-valley transitions happening in ZnO due to its high non-parabolicity coefficient, we limit our discussion in Figure 5.6b to the lower energy valley, where the bulk of the electrons will reside, even under the application of very high electric field strengths [24]. It is clear from Figure 5.6b that the implicit assumption of the semi-analytical result, that the effective mass of the electrons within a valley will be solely determined by the effective mass of the electrons at the minimum point in the valley, loses its validity as the energies of the electrons increase as a result of very high field strengths. Therefore, unlike the cases of GaN and GaAs, electrons within bulk wurtzite ZnO can gain significant mass when highly energized, due to very high electric field strengths, even if they stay in the lower valley and do not perform any inter-valley transitions. This undervalued electron effective mass employed when solving the momentum and energy balance equations, i.e., Eqs. (5.1) and (5.2), becomes responsible for the exaggerated estimates of the overshoot velocities, and consequently, the lower predictions for the optimal electric fields for channel lengths less than 40 nm, as observed in Figure 5.4. Similarly the exaggerated overshoot velocity accounts for the higher predictions for the cut-off frequencies for channel lengths less than 40 nm, as the semi-analytical electron transit-times predictions would be lower than their Monte Carlo counterparts; recall Figure 5.5. This puts a limitation on the applicability of the semi-analytical approach when studying the transient electron transport response of an ensemble of electrons within bulk wurtzite bulk ZnO for very high electric field strengths.

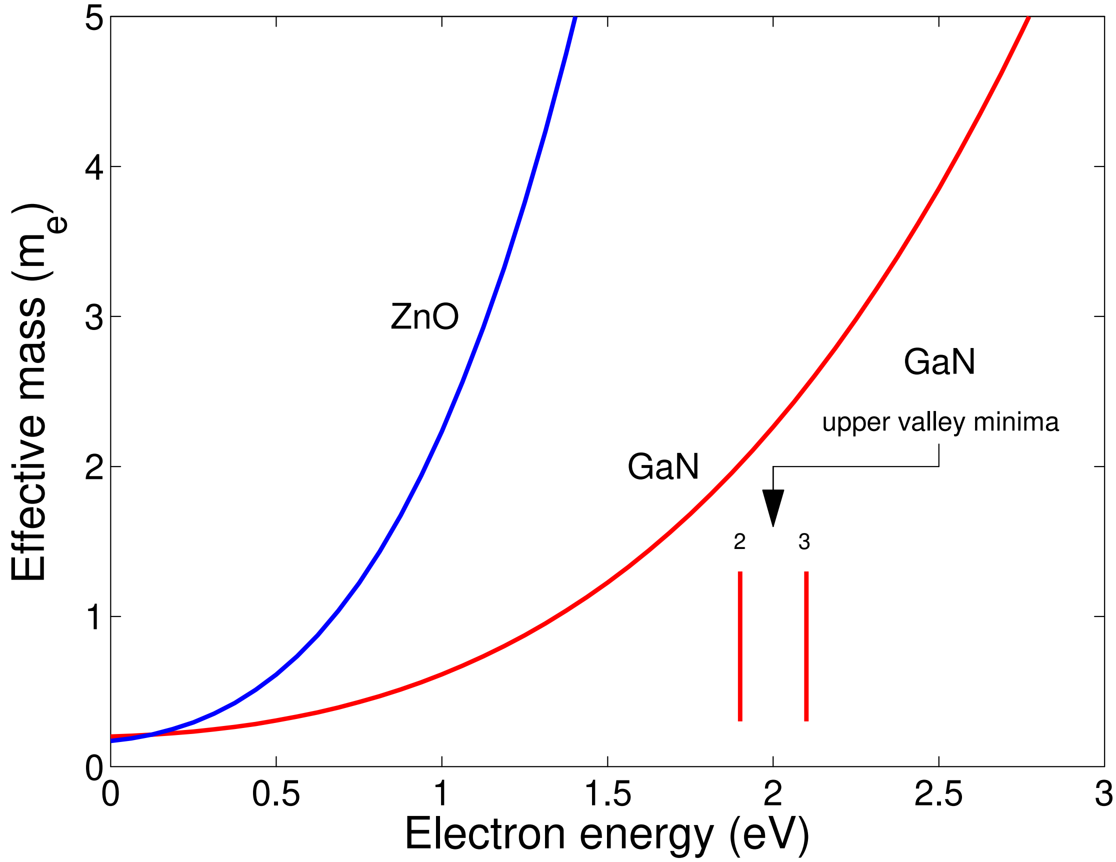

Figure 5.6b: The electron effective mass as a function of energy for the cases of wurtzite GaN and wurtzite ZnO. The GaN result is depicted with the red line and the ZnO result is represented with the blue line. The upper valley minima, corresponding to the case of wurtzite GaN, is also depicted; the upper valley minima corresponding to the case of wurtzite ZnO lies beyond the range of this figure. The online version is depicted in color.

5.7 Conclusions

We critically examined the applicability of the semi-analytical approach of Shur [5] in determining the optimal performance of wurtzite ZnO-based high field electron device. In particular, we contrasted results of the semi-analytical approach of Shur [5] with those obtained from Monte Carlo simulations of the electron transport that we use as a reference. For both methods, we examined the response of an ensemble of electrons to the application of a constant and uniform applied electric field. For the purposes of this analysis, we examined the following aspects of the transient electron transport response: (1) the transient electron drift velocity as a function of the time elapsed since the application of the electric field, (2) the average electron displacement as a function of the time elapsed since the application of the electric field, (3) the optimal electric field strength required in order to obtain the minimum electron transit time as a function of channel length, and (4) the upper bound optimal cut-off frequency as a function of the channel length. The results obtained showed that this semi-analytical approach of Shur [5] is an efficient and valuable method that can be used in the field optimization of wurtzite ZnO-based devices. The semi-analytical method results were found to be very similar to those of the Monte Carlo simulations for devices with channel lengths greater than 40 nm and for electric field strengths less than 800 kV/cm. The limitations of the semi-analytical approach of Shur [5] in the field optimization of ZnO-based devices at very high field strengths were also discussed. Despite those very high field limitations, the validity and the practicality of the method as a tool that can be used by researchers in studying field optimization in short-channel devices was evident in our results. As such, the approach could potentially be used to study field optimization in other material based devices, such as GaAs and GaN.

References

[1] C. Jagadish and S. J. Pearton, *Zinc Oxide Bulk, Thin Films, and Nanostructures*. New York, New York: Elsevier, 2006.

[2] V. Srikant and D. R. Clarke, “On the optical band gap of zinc oxide,” *Journal of Applied Physics*, vol. 83, no. 10, pp. 5447-5451, 1998.

[3] D. K. Ferry, “High-field transport in wide-band-gap semiconductors,” *Physical Review B*, vol. 12, no. 6, pp. 2361-2369, 1975.

[4] B. E. Foutz, S. K. O’Leary, M. S. Shur, and L. F. Eastman, “Transient Electron Transport in Wurtzite GaN, InN and AlN,” *Journal of Applied Physics*, vol. 85, no. 11, pp. 7727-7734, 1999.

[5] M. S. Shur, “Influence of non-uniform field distribution on frequency limits of GaAs field-effect transistors,” *Electronics Letters*, vol. 12, no. 23, pp. 615-616, 1976.

[6] S. K. O'Leary, B. E. Foutz, M. S. Shur, and L. F. Eastman, “Potential performance of indium-nitride-based devices,” *Applied Physics letters*, vol. 88, no. 15, pp. 152113-1-3, 2006.

[7] S. J. Pearton, D. P. Norton, K. Ip, Y. W. Heo, and T. Steiner, “Recent advances in processing of ZnO,” *Journal of Vacuum Science and Technology B*, vol. 22, no. 3, pp. 932-938, 2004.

[8] J. D. Albercht, P. P. Ruden, S. Limpijumnong, W. R. L. Lambrecht, and K. F. Brennan, “High field electron transport properties of bulk ZnO,” *Journal of Applied Physics*, vol. 86, no. 12, pp. 6864-6867, 1999.

[9] B. Guo, U. Ravaioli, and M. Staedele, “Full band Monte Carlo calculations of velocity-field characteristics of wurtzite ZnO,” *Computer Physics Communications*, vol. 175, no. 7, pp. 482-486, 2006.

[10] F. Bertazzi, M. Goano, and E. Bellotti, “Electron and Hole Transport in Bulk ZnO: A Full Band Monte Carlo Study,” *Journal of Electronic Materials*, vol. 36, no. 8, pp. 857-863, 2007.

[11] E. Furno, F. Bertazzi, M. Goano, G. Ghione, and E. Bellotti, “Hydrodynamic transport parameters of wurtzite ZnO from analytic and full-band Monte Carlo simulation,” *Solid-State Electronics*, vol. 52, no. 11, pp. 1796-1801, 2008.

[12] S. K. O’Leary, B. E. Foutz, M. S. Shur, and L. F. Eastman, “Steady-state and transient electron transport within bulk wurtzite zinc oxide,” *Solid State Communications*, vol. 150, no. 43, pp. 2182-2185, 2010.

[13] W. A. Hadi, M. S. Shur, and S. K. O'Leary, "A transient electron transport analysis of bulk wurtzite zinc oxide," *Journal of Applied Physics*, vol. 112, no. 3, pp. 033720-1-5, 2012.

[14] W. A. Hadi, S. Chowdhury, M. S. Shur, and S. K. O'Leary, "A detailed characterization of the transient electron transport within zinc oxide, gallium nitride, and gallium arsenide," *Journal of Applied Physics*, vol. 112, no. 12, pp. 123722-1-6, 2012.

[15] W. A. Hadi, M. S. Shur, and S. K. O'Leary, "The sensitivity of the steady-state and transient electron transport within bulk wurtzite zinc oxide to variations in the crystal temperature, the doping concentration, and the non-parabolicity coefficient," *Journal of Materials Science: Materials in Electronics*, vol. 24, no. 1, pp. 2-12, 2013

[16] W. A. Hadi, M. S. Shur, and S. K. O'Leary, "On the applicability of a semi-analytical approach to determining the transient electron response of gallium arsenide, gallium nitride and zinc oxide," *Journal of Materials Science: Materials in Electronics*, vol. 24, no. 5, pp. 1624-1634, 2013.

[17] E. O. Kane, "Band structure of indium antimonide," *Journal of Physics and Chemistry of Solids*, vol. 1, no. 4, pp. 249-261, 1957.

[18] W. Fawcett, A. D. Boardman, and S. Swain, "Monte Carlo determination of electron transport properties in gallium arsenide," *Journal of Physics and Chemistry of Solids*, vol. 31, no. 9, pp. 1963-1990, 1970.

[19] P. Lugli and D. K. Ferry, "Degeneracy in the ensemble Monte Carlo method for high-field transport in semiconductors," *IEEE Transactions on Electron Devices*, vol. 32, no. 11, pp. 2431-2437, 1985.

[20] K. Seeger, *Semiconductor Physics*: *An Introduction*, 9th ed. Berlin, Germany: Springer, 2004.

[21] B. E. Foutz, L. F. Eastman, U. V. Bhapkar, and M. S. Shur, "Comparison of high field electron transport in GaN and GaAs," *Applied Physics Letters*, vol. 70, no. 21, pp. 2849-2851, 1997.

[22] B. E. Foutz, S. K. O'Leary, M. S. Shur and L. F. Eastman, "Transient electron transport in wurtzite GaN, InN and AlN," *Journal of Applied Physics*, vol. 85, no. 11, pp. 7727-7734, 1999.

[23] S. K. O'Leary, B. E. Foutz, M. S. Shur, and L. F. Eastman, "Steady-state and transient electron transport within bulk wurtzite indium nitride: An updated semiclassical three-valley Monte Carlo simulation analysis," *Applied Physics Letters*, vol. 87, no. 22, pp. 222103-1-3, 2005.

[24] W. A. Hadi, S. K. O'Leary, M. S. Shur, and L.F. Eastman, "The sensitivity of the steady-state electron transport within bulk wurtzite zinc oxide to variations in the non-parabolicity coefficient," *Solid State Communications*, vol. 151, no. 12, pp. 874-878, 2011.

[25] S. K. O'Leary, B. E. Foutz, M. S. Shur, U. V. Bhapkar, and L. F. Eastman, "Electron transport in wurtzite indium nitride," *Journal of Applied Physics*, vol. 83, no. 2, pp. 826-829, 1998.

[26] S. K. O'Leary, B. E. Foutz, M. S. Shur, U. V. Bhapkar, and L. F. Eastman, "Monte Carlo simulation of electron transport in wurtzite aluminum nitride," *Solid State Communications*, vol. 105, no. 10, pp. 621-626, 1998.

[27] S. K. O'Leary, B. E. Foutz, M. S. Shur, and L. F. Eastman, "Polar optical phonon instability and intervalley transfer in III-V semiconductors," *Solid State Communications*, vol. 118, no. 2, pp. 79-83, 2001.

[28] S. K. O'Leary, B. E. Foutz, M. S. Shur, and L. F. Eastman, "Steady-state electron transport in the III–V nitride semiconductors: A sensitivity analysis," *Journal of Electronic Materials*, vol. 32, no. 5, pp. 327-334, 2003.

[29] S. K. O'Leary, B. E. Foutz, M. S. Shur, and L. F. Eastman, "Steady-state and transient electron transport within the III–V nitride semiconductors, GaN, AlN, and InN: A review," *Journal of Materials Science: Materials in Electronics*, vol. 17, no. 2, pp. 87-126, 2006.

[30] S. K. O'Leary, B. E. Foutz, M. S. Shur, and L. F. Eastman, "The sensitivity of the electron transport within bulk wurtzite indium nitride to variations in the crystal temperature, the doping concentration, and the non-parabolicity coefficient: an updated Monte Carlo analysis," *Journal of Materials Science: Materials in Electronics,* vol. 21, no. 3, pp. 218-230, 2010.

[31] B. Carnez, A. Cappy, A. Kasznski, E. Constant, and G. Salmer, "Modeling of a submicrometer gate field-effect transistor including effects of nonstationary electron dynamics," *Journal of Applied Physics*, vol. 51, no. 1, pp. 784-790, 1980.

[32] S. Adachi, *Properties of Group-IV, III-V and II-VI Semiconductors*. Chichester, England: John Wiley and Sons, 2005.

CHAPTER 6

Conclusions

In this thesis, the electron transport that occurs within two particular wide energy gap semiconductors of current interest, GaN and ZnO, was considered. Electron transport within GaAs was also examined, albeit primarily for benchmarking purposes. The over-arching goal of this thesis was to provide the materials community with tools for device performance analysis and optimization, to be used when evaluating the consequences of transient electron transport within these compound semiconductors, with the potential application for other materials. Providing fresh insights into the character of the electron transport within ZnO, a material whose electron transport characteristics were poorly understood prior to our investigations, with particular focus on the device implications thus engendered, was another central aim of this analysis. Device performance was assessed through the evaluation of the electron time-to-transit, the cut-off frequency of a device being inversely proportional to this time. Data from Monte Carlo simulations of the electron transport within these materials, performed by others, provided the input data needed for this analysis. The intellectual contributions provided throughout this thesis reside in the novel means of interpreting and processing the Monte Carlo results for the different materials considered in this analysis.

Initially, three-valley Monte Carlo simulation electron transport results were used for a detailed and quantitative analysis of the transient electron transport that occurs within bulk zinc-blende GaAs and bulk wurtzite GaN. We found that, for both cases, the electron drift velocity and the average electron energy field-dependent "settling times" are strongly correlated, and that the electric field resulting in the shortest electron transit-time is a function of the channel length. The calculated dependence of the peak transient electron drift velocity on the applied electric field strength was then used for the design optimization of short-channel high-frequency devices.

Then, the applicability of the semi-analytical approach of Shur [1] in evaluating the transient electron transport response of bulk zinc-blende GaAs, bulk wurtzite GaN, and bulk wurtzite ZnO was critically examined. In particular, results obtained using this semi-analytical approach of Shur [1] were contrasted with those obtained using three-valley Monte Carlo simulations of the electron transport. The approach adopted was to examine the response of an ensemble of electrons to the application of a constant and uniform applied electric field that is applied at time-zero. For the purposes of this analysis, three aspects of the transient electron transport response were considered: (1) the dependence of the electron drift velocity on the time elapsed since the onset of the applied electric field, (2) the dependence of the average electron energy on the time elapsed since the onset of the applied electric field, and (3) the dependence of the average electron displacement on the time elapsed since the onset of the applied electric field. The results obtained showed that this semi-analytical approach of Shur [1] produces results that are very similar to those produced using Monte Carlo simulations. Thus, this semi-analytical approach of Shur [1] should be applicable for the treatment of non-uniform and time-varying electric fields, making it a useful tool for the treatment of the transient electron transport response within general electron device configurations.

Then, how electrons, initially in thermal equilibrium, drift under the action of an applied electric field within bulk wurtzite ZnO, was considered. In particular, within the framework of a transient Monte Carlo analysis of the electron transport within this material, the applied electric field strength that ensures the minimum time-to-transit for a give electron transit displacement, $\tau_{\min}$, was determined. This analysis was performed for a range of displacements, and the optimal applied electric field strength was plotted as a function of the displacement considered. These results were then used in order to provide an upper bound on the potential performance of ZnO-based devices, assuming that the transit across a ZnO-based device occurs solely across the device length. The optimal cut-off frequency was found to range from around 50.3 GHz when the device length is set to 1000 nm to about 11.5 THz when the device length is set to 10 nm. These results suggest that ZnO holds great promise for future high-speed electron device applications.

Finally, the utility of the semi-analytical approach of Shur [1], for the purposes of device design optimization, was considered for the specific case of bulk wurtzite ZnO. In particular, the device optimization procedure performed previously through the use of Monte Carlo simulations of the electron transport was performed within the framework of the semi-analytical approach of Shur [1]. How the results obtained through the Monte Carlo simulations compared with those produced through the semi-analytical approach was then critically examined, for each step of the analysis. It was found that the results produced through the semi-analytical approach of Shur [1] are, in many cases, imperceptibly different from those of the Monte Carlo simulations. This suggests that the semi-analytical approach of Shur [1] may be employed for the purposes of device design and optimization, offering a substantial computational benefit to the device designer community. It is probable that the semi-analytical approach of Shur [1] may also be used for other compound semiconductors. It should be noted that further investigation would have to be performed in order to confirm this supposition.

The intellectual contributions provided by this analysis are numerous and varied. They primarily focus on adding value to the results of Monte Carlo simulations of the electron transport that occurs within these compound semiconductors and in providing tools and fresh insights into the nature of these materials that may be employed by the device design community. In the first phase of the analysis, the novelty rests in providing a new means of visualizing the impact of transient electron transport and in exploring the implications of this visualization technique for short-channel device optimization purposes. In the second phase of the analysis, establishing the suitability of the semi-analytical approach of Shur [1] in the characterization of the transient electron transport response is the primary achievement. This provides device designers with a much more computationally efficient means of determining the transient electron transport response which may be used for device simulation and optimization purposes. In the third phase of the analysis, the application of a device optimization procedure to the specific case of wurtzite ZnO and the determination of an upper bound on the performance of ZnO-based devices, which can be used by subsequent generations of device designers, are the primary accomplishments. In the final phase of the analysis, the assessment as to whether or not the semi-analytical approach of Shur [1] may be employed for device optimization purposes, for the specific case of bulk wurtzite ZnO, is the primary contribution.

Building upon the insights gleaned from this thesis, there are a variety of topics that one can further explore. For the visualization technique presented in the first phase of the analysis, it would be interesting to explore the consequences of this visualization technique for the specific case of bulk wurtzite ZnO, something that was not pursued during the course of this thesis. Plotting the transient electron drift velocity as a function of the applied electric field strength for a fixed distance displaced since the onset of the applied electric field, rather than the time elapsed, would also be interesting. In reference to the second phase of the analysis, establishing, in a more rigorous sense, the limits of the applicability of the semi-analytical approach, and suggesting possible model enhancements that would remedy these limitations, would be of use. The applicability of the semi-analytical approach of Shur [1] to other compound semiconductors would also be worthy of further investigation. In reference to the third phase of the analysis, i.e., the device optimization analysis based upon Monte Carlo results, the application of this approach to other materials of interest would be of value. Finally, for the final phase of this analysis, the use of this device optimization procedure to cases with non-uniform and time-varying electric fields should also be considered. These topics will have to be pursued in the future.

References

[1] M. S. Shur, “Influence of non-uniform field distribution on frequency limits of GaAs field-effect transistors,” *Electronics Letters*, vol. 12, no. 23, pp. 615-616, 1976.

Appendix A

The Monte Carlo method

The Monte Carlo electron transport simulation results, used for the purposes of this thesis, were acquired using the algorithm shown in Figure A.1 [1]. For all cases, the number of electrons in the ensemble is set to 3,000 for steady-state simulations and 10,000 for transient simulations. Using Fermi-Dirac occupation statistics, distinct electron-wave vectors are initially assigned to each electron. During a free-flight, an electron does not encounter any scattering events and moves semi-classically in accordance with the following equations [1]:

$$v = \frac{1}{\hbar}\vec{\nabla}_k \varepsilon(\vec{k}), \tag{A.1}$$

and

$$\hbar\frac{d\vec{k}}{dt} = -q\vec{\xi}, \tag{A.2}$$

where v is the electron velocity, $\vec{k}$ is the electron wave-vector, $\vec{\xi}$ is the electric field, q is the electron charge, and $\varepsilon(\vec{k})$ is the electron energy as a function of the electron wave-vector. The free-flight time, t_s, is chosen according to [2]:

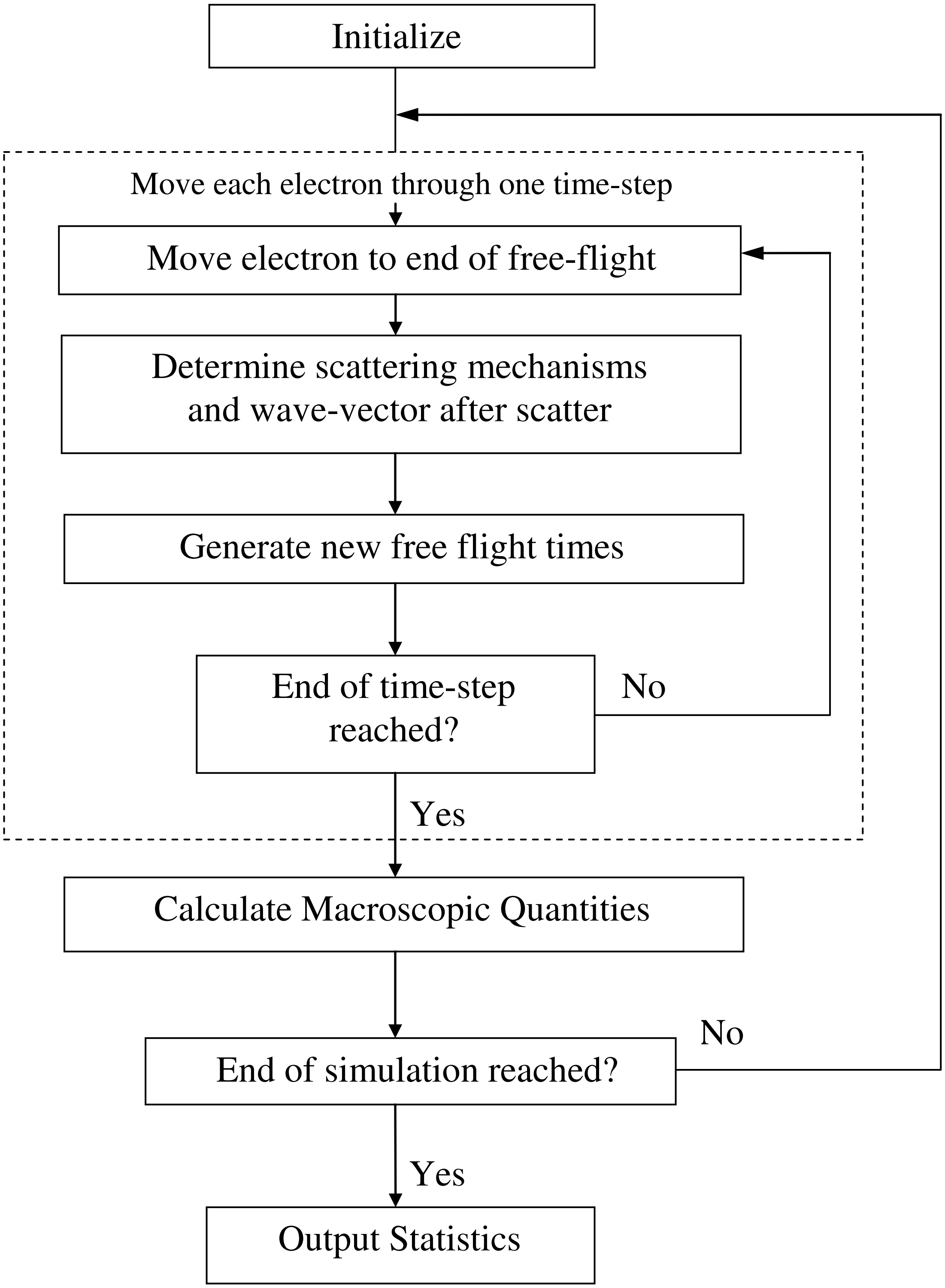

Figure A1: A flow chart of the Monte Carlo simulation algorithm used in order to determine the results employed throughout this thesis [1].

$$t_s = \frac{-1}{\lambda}\ln(1-r), \tag{A.3}$$

where r is a uniformly distributed random number, between 0 and 1, $\lambda = \sum_{m=1}^{n}\lambda_m$ is the total scattering rate, λ_m being the scattering rate associated with the m^{th} scattering mechanism.

At the end of a free-flight, each electron is subjected to random scattering events, selected with probabilities proportional to the scattering rate associated with each scattering mechanism. The scattering mechanisms considered are: (1) ionized impurity, (2) polar optical phonon, (3) piezoelectric, (4) acoustic deformation potential, and (5) intervalley scattering. After an electron scatters, a new free-flight time is chosen and the process is repeated until that electron reaches the end of the current time-step. After all of the electrons go through a time-step, macroscopic quantities, such as the electron drift velocity, the average electron energy, and the electron valley occupancy, are extracted from the electron distribution.

The scattering rates associated with aforementioned scattering mechanisms are determined as follows [2]:

1. Ionized impurity scattering:

$$\lambda_i(\varepsilon) = 4.84\times10^{11}(m^*)^{\frac{1}{2}}\frac{T}{K_o}\left(\frac{1+2\alpha\varepsilon}{[\varepsilon(1+\alpha\varepsilon)]^{\frac{1}{2}}}\right) \quad (\mathrm{s}^{-1}), \tag{A.4}$$

where ε is the electron energy, m^* is the electron effective mass at the bottom of the valley, α is the non-parabolicity coefficient, K_o is the relative static dielectric constant, and T is the temperature.

2. Polar optical phonon scattering:

$$\lambda_o(\varepsilon) = 5.61\times 10^{15}(m^*)^{\frac{1}{2}}\varepsilon_{op}\left(\frac{1}{K_\infty}-\frac{1}{K_o}\right)\left(\frac{1+2\alpha\varepsilon'}{\gamma^{\frac{1}{2}}(\varepsilon)}\right)F_o(\varepsilon,\varepsilon')$$

$$\times\begin{cases} N_o & \text{(absorption)} \\ N_o+1 & \text{(emission)} \end{cases} \quad (\mathrm{s}^{-1}), \tag{A.5}$$

where K_∞ is the relative high frequency dielectric constant, $\varepsilon_o = \dfrac{\hbar w_o}{q}$ is the polar optical phonon energy,

$$\varepsilon' = \begin{cases} \varepsilon+\varepsilon_o & \text{(absorption)} \\ \varepsilon-\varepsilon_o & \text{(emission)} \end{cases}, \tag{A.6}$$

$$N_o = \frac{1}{\exp(\hbar w_o / k_b T) - 1}\ , \tag{A.7}$$

where k_b is the Boltzmann constant,

$$\gamma(\varepsilon) = \varepsilon(1+\alpha\varepsilon)\,, \tag{A.8}$$

$$F_o(\varepsilon,\varepsilon^{'}) = C^{-1}\left[A\times\ln\left[\frac{\gamma^{\frac{1}{2}}(\varepsilon)+\gamma^{\frac{1}{2}}(\varepsilon^{'})}{\gamma^{\frac{1}{2}}(\varepsilon)-\gamma^{\frac{1}{2}}(\varepsilon^{'})}\right]+B\right], \tag{A.9}$$

$$A = \left\{2(1+\alpha\varepsilon)(1+\alpha\varepsilon^{'})+\alpha\left[\gamma(\varepsilon)+\gamma(\varepsilon^{'})\right]\right\}^2, \tag{A.10}$$

$$B = -2\alpha\gamma^{\frac{1}{2}}(\varepsilon)\gamma^{\frac{1}{2}}(\varepsilon^{'})\left\{4(1+\alpha\varepsilon)(1+\alpha\varepsilon^{'})+\alpha\left[\gamma(\varepsilon)+\gamma(\varepsilon^{'})\right]\right\}, \tag{A.11}$$

and

$$C = 4(1+\alpha\varepsilon)(1+\alpha\varepsilon^{'})(1+2\alpha\varepsilon)(1+2\alpha\varepsilon^{'}), \tag{A.12}$$

3. Piezoelectric scattering [3, 4]:

$$\lambda_{pz}(\varepsilon) = \frac{\sqrt{m^*}(qe_{pz})^2 k_b T}{4\sqrt{2}\pi\hbar^2 K_o e_o}\gamma^{\frac{-1}{2}}(\varepsilon)(1+2\alpha\varepsilon)^2\times\left[\ln\left(1+\frac{8m^*\gamma(\varepsilon)}{\hbar^2\beta^2}-\frac{1}{1+\frac{\hbar^2\beta^2}{8m^*\gamma(\varepsilon)}}+\left(\frac{\sqrt{2}\alpha\varepsilon}{1+2\alpha\varepsilon}\right)^2\right)\right] (\mathrm{s}^{-1}), \tag{A.13}$$

where e_{pz} is the piezoelectric constant, e_o is the permittivity of vacuum, ρ is the material density, v_s is the sound velocity, $\beta = \sqrt{\frac{q^2 N_D}{e_o k_b T}}$ is the inverse screening length [2], and N_D is the donor concentration.

4. Acoustic deformation potential scattering:

$$\lambda_a(\varepsilon) = \frac{0.449\times 10^{18}(m^*)^{\frac{3}{2}} T D_a{}^2}{\rho v_s{}^2}\varepsilon^{\frac{1}{2}}(1+\alpha\varepsilon)^{\frac{1}{2}}\left(\frac{(1+\alpha\varepsilon)^2+\frac{1}{3}(\alpha\varepsilon)^2}{1+2\alpha\varepsilon}\right) \quad (\mathrm{s}^{-1}), \quad \text{(A.14)}$$

where D_a is the acoustic deformation potential.

5. Intervalley scattering between the i^{th} valley and the j^{th} valley:

$$\lambda_{ij}(\varepsilon) = 1.129\times 10^{-5} Z_j (m^*)^{\frac{3}{2}} \frac{D_{ij}{}^2}{\rho E_{ij}}\varepsilon^{\frac{1}{2}}(1+\alpha\varepsilon)^{\frac{1}{2}}\left(1+2\alpha_j\varepsilon'_j\right)F_{ij}(\varepsilon_i,\varepsilon'_j)$$

$$\times\begin{cases} N_{ij} & \text{(absorption)} \\ N_{ij}+1 & \text{(emission)} \end{cases} \quad (\mathrm{s}^{-1}), \qquad \text{(A.15)}$$

where $\varepsilon_{ij} = \dfrac{\hbar w_{ij}}{q}$ is the intervalley scattering phonon energy, D_{ij}, is the intervalley deformation potential, Z_j is the number of equivalent valleys,

$$N_{ij} = \frac{1}{\exp(\hbar w_{ij}/k_B T)-1}\ , \qquad \text{(A.16)}$$

$$F_{ij}(\varepsilon_i,\varepsilon'_j) = \frac{(1+\alpha_i\varepsilon_i)(1+\alpha_j\varepsilon'_j)}{(1+2\alpha_i\varepsilon_i)(1+2\alpha_j\varepsilon'_j)}\ , \qquad \text{(A.17)}$$

and

$$\varepsilon'_j = \begin{cases} \varepsilon_i+\varepsilon_{ij} & \text{(absorption)} \\ \varepsilon_i-\varepsilon_{ij} & \text{(emission)} \end{cases} \ . \qquad \text{(A.18)}$$

References

[1] S. K. O'Leary, B. E. Foutz, M. S. Shur, and L. F. Eastman, "Steady-state and transient electron transport within the III–V Nitride semiconductors, GaN, AlN, and InN: A review," *Journal of Electronic Materials*, vol. 17, no. 2, pp. 87-126, 2006.

[2] M. Shur, *GaAs Devices And Circuits*, New York, New York: Plenum Press, 1987.

[3] C. Jacoboni, and P. Lugli, *The Monte Carlo Method for Semiconductor and Device Simulation*, New York, New York: Springer-Verlag, 1989.

[4] C. Moglestue, *Monte Carlo Simulation of Semiconductor Devices*, New York, New York: Springer, 1993.

VITA AUCTORIS

Name:	Walid Abdul Hadi
Place of birth:	Sidon, Lebanon
Year of birth:	1973
Education:	Ph.D., Electrical and Computer Engineering, University of Windsor, Windsor, ON, Canada, 2014
	M.S., Electrical and Computer Engineering, Oklahoma State University, Stillwater, OK, U.S.A, 1998
	B.E. Electrical Engineering, American University of Beirut, Beirut, Lebanon, 1996
Work Experience:	Instructor Electronics Engineering Technologies Saint Clair College, Windsor, ON, 2013-present.
	Instructor Lebanese International University Sidon, Lebanon, 2003-2008
	Transmission Planning Engineer American Electric Power Tulsa, Oklahoma, 1998-2003
Awards	Graduate student society award, winter 2013. A. R. and E .G. Ferriss award, winter 2013. Fredrick Atkins Graduate award, winter 2013. Doctoral tuition scholarship 2008 – 2012. A. R. and E .G. Ferriss award, winter 2012.

Publications

W. A. Hadi, E. Baghani, M. S. Shur, and S. K. O'Leary, "Electron transport within the two-dimensional electron gas formed at a ZnO/ZnMgO heterojunction: Recent progress," in *Materials Research Society Symposium Proceedings*, 2013, vol. 1577.

W. A. Hadi, M. S. Shur, and S. K. O'Leary, "Steady state and transient electron transport within bulk wurtzite zinc oxide and the resultant electron device performance," in *Materials Research Society Symposium Proceedings*, 2013, vol. 1577.

W. A. Hadi, M. S. Shur, and S. K. O'Leary, "The electron transport within bulk wurtzite zinc oxide in response to strong applied electric field pulses," in *Materials Research Society Symposium Proceedings*, 2013, vol. 1577.

W. A. Hadi, M. S. Shur, and S. K. O'Leary, "Steady-state and transient electron transport within wurtzite and zinc-blende indium nitride," *Journal of Applied Physics*, vol. 113, no. 11, pp. 113709-1-6, 2013.

W. A. Hadi, M. S. Shur, and S. K. O'Leary, "The sensitivity of the steady-state and transient electron transport within bulk wurtzite zinc oxide to variations in the crystal temperature, the doping concentration, and the non-parabolicity coefficient," *Journal of Materials Science: Materials in Electronics*, vol. 24, no. 1, pp. 2-12, 2013.

W. A. Hadi, R. Cheekoori, M. S. Shur, and S. K. O'Leary, "Transient electron transport in the III-V compound semiconductors gallium arsenide and gallium nitride," *Journal of Materials Science: Materials in Electronics*, vol. 24, no. 2, pp. 807-813, 2013.

W. A. Hadi, M. S. Shur, and S. K. O'Leary, "On the applicability of a semi-analytical approach to determining the transient electron response of gallium arsenide, gallium nitride and zinc oxide," *Journal of Materials Science: Materials in Electronics*, vol. 24, no. 5, pp. 1624-1634, 2013.

W. A. Hadi, M. S. Shur, and S. K. O'Leary, "A transient electron transport analysis of bulk wurtzite zinc oxide," *Journal of Applied Physics*, vol. 112, no. 3, pp. 033720-1-5, 2012.

W. A. Hadi, S. Chowdhury, M. S. Shur, and S. K. O'Leary, "A detailed characterization of the transient electron transport within zinc oxide, gallium nitride, and gallium arsenide," *Journal of Applied Physics*, vol. 112, no. 12, pp. 123722-1-6, 2012.

W. A. Hadi, S. K. O'Leary, M. S. Shur, and L.F. Eastman, "The sensitivity of the steady-state electron transport within bulk wurtzite zinc oxide to variations in the non-parabolicity coefficient," *Solid State Communications*, vol. 151, no. 12, pp. 874-878, 2011.

W. A. Hadi, S. K. O'Leary, M. S. Shur, and L. F. Eastman, "Steady state and transient electron transport in Zinc Oxide: recent progress," in *Materials Research Society Spring Meeting*, San Francisco, CA, 2011, vol. 1327.

J. J. Sanchez-Gasca, D. W. Matthews, and W. A. Hadi, "Small-signal stability assessment based on transient events," in *IEEE Power Engineering Society Summmer Meeting.,* Edmonton, Alberta, 1999, vol. 2, pp. 1292-1296.